Towards Environmentally Benign Wastewater Treatment – Photocatalytic Study of Degradation of Industrial Dyes

---

A thesis submitted in partial fulfillment of the requirements for the degree of

Masters of Science

in

Chemistry

at the

University of Canterbury

by

Ida Nuramdhani

University of Canterbury
July 2011

Acknowledgements

I would like to take this opportunity to express my sincere gratitude to many people who helped me with this project.

First and foremost, my thanks go to my supervisors, Dr. Vladimir Golovko and Dr. Deborah Crittenden for their support and help. It would have been next to impossible to finish this thesis writing without their continual guidance and commitment. Separately, I would like to thank Vladimir who welcomed me to be a part of his research group that provided me valuable experiences of learning and research in Chemistry. He (with Professor Ian Shaw) also cared for my health and safety to work in the laboratory during my pregnancy.

Thank you to NZAID – the international agency for development of New Zealand Ministry of Foreign and Trade for the scholarship, by which I have had the experiences of studying and living here in Christchurch, New Zealand.

I would especially like to thank Nick Oliver and Danny Leonard from the Mechanical Workshop, Roger Merryweather and Steven Graham from the West Precinct Electronic Workshop, as well as Robert McGregor from the Glassblowing workshop, for their excellent collaboration in constructing the photocatalytic chamber, without which the project would not have been possible. Thanks also go to Dr. Matthew Polson for the UV-Vis spectroscopy facilities.

My thanks go to Jan-Yves Ruzicka and David Anderson for providing me their catalysts, Anthony and Farida who helped me during my critical times, and the other members of the Golovko group who have made my study life an enjoyable experience. Thanks separately go to Jan-Yves for his help with experimental (especially in my first months), studying, and editing the English of my thesis.

I am greatly appreciative of academic, technical, and administration staff of the Department of Chemistry at the University of Canterbury, for being so helpful and friendly in taking care of my academic welfare. Thanks also go to Jonnie Chang, Sarah Beaven, and Mohammad Zeidan, my advisers from the International Student Office, who managed my scholarship and looked after the social welfare of me and my family. Being an international student became much easier for me with their helps.

Finally, my heartfelt appreciation goes to my husband, Tisna Kusumah, for his countless loves, patience, and support financially and spiritually, as well as my lovely daughter Yashilla and my "New Zealand-made" baby Alfarras, who always colour and fill my days with joys and happiness, especially during this challenging time. I would like to extend my thanks to my mum (Darsih Mulyani) and dad (Dayat Hidayat) for their endless loves, supports, and prayers.

Table of Contents

List of Tables

List of Figures

Abstract

Pollution created by textile dyeing operations attracts significant attention because an effluent containing a complex mixture of coloured and potentially toxic compounds can be released with the discharged water. Developing dyes and dyeing conditions to reduce the amount of residual dye contained in any effluent has been one of many approaches to minimise this environmental impact. However, the presence of coloured discharge cannot be totally eliminated using only this strategy. Thus, development of efficient post-dyeing wastewater treatment methods capable of removing coloured products from the water is of paramount importance.

TiO_2-mediated photocatalytic degradation of organic dye molecules *via* oxidation is the focus of the study reported in this thesis. TiO_2 significantly increases the rate of photodegradation of a wide range of organic dyes under mild operating conditions, and is able to mineralise a wide spectrum of organic contaminants. TiO_2 is also one of the very few substances appropriate for the industrial applications.

One of primary aims of this thesis is to test the hypothesis that augmenting standard TiO_2 photocatalysts with Au nanoparticles could increase performance of a catalyst, while immobilizing TiO_2 on a SiO_2 support may improve the cost of the process efficiency, *i.e.* more photocatalytic degradation per particle of TiO_2. Combining TiO_2 doped with gold nanoparticles on SiO_2 support has the potential to provide the highest photocatalytic ability at the lowest cost.

The first half of the thesis is concerned with establishing and optimizing experimental conditions for monitoring photodegradation *via* UV-Visible spectroscopy. Effects of various conditions such as temperature, sequence of addition of reagents, exposure to light *vs.* experiments in dark, sampling methods, and the use of quenching agent were examined.

The main conclusions from this study are that light-induced photodegradation using titanium dioxide nanoparticle catalysts is comparatively more efficient than purely chemical catalytic (*e.g.* non-light

mediated) degradation, even if the latter is performed at elevated temperature. Further, the rate of dye degradation is affected considerably by the parameters of the system.

The degradation rate depends strongly on the pH of the solution, due to charges on the catalyst surface and in the dye. In general, at pH $\leq$ 6.8, which is the zero charge point for TiO_2, reactions proceeded faster than those at higher pH. Six dyes from four different classes of dyes used in industry were used in this study, and all showed different photodegradation behaviour.

The second half of thesis tests the photocatalytic abilities of various TiO_2-based catalysts: pure TiO_2 (commercial and custom-made in our laboratory), TiO_2-supported gold nanoparticles (Au/TiO_2), SiO_2-supported TiO_2 (TiO_2/SiO_2), and SiO_2-supported Au/TiO_2. The best photocatalytic performance was observed for the custom-made TiO_2 code-named as e-TiO_2, which was synthesized using the sol-gel method in dry ethanol. TiO_2-supported Au55 nanoparticles showed a similar level of catalytic ability but are significantly more expensive. It was observed that dye adsorption played a significant role in the case of SiO_2-immobilized photocatalysts.

Chapter 1 - Introduction

1.1 Research Background

Pollution created by the textile industry attracts significant attention because large quantities of water are consumed at each stage of various processes. Approximately 80 kg of water are required to produce 0.5 kg of textile product.[1] The dyeing process in particular is a major problem for this industry. A number of dyes from different classes of chemical substances can be used in a single dyeing operation, resulting in an effluent containing a complex mixture of coloured and potentially toxic compounds. It is estimated that, during the coloration process, about 1 – 20% of the global production of dyes is released in the textile effluent.[2]

To minimise environmental impact, the textile dyeing industry is required to minimise the environmental release of chemicals as a result of the dyeing process.[3] It is also the responsibility of the dye manufacturers to develop dyes and dyeing conditions that increase the exhaustion of dye on textile fibres, and hence reduce the amount of residual dye contained in any effluent. Despite these preventive approaches, the presence of coloured discharge cannot be totally eliminated. Thus treatment methods that remove coloured waste products from the water are still required.

In general, traditional clean-up methods are classified as biological, physical or chemical. These methods have been widely applied in textile industries, yet are still plagued with further, secondary problems. Biological treatment, which is beneficial due to its low cost and simplicity, is generally not effective as synthetic dyes are generally resistant to aerobic bio-degradation.[4,5,6] Dye removal by physical treatment (such as filtration, adsorption or coagulation/flocculation) is usually effective, but suffers from high operational costs of post treatment of solid and coagulated wastes.[6,7,8] Chemical treatment also suffers drawbacks, such as the production of toxic and carcinogenic by-products, the high dosage of chemicals required, low efficiency and incomplete mineralisation.[4,5,9] Since all current

systems have their limitations, development of a significantly improved method of wastewater treatment is of paramount importance for long-term environmental viability of the textile industry.

The most successful methods to remove colour generally involve the oxidative degradation of dyes. These methods are collectively known as advanced oxidation processes (AOPs). One example of an AOP is TiO_2-mediated photocatalysis,[5,10] in which dye molecules adsorbed on the surface of TiO_2, activated by light, are broken down. This process is the focus on the study reported in this thesis.

Titanium dioxide (TiO_2) has been shown to be a promising heterogeneous photocatalyst because it is a low-cost material, capable of catalyzing photodegradation of dyes quickly under mild operating conditions, and is able to mineralise (i.e. degrade fully to water and CO_2) a wide spectrum of organic contaminants without side-reactions.[8,11] Importantly, it is also biologically and chemically inert as well as non-toxic.[6] Due to its remarkable properties, TiO_2 is one of the very few substances appropriate for the industrial application of AOP-mediated dye degradation.[9,12,13,14]

Additionally, the presence of noble metals such as silver,[15] platinum,[16] palladium,[16] and gold[16,17] has been reported to enhance the photocatalytic performance of TiO_2. It is believed that photo-generated electrons in the TiO_2 are trapped by the noble metal particles, leading to high efficiency of charge separation.[17,18,19] Of those listed above, gold is the most attractive dopant in terms of enhancing the photocatalytic activity of TiO_2 and enabling dye degradation because gold nanoparticles have been shown to possess the ability to activate oxygen from air, and thus they could potentially be used to decompose organic colourants.[20] Consequently, the use of harsh oxidants can be avoided, which is not only environmentally but also economically beneficial. Therefore, the photocatalytic study of dye degradation catalyzed by gold nanoparticles deposited on the surface of TiO_2 is anotherimportant part of this study.

1.2 Dye-Containing Textile Wastewater and the Environment

The principal aim of this thesis is to explore the synthesis and application of photocatalysts for the decolourisation of dyes in textile wastewater. A complete appreciation of the problems addressed by this thesis, however, cannot be achieved without sufficient knowledge about the chemistry of dyes and the colouration of textiles. This section therefore presents an introduction to some of the basic chemical principles associated with coloured compounds, and an overview of the ways in which the chemical structure of a molecule influences its colour properties. This is then followed by a description of how dyes (and pigments) may be classified. The discussion then focuses on the characteristics of textile effluent, with a closer look at coloured wastewater resulting from the dyeing process and its effect on the environment.

1.2.1 An Introduction to Colour and Dyes

"Colours," said 19th-century poet Leigh Hunt, "are the smiles of nature". Both natural and synthetic colours are all around us and commonly influence our moods and emotions. It is generally understood that colour generally serves a purely decorative or aesthetic purpose; in some cases, however, specific colours may be used to convey vital information, such as in traffic lights, colour-coded electrical cables and work safety equipment. In contrast, the presence of colour can sometimes be a problem, as is the case with dyeing effluent.

In scientific terms, colour is light.[21] Colour is a psychological phenomenon of human sensation interpreted in the brain when light of a particular wavelength (see Figure 1) stimulates the retina of the eye. An object will appear coloured if it selectively absorbs some wavelengths of light, and reflects or transmits others, within the visible region.[22] Table 1 presents a list of colours that result from light absorption and reflection of a substrate within the visible light spectral region.

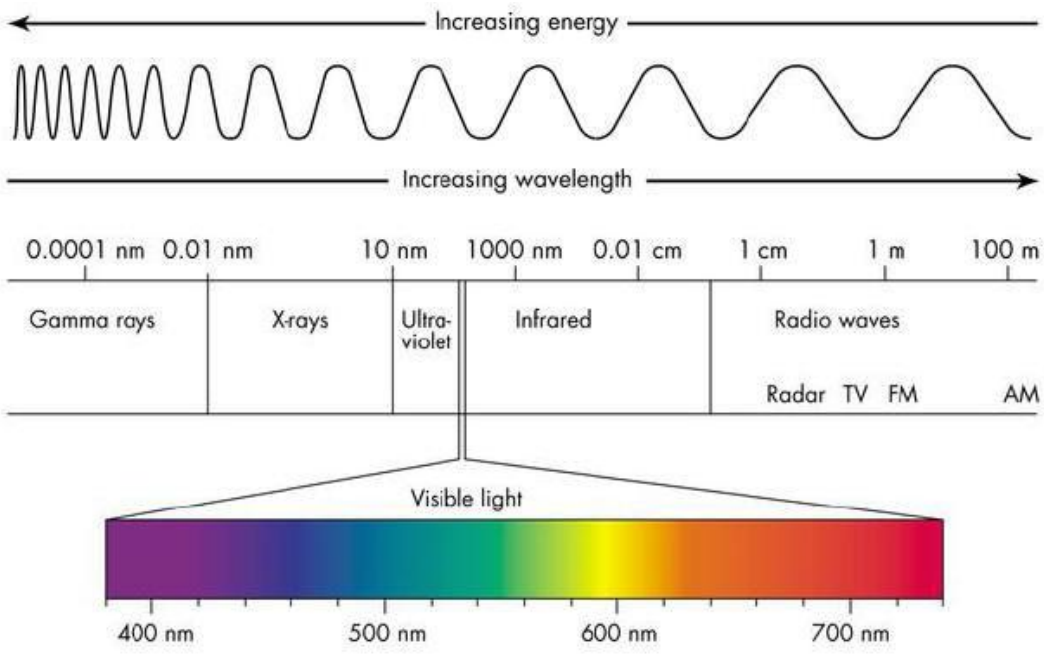

Figure 1: Visible Light Spectrum[i]

Table 1: Colours of typical spectral bands and colours perceived after their absorption by a material viewed in white light [22]

Wavelength absorbed (nm)	Colour of the light absorbed	Visible colour of the reflected light (complementary colour)
400-440	Violet	Greenish-yellow
440-480	Blue	Yellow
480-510	Blue-green	Orange
510-540	Green	Red
540-570	Yellowish-green	Magenta
570-580	Yellow	Blue
580-610	Orange	Greenish-blue (cyan)
610-700	Red	Blue-green

According to Nassau,[23] there are fifteen specific causes of colour. He has organized these colours in accordance with the physical and chemical mechanisms that govern them into five groups:

(1) colours from vibrations and simple excitations, which include those from incandescence, gas excitation, vibrations and rotations;

(2) colours from ligand field effects as observed in transition metal compounds and impurities;

(3) colours from transitions involving energy bands, as is the case with metals, semiconductors and doped semiconductors;

[i] Image was taken from http://quarknet.fnal.gov/quarknet-summer-research/QNET2010/Astronomy/

(4) colours from geometrical and physical optics, which include those generated from dispersion, scattering, interference and diffraction; and

(5) colours from transitions between molecular orbitals, which are generated by organic compounds such as dyes and pigments and by charge transfer.

In textiles, colour is introduced into materials using substances known as dyes and, to a much lesser extent, pigments. Both dyes and pigments may be classified as types of colourants – that is, substances capable of selectively modifying the reflection or transmission properties of a substrate. However, dyes and pigments have different behaviours when applied to a material, and therefore have different toxicological and environmental profiles.[24] A dye is soluble in the solvent medium used in the application process. It can be incorporated into a substrate through either physical or chemical (ionic, coordinative, or covalent) bonding. A pigment is insoluble and has no substantivity[ii] to the substrate.[22,24] These definitions are not universally true: for example, disperse and vat dyes are not readily soluble in water, but are referred to as dyes due to the way in which they are introduced onto fibres. This fact therefore suggests that, in addition to their solubility characteristics, it is always necessary to take into account the actual use to which the colourants is being put into.[10]

During the early years in the history of dye synthesis, new organic dyes were generally developed by a process of trial-and-error, as dye manufacturers attempted to mimic the structure of natural dyes.[24] Nonetheless, the relationship between colour and the chemical structure of a dye molecule had been of great concern until O. N. Witt proposed his empirical approach in 1876, which was subsequently followed by several works of others in the field.[10,22] A molecule of dye, according to the Witt theory of colour, must contain both a *chromophore* (colour bearing) and an *auxochrome* (colour enhancer) attached to an aryl ring. In 1907, Hewitt and Mitchell suggested that conjugation a system is vital to the production of colour. Dilthey and Witzinger (1928) brought all these concepts together,

[ii] Substantivity is dye retention: the affinity of a dye for a given substrate through particular interactions (polar or ionic interactions, hydrogen bonding, Van der Waals forces, and solubilities) is termed its substantivity. Dyes can be classified by their substantivity, which depends, in part, on the nature of the substituents in the dye molecule. (source*: Encyclopaedia Brittannica*)

concluding that the chromophore and auxochrome are respectively electron-withdrawing and electron-donating groups, that are linked to one another through a conjugated system.[10,22]

Chromophores are generally unsaturated groups. Examples of common chromophores include the azo (–N=N–), thio (>C=S), methano (R_1–CH=R_2), nitroso (–N=O) and nitro (–NO_2) groups. To produce colour, it is essential for an organic compound to contain at least one group of chromophores on an aryl ring forming an alternating single and double bonds.[24] For example, attaching a nitro group into a benzene ring (which would otherwise be colourless) gives a pale yellow substance, whereas the colour of azobenzene is orange-red. In addition, *p*-quinones are yellow, but *o*-quinones are orange or red.

Commonly encountered auxochromes include –OH (hydroxyl), –OR (alkoxy), –NH_2 (amino), and –N–R (alkylated amino) groups. These groups are all able to intensify the colour of the dye as their presence in the dye molecule can give greater quantum absorption of photons. Nitroanilines, for example, are more strongly coloured (deep yellow to orange) than nitrobenzene and aniline. An increase in the electron withdrawing or donating power, or the length of the conjugation, of the auxochrome causes the absorption band to shift to longer wavelength. This shift is referred to as a *bathochromic* shift, or red shift. A shift in the opposite direction is termed a *hypsochromic* shift, or blue shift. This concept of the origin of colour may be applied to most chemical classes of dyes, except for those that are not of the donor-acceptor type such as phthalocyanines.[10,24]

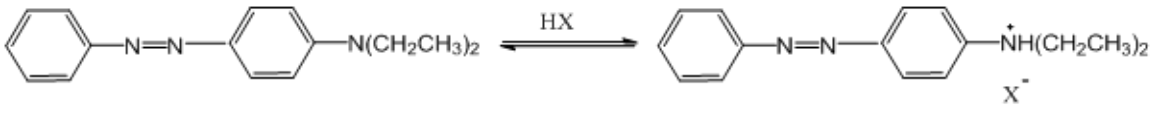

Figure 2: Protonation of N-N, diethylaminoazobenzene

A more precise understanding of the relationship between colour and molecular structure is given by various modern electronic structure theories.[25] These theories are able to predict the transition energies of organic molecules by using equations. The molecular orbital method can provide an accurate understanding of the relationship between colour and chemical composition. Importantly, it

also allows for the prediction of a dye's colour properties without the need to synthesise the dye itself.[10] For example, a prediction of the intensity and colour of the azonium cation from N,N-diethylaminoazobenzene (Figure 2) can be made by modifying the PPP-MO[iii] parameters of the protonated N atoms. The calculation results in a bandwidth that correlates well to experimental values.[24] The molecular orbital method also allows for the quantification of halochromism (change of colour due to change of pH) for more complex bis-azonium ions with insulated chromogens.[26]

Table 2: The effect of different substituent of azobenzene to its λ_{max} values[10]

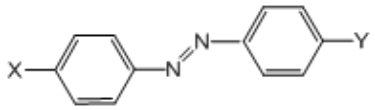

Substituent X	Substituent Y	Maximum wavelength (nm)
H	H	320
NO_2	H	332
H	NH_2	385
H	NMe_2	407
H	NEt_2	415
NO_2	NEt_2	486

The energy difference between the excited and ground states of the molecule determines the wavelength of light absorbed. The smaller the difference between two states (HOMO-LUMO gap), the longer the wavelength of the light absorbed (due to the Bohr-Einstein frequency relationship, $\Delta E=hc/\lambda$). Conjugated molecules can stabilize the excitation state by sharing and delocalizing the excited electrons.[27] Increasing conjugation will result in an increase in the wavelength of absorbed light, affecting the colour of the molecule. Thus, the resonance and conjugation system in a molecule of dyes determine its characteristics and depth of colour. Examples are given in Reference 10.

[iii] PPP-MO is a self-consistent molecular orbital method specifically taking into account antisymmetrisation and electron repulsion effects developed by Parises, Parr and Pople in 1953. The PPP-MO method established itself over the next two decades as the most useful and versatile technique for colour prediction, especially when the microelectronics revolution provided facilities for overcoming the complexity of the necessary calculation. (source: Shore, 2002) [24].

1.2.2 Classification of Dyes

The Colour Index (CI), which is usually used to classify dyes, has been the most popular and well-known classification system of dyes and pigments since its first publication in 1924. The second and third revised editions by the Society of Dyers and Colourists (SDC) jointly with the Association of American Textile Chemists and Colourists (AATCC) established the Colour Index as a leading standard reference internationally used by industries and importing authorities.[22, 24]

The CI designation comprises the name of the dye class, its hue, and a number: for example, CI Disperse Red 1, the first red dye in the disperse class. The name of the dye class is given in accordance with the different characteristics of the dyes.

Reactive dyes, for example, are so named because of their excellent reactivity due to the presence of reactive groups that are able to form covalent bonding with cellulosic and protein fibres. Typical reactive groups include: (1) an activated halogeno substituent (Cl or F) that undergoes nucleophilic substitution with a *cellulosate* anion; and (2) an activated unsaturated vinyl group that reacts with cellulose through an addition reaction.

Figure 3 presents CI Reactive Red 1 and CI Reactive Blue 19 as examples of different reactive groups.[28] The latter is one of the dyes mainly used in this study.

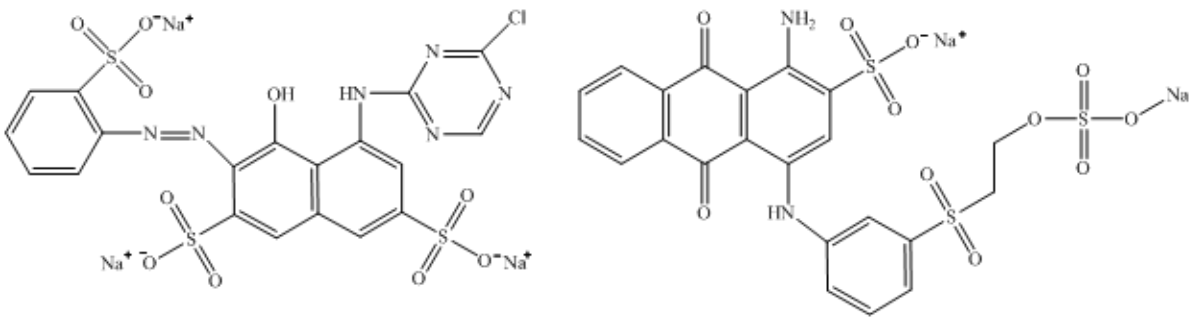

CI Reactive Red 1 CI Reactive Blue 19

Figure 3: Example of reactive dyes with triazinyl (left) and vinyl sulfone (right) reactive group

Disperse dyes are so-named because they are applied onto fabrics in the form of fine dispersion in water. These dyes are generally used to colour hydrophobic fibres such as polyester. Acid and basic dyes are so-named because they have negative and positive charges respectively.[29] Acid dyes usually contain sulphonic groups that provide negative charges and attract the protein fibres such as wool and silk that are protonated under acidic conditions. Basic dyes are typified by a delocalized positive charge and have good affinity for fibres that possess significant numbers of negative charges such as nylon and polyacrylic. Examples would be CI Disperse Yellow 211, CI Acid Red 42 and CI Basic Blue 9 (Figure 4), these are also used in this study.

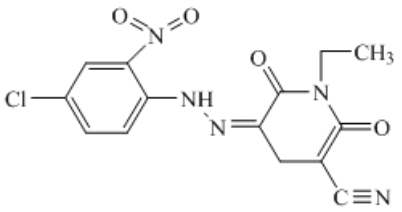

CI Disperse Yellow 211

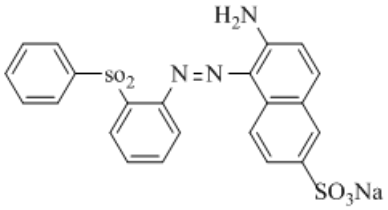

CI Acid Red 42

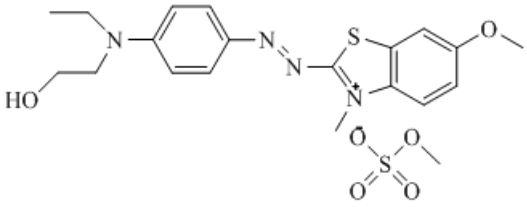

CI Basic Blue 41

Figure 4: Examples of Disperse, Acid and Basic Dyes

In addition, dyes may be classified based on their chemical constitution in the CI classification system. Azo dyes are the largest chemical class of dyes, and account for 75-80% of all dyes produced. These dyes are still used and produced globally, although their widespread use has been questioned in the recent years due to safety issues. Possible hazards of such dyes are described in more detail in the following section.

There are 19 groups of generic-name and 25 structural classes of colorants recorded in the Colour Index.[24] Table 3 presents the major classes of dyes according to method of application (generic name) and chemical constitutions.

Table 3: Classification of dyes according to method of application and chemical constitution

Classification according to method of application		Classification according to chemical constitution	
Generic name groups	Percentage of availability in commercial use	Chemical classes	Composition of total
CI Acid dyes	55%	Azo	~ 80%
CI Direct dyes	40%	Anthraquinone	15%
CI Disperse dyes	60%	Triarylmethane	3%
CI Reactive dyes	75% (continue to progress)	Phthalocyanine	2%
CI Basic dyes	60% (continue to progress)	Other minor classes	Less than 1%
CI Solvent dyes	60% (continue to progress)	(e.g. indigoid,	
CI Pigments	60% (continue to progress)	quinophthalone,	
CI Vat dyes	45% (in decline)	aminoketone,	
CI Mordant dyes	33% (in decline)	formazan, nitro,	
Other minor groups (e.g. CI Food dyes, CI Leather dyes, CI Fluorescent Brighteners, etc.)		nitroso, etc.)	

1.2.3 Colour in Dyeing Effluent and Its Effect on the Environment

During the colouration process, a small proportion of colorants (which by their nature are highly visible substances) may be released into open waters due to incomplete exhaustion of the colorants onto textile fibres. Thus, even a minor release may cause an obvious appearance of colour in the body of discharged wastewater. Shore (2002)[24] notes that a typical limit of visibility of coloured discharge in a river varies between 0.1 to 1 g/L, depending on colour, illumination and degree of clarity of the water. In pure water, a reactive dye solution with a concentration of as little as 0.005 mg/L may be visible, especially if the dye is red or violet in hue.

The nature of the effluent depends heavily on the type of dye used in the dying process and the depth of shade of the dye required.[30] For instance, several textile factories in Indonesia have seen high production of deep-coloured (e.g. dark red, navy blue and maroon) materials of cotton, polyester or combination cotton-polyester over the last decade. These processes require high concentrations of reactive and disperse dyes, which will produce relatively high concentrations of dyes in discharged wastewater.

Reactive dyes have been known to produce large volumes of coloured effluent compared to other dyes, due to their typically low rates of fixation on the fibre (*ca.* 50%-70%,[31] especially for dichlorotriazine dyes). The fixation rate for reactive dyes in particular is low due to the tendency of the dyes to react with water during the dyeing process. This reaction results in a hydrolysed dye that has a comparatively low affinity for the fibre.

O'Neill and co workers[32] have shown that technological and economic factors also play an important role in determining the nature of the textile effluent. Modern textile dyes are designed to possess a degree of chemical stability, which grants them good fastness to sunlight exposure, water, soap, and other environmental factors such as bleach and perspiration. The use of antimicrobial agents in natural fibres such as cotton and wool can often result in the resistance of effluents to biological degradation. Those factors therefore hinder removal of dyes from textile wastewater.

As well as being considered a pollutant, the chemicals in the coloured wastewater may become a source of eutrophication[iv] and yield dangerous by-products through oxidation, hydrolysis, or other chemical reactions in the wastewater phase.[30] The major question concerning the environmental impact of dye residues has been at what concentration the coloured effluent posses a significant hazard for the aquatic life. Debate continues regarding this topic as, in general, organic dyes have

[iv] Eutrophication is the gradual increase in the concentration of phosphorous, nitrogen, and other plant nutrients in an aging aquatic system such as a lake. The productivity or fertility of such an ecosystem increases as the amount of organic material that can be broken down into nutrients increases. This material enters the ecosystem primarily by runoff from land that carries debris and products of the reproduction and death of terrestrial organisms. Blooms, or great concentration of algae and microscopic organisms, often develop on the surface, preventing the light penetration and oxygen absorption necessary for underwater life. (*source: Encyclopaedy Brittannica*)

demonstrated low toxicity to fish and organisms. This is represented by the value of LC_{50}, the concentration of substance required to kill half of the organisms exposed. Bae and Freeman[33] reported that several types of new direct dyes were observed to be non-toxic with 24 hours LC_{50} > 100 mg/L, whereas the other dyes containing copper molecule were found to have 24 hours LC_{50} > 6.0 mg/L and 48 hours LC_{50} > 3.6-6.0 mg/L. Other results also suggest that biological toxicity in dye wastewater stems chiefly from dyes containing copper.[34] In contrast, it has been found that dye wastewater has a considerable effect on algae, a life-form vital to the aquatic ecosystem. There is evidence that the presence of coloured effluent (especially from basic dyes) inhibits the growth of algae at concentrations as low as 1 mg/L.[24] These facts give no general conclusion regarding the toxicity of dyes to the biological aquatic ecosystem.

Textile dyes are considered non-toxic and safe for people simply because consumers have no contact with the free dyes directly, rather only through the coloured materials used in daily life. This is not the case for plant workers, however. For these people, dyes pose a high risk of acute toxicity such as skin irritation and skin sensitization. Moreover, evidence of high incidences of bladder cancer found in plant workers involved in the manufacture of particular dyes (containing benzidine and 2-naphthylamine) during 1930-1960 indicates that the long-term effects of certain textile dyes are more harmful, and can be lethal. Unfortunately, the statistics of this were not reported.[35] A study conducted in 1985 on 414 workers involved in the various departmental sections in a dye manufacturer found that 21 of them were found to have allergic reactions, including occupational asthma.[36] For the general public, exposure will likely only occur through discharge of unfixed dyes into open water.

One documented example of possible dye toxicity is the azo class of dyes, which may be carcinogenic and biologically active either because of the dye itself, or due to metabolites of the dye.[37,38] Figure 5 shows the mechanism of *N*-hydroxylation, which can cause the carcinogenicity of the dye.[35]

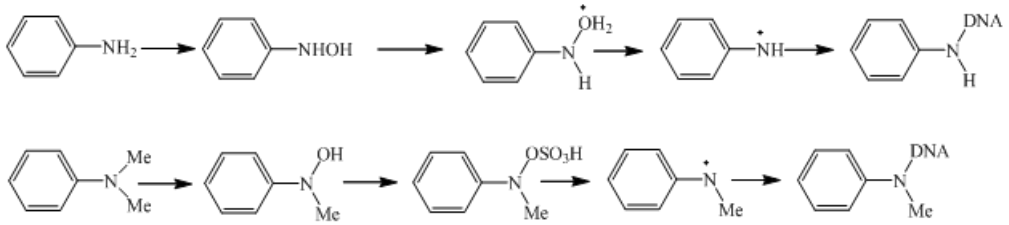

Figure 5: Mechanisms of activation of amino-group in azo-dyes

For water-soluble azo dyes, metabolites such as benzidine and 2-naphthylamine may also be carcinogenic. Figure 6 shows a typical example of such dyes.[35]

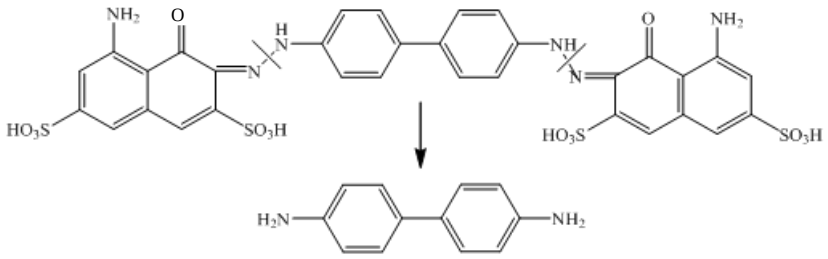

Figure 6: Typical example of carcinogenic water-soluble azo dyes

1.3 Titanium Dioxide and Photocatalysis

This section presents an overview of titanium dioxide and its chemical modification in association with photocatalytic activity. The chapter will conclude with a brief review of past studies on the photocatalytic decolourisation of wastewater dyes. These topics are presented so as to lay the foundation for subsequent work and as a prelude to the more detailed and comprehensive account of the synthesis and application of titanium dioxide for the decolourisation of wastewater dyes presented in Chapters 2 and 4.

1.3.1 Properties of Titanium Dioxide

Titanium dioxide (TiO_2) is a semiconducting material that may be chemically activated by light. It has an energy band gap of 3.0-3.2 eV, which is equivalent to the energy of near UV radiation (< 400 nm).[39]

Since its discovery as a catalyst for the photo-splitting of water by Fujishima and Honda,[40] the photoactivity of titanium dioxide has been extensively investigated due to its potential in myriad applications, ranging from photovoltaics and photocatalysis to photo-electrochromics and sensors.[40,41,42] Due to its outstanding properties, titanium dioxide has become the ideal photocatalyst for commercial use due to its low cost, high stability, and non-toxicity.

Titanium dioxide exhibits three major crystalline phases: rutile, anatase and brookite. Rutile is the most stable phase for small crystals (< 11nm), anatase for large crystals (> 35nm) and brookite in between.[42] Rutile and anatase (see Figure 7) are the most studied of the phases, particularly in the field of surface science.[43] Sclafani and Herrmann[44] reported that anatase is the most active phase of TiO_2 compared with the amorphous and the rutile phases, whereas brookite is photocatalytically inactive.

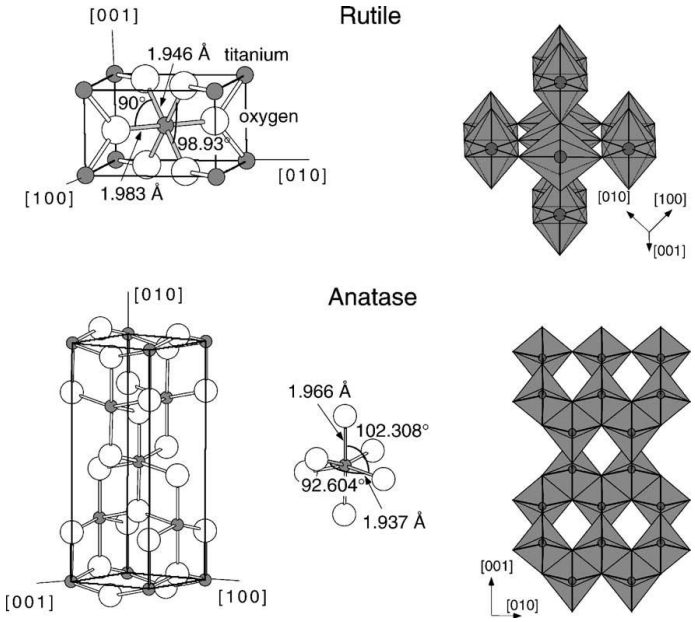

Figure 7: Bulk Structure of Rutile and Anatase TiO_2[v]

[v] Image was taken from Diebold © 2002 Elsevier Science [39]

Rutile is the most thermodynamically stable phase at high temperature.[44,45] Its structure can be observed at temperature between 673–1073 K.[46] The surface enthalpies of the three crystal structures of TiO_2 are also different. Upon heating, anatase and brookite are observed to form rutile, but also to coarsen, showing the balanced energetics as a function of particle size. The change of thermodynamic stability of the three polymorphs can take place under conditions that prevent coarsening, with anatase and/or brookite being stable at small particle size regimes.[47]

As a semiconductor, TiO_2 possesses a fully occupied valence band and totally empty conduction band, that are separated by a forbidden "band gap" of energies.[48] The absorption of a photon with an energy equivalent to or greater than its band gap (≥3.0 eV) can excite an electron from the filled valence band into the empty conduction band, creating an excited electron in the conduction band and hole in the valence band. Further, one of two possible mechanisms can occur to this charge pair:[49]

(1) Reaction between the charge pair and an electron donor or acceptor

(2) Recombination of the photogenerated electron-hole pair, either radiatively or non-radiatively

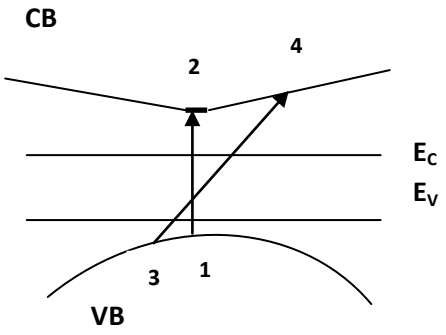

Figure 8: Schematic band structure of crystalline TiO_2 [50]
[E_v and E_c are the interface levels. The arrow indicates two ways that light absorption takes place: direct electron transition (1 to 2) and indirect (3 to 4) that occurs at the interface]

In order to be a suitable photocatalyst, it is important for TiO_2 to be efficient at capturing energy from ambient light. TiO_2 is classified as an indirect semiconductor, and thus the mechanism of light absorption through the interband electron transition described above is not effective as it is prevented by the symmetry of the crystal.[47,49] When the absorption occurs at the surface of a crystal, or at the interface between two crystals, momentum that the electron obtained from the light wave is not conserved.[51]

It is far more efficient for the TiO_2 crystal to absorb light through indirect electron transitions. In small nanocrystals of TiO_2, as well as in porous and microcrystalline semiconductors, a large dipole matrix element and high electron density in the valence band results in a large share of the interface atoms, which allows for such indirect transitions (see Figure 8).[50] For crystallites with dimensions smaller than 20 nm, absorption on the crystal interface is actually the most important mechanism of light absorption.

The band gap of bulk TiO_2 is narrower than that of TiO_2 nanomaterials because the former has a large dimensionality.[47] Thus, it can be seen that the size of a TiO_2 particle plays a key role in defining its properties and, as a result, in its overall performance as a photocatalyst.

1.3.2 Modified Titanium Dioxide

There are some unattractive properties of TiO_2 that impede its efficiency as a photocatalyst. First, bulk TiO_2 is known to possess a relatively wide intrinsic band gap – 3.0 eV for rutile and 3.2 eV for anatase. This can restrict its utilization of the solar energy spectrum, as these energy band gaps correspond to the energy of near-UV light (which is only less than 10% of the total energy radiated from the sun).[47] Second, TiO_2 photocatalytic efficiency can be lowered by the unexcitation of the photoexcited electrons (recombination).[52] As shown by Figure 9, photoexcitation causes the formation of a region of positive charge density (hole) created by the removal of an electron from a site. Holes are positively charged nuclei and they are held fixed in position in the crystalline lattice. Electrons

from another source can fill the hole, such as from another site in the crystal, from an external anion, or from the drop of the original electron back into its original molecular orbital (recombination). This is not desired in photocatalysis. One of the reasons for the latter is the presence of defect sites in the lattice structure, which can behave as recombination centres and generate a lower quantum yield and, as a result, a poor efficiency for photocatalytic reactions.[53,54] This occurrence can be explained by the scheme presented in Figure 9. Photoexcited electrons from the valence band can be trapped either in the conduction band (a), or in a defect site close to the conduction band (shallow traps) (b).[44]

There has been great interest in modifying TiO_2, either to shift the band gap into the visible light region and/or to prevent the recombination of photogenerated electron/hole pairs.[13, 19, 47, 54] According to Chen,[47] there are two major methods that have been widely employed to modify the optical properties of TiO_2:

(1) surface chemical modification (sensitization)

(2) bulk chemical modification (doping)

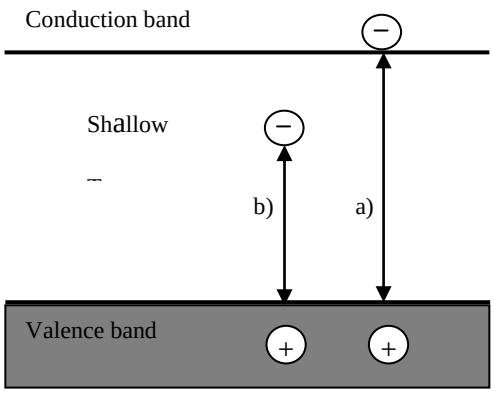

Figure 9: Scheme of UV-Induced Charge Separation in TiO_2[44]

Sensitization is a way to treating the TiO_2 to enable production of photocurrent. This sensitizer may be a metallic, inorganic, or organic material. A variety of inorganic and organic dyes have been

studied as sensitizers for TiO_2, particularly in the field of dye-sensitized solar cells (DSSCs).[55,56] In a DSSC, the sensitizer produces higher energy electrons than available in TiO_2 normally.[57,58]

Doping is a commonly-used method to narrow the band gap and change the electronic properties of TiO_2. TiO_2 is doped by loading other components, either organic or inorganic, into the bulk material, modifying its optical activity. The chemical composition of TiO_2 can be altered in this way by replacing either the cations (Ti^{4+}) with other transition metals or the anions (O^{2-}) with other anions. These changes may also affect the material's electronic properties and thermal stability.[43] Doping with non-metals tends to raise the valence band maximum energy level (threshold), as most non-metallic dopants are less electronegative than oxygen. On the other hand, doping with metallic elements tends to lower the conduction band minimum energy level, as most metals used in doping are more electronegative than titanium. Noble metal dopants may also act as sinks for the photogenerated charge carriers, and may support interfacial charge-transfer processes, inhibiting electron-hole recombinations.[44, 54,59]

As mentioned earlier, one of the catalysts presented in this thesis consists of gold nanoparticles immobilized on the surface of TiO_2 (Au/TiO_2). This approach to TiO_2 modification is related to metal doping, but the characteristics of the modified material are conceptually different. Here, the presence of the noble metal (i.e. gold nanoparticles) does not change the solid framework – instead, the nanoparticle is simply in an interfacial contact with the semiconducting TiO_2. Here, our hypothesis is that gold nanoparticles on the TiO_2 surface will trap the photoexcited electrons (e_{CB}^-) and so help to prevent the recombination of electron-hole pairs.

1.3.3 Photocatalytic Degradation of Textile Dyes

Photocatalysis refers to a reaction when the catalyst is activated by light. TiO_2's photocatalytic abilities are due to the production of an excited electron/hole pair when the material is exposed to UV light. The UV radiation leads to a charge separation due to excitation of an electron (e^-) from the

valence band to the conduction band of TiO_2, simultaneously forming a hole (h^+, a region of positive charge density) in the valence band. The mechanism of photocatalysis is illustrated by Figure 10.[60]

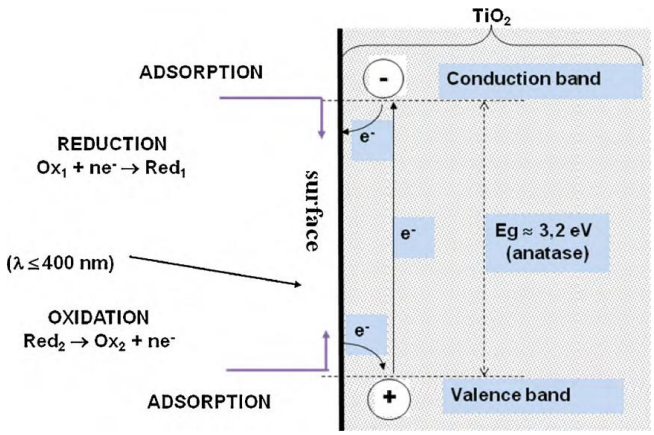

Figure 10: Electron energy plotted upwards as a function of the distance from the surface to the bulk of titanium dioxide[vi] (Eg is the band gap energy)

As expressed in Scheme 1, this process generates a photoexcited electron and hole (see Eq.1). Possible further reactions are represented by Eqs. 2-6, while Eqs. 7-9 represent the possible recombination pathways. Eqs. 3 and 4 illustrate the formation of OH radicals and O vacancies due to competition for holes.[49]

Scheme 1: *Excitation process of TiO_2 and its further mechanisms*[61]

$TiO_2 + h\upsilon$	$\longrightarrow$	$e^- + h^+$	(Eq. 1)
e^- + Ti(IV)O─H	$\longrightarrow$	Ti(III)O─H^- (X)	(Eq. 2)
h^+ + Ti(IV)O─H	$\longrightarrow$	Ti(IV)O·─H (Y)	(Eq. 3)
$h^+ + ½\ O^{2-}_{lattice}$	$\longleftrightarrow$	¼ O_2 (g) + vacancy	(Eq. 4)
$e^- + O_{2,(surface)}$	$\longrightarrow$	$O_2^-{}_{(surface)}$	(Eq. 5)
$O_{2,s}^-$ + H^+	$\longleftrightarrow$	$HO_{2,s}$	(Eq. 6)
h^+ + Ti(III)O─H^-	$\longrightarrow$	Ti(IV)O─H	(Eq. 7)
e^- + Ti(IV)O·─H	$\longrightarrow$	Ti(IV)O─H	(Eq. 8)
$O_2^-{}_{(surface)}$ + Ti(IV)O─H	$\longrightarrow$	Ti(IV)O─H + $O_{2(surface)}$	(Eq. 9)

[vi] Image was taken from J.-M. Herrmann @ 2010 Elsevier BV [58]

Oxidant radical species such as superoxide ($O_2^{\bullet-}$), hydroxyl ($OH^{\bullet}$), or peroxide ($OOH^{\bullet}$) may result from redox reactions of the photogenerated electron-hole pairs. These radicals are responsible for the heterogeneous photodegradation of organic substrates such as dyes on the TiO_2 surface. Akpan and Hameed[62] have reported that these radicals will readily oxidize most azo dyes. Reactions relevant to the photodegradation of organic dyes on the surface of TiO_2 are described in Scheme 2.

Scheme 2: *Relevant reactions of degradation of dyes at the surface of TiO_2*[30]

$$TiO_2\ (h_{VB}^{+}) + H_2O \longrightarrow TiO_2 + H^{+} + OH^{\bullet} \quad \text{(Eq. 10)}$$

$$TiO_2\ (h_{VB}^{+}) + OH^{-} \longrightarrow TiO_2 + OH^{\bullet} \quad \text{(Eq. 11)}$$

$$TiO_2\ (e_{CB}^{-}) + O_{2(surface)} \longrightarrow TiO_2 + O_2^{-\bullet}{}_{(surface)} \quad \text{(Eq. 12)}$$

$$O_2^{-\bullet}{}_{(surface)} + H^{+} \longrightarrow HO_2^{\bullet} \quad \text{(Eq. 13)}$$

$$Dye + OH^{\bullet} \longrightarrow \text{degradation products} \quad \text{(Eq. 14)}$$

$$Dye + h_{VB}^{+} \longrightarrow \text{oxidation products} \quad \text{(Eq. 15)}$$

$$Dye + e_{CB}^{-} \longrightarrow \text{reduction products} \quad \text{(Eq. 16)}$$

Most of these degradation reactions occur due to the presence of the hydroxyl radical, which is a very strong oxidizing agent (Eq. 14). Dyes that will not react with the hydroxyl radical can follow either oxidation or reduction pathways as shown by Eqs. 15-16, but these routes are less effective overall.[30]

Scheme 3: *Excitation process of Au-TiO_2*[17]

$$Au\text{–}TiO_2 \xrightarrow{h\upsilon} Au\text{–}TiO_2(e_{CB}^{-}) + Au\text{–}TiO_2(h_{VB}^{+}) \quad \text{(Eq. 17)}$$

$$Au\text{–}TiO_2(h_{VB}^{+}) + Dye \longrightarrow \text{products} \quad \text{(Eq. 18)}$$

$$Au + e_{CB}^{-} \longrightarrow Au\ (e^{-}) \quad \text{(Eq. 19)}$$

$$Au(e) + O_2 \longrightarrow O_2^{\bullet-} \quad \text{(Eq. 20)}$$

In the presence of gold nanoparticles on the surface of TiO_2, it is hypothesized[17] that the accumulation of e_{CB}^- in the gold sites producing Au(e^-) (Eq. 19) can prevent the electron-hole pairs recombination. The lifetime of the charge separation is thought to be longer, thus, increasing the photocatalytic activity on the surface of TiO_2 (as shown in *Scheme* 1 and 2). In this case, the presence of oxygen and the superoxide anions, which are important species for photooxidation, can be formed (Eq. 20).

1.3.4 Brief Overview of Relevant Past Studies

Most previous studies on photocatalytic degradation of dyes have employed ionic dyes (basic and/or acid dyes),[6,30,39,62, 63] catalyzed by commercially available TiO_2 . The most commonly used TiO_2 catalyst is Degussa P25, which is mostly (*ca.* 80%) anatase with a BET (Brauer, Emmet, Teller) surface area of 50 m^2/g and a mean particle size of *ca.* 30 nm.[62] Lachheb *et al.*[63] reported that Degussa P25 could photodegrade five different types of dyes (see Table 4), four of which are simple

Table 4: Stoichiometric equation of total oxidation of five-selected dyes[63]

Name of the selected dyes	Stoichiometric equation of total oxidation
Methylene Blue	$C_{16}H_{18}N_3S^+ + 51/2O_2 \rightarrow 16CO_2 + 3NO_3^- + SO_4^{2-} + 6H^+ + 6H_2O$
Orange G	$C_{16}H_{11}N_2O_3S^- + 20O_2 \rightarrow 12CO_2 + 2NO_3^- + SO_4^{2-} + 3H^+ + H_2O$
Alizarin S	$C_{14}H_7O_7S^- + 14O_2 \rightarrow 14CO_2 + SO_4^{2-} + H^+ + H_2O$
Methyl Red	$C_{15}H_{15}N_3O_2 + 43/2O_2 \rightarrow 15CO_2 + 3NO_3^- + 3H^+ + 6H_2O$
Congo Red	$C_{33}H_{22}N_6O_6S_2^{2-} + 91/2O_2 \rightarrow 32CO_2 + 6NO_3^- + 2SO_4^{2-} + 8H^+ + 7H_2O$

model dyes usually used as pH indicators. Complete mineralization of these dyes (in which all carbon is converted into CO_2) was achieved after 60 minutes of irradiation, regardless of initial concentration, with the stoichiometric equation of total oxidation expressed in Table 4.

In contrast, Mahmoodi *et al*[6] reported that the rate of degradation of an acid dye (acid blue 25) depended greatly on the initial concentration of the dye solution and the presence of electron

acceptors on the surface of TiO_2. After 80 minutes of irradiation the group observed no decolourisation of 75 and 100 mg/L dye solutions (0.18×10^{-3} and 0.24×10^{-3} mol/L respectively) . To achieve complete degradation, a large amount of H_2O_2 (600 mg/L or 15.8×10^{-3} mol/L) had to be added to the solution. The molar amount of H_2O_2 added in these experiments was 88 and 66 times (very high) more than the molar amount of the dye. In addition, they showed that the residual acute toxicity of the dye decreased during the colour degradation, as was demonstrated by a *Daphnia Magna*[vii] bioassay. Here, the photocatalytic reaction was carried out under UV irradiation. The catalyst used was Degussa P25, immobilized on a synthetic polymer. This can be compared with the work done by Lachheb and co-workers, who used a suspension of P25 catalyst in the dye solution. Other studies have also shown that the rate of degradation can depend on other process parameters, including pH, catalyst concentration, and spectrum of light used to irradiate the sample.[6,30,39, 62]

Arbuj *et al.*[64] reported in 2010 a method to synthesise TiO_2 of comparable photoactivity to Degussa P25. Their synthesis was carried out by hydrolysis of titanium tetrachloride ($TiCl_4$) precursor followed by drying at 100 ^{0}C. Calcination at 750 ^{0}C resulted in an 80:20 ratio of anatase:rutile, which gave the best photocatalytic degradation of methylene blue dye.

Several attempts to enhance the photocatalytic performance of TiO_2 have been carried out by depositing gold metal on the surface of TiO_2. Kumar *et al.*[17] observed that the photocatalytic degradation of acid red 88 under visible light irradiation in the presence of electron acceptors was considerably higher than that demonstrated by pure TiO_2. However, Dozzi *et al.*[19] have shown that the presence of gold on the surface of TiO_2 can result in a decrease of the reductive-oxidative photoprocess under visible light irradiation.

Of those previous studies, most researchers have been concerned only with the photocatalytic degradation of typical (model) dyes, limiting the real-life applicability of the generated data and

[vii] a species of Daphnia, widely used for a 48 hour acute toxicity study [6]

conclusions. Thus, a systematic study focused on industrially applicable dyes would be of great importance and relevance to the field. The synthesis (and modification) of novel TiO_2 to produce more effective catalysts than those currently available is still a challenging field of research.

1.4 Aims of Present Study

The objective of this project is to develop an environmentally friendly low cost wastewater treatment system for use in the textile industry, using a TiO_2-based catalyst under irradiation by UV light. The present study may be divided into the following sections:

1. Systematic study of photocatalytic dye degradation using industrially-available TiO_2 catalysts and various types of industrially-relevant dyes. The effect of altering parameters such as catalyst concentration, the use of oxidants, and pH has been studied.
2. Systematic study of photocatalytic dye degradation using novel TiO_2 catalysts. The effect of different preparation methods has been studied. The TiO_2 catalysts have been synthesized by Jan-Yves Ruzicka, a Ph.D. student in the Golovko group.
3. Systematic study of photocatalytic dye degradation using modified TiO_2: i.e. Au/TiO_2 (gold nanoparticles deposited on the surface of TiO_2) and $Au/TiO_2/SiO_2$ (gold nanoparticles deposited on the surface of TiO_2 loaded on a SiO_2 support). Both industry-standard and custom-made TiO_2 were used as supports for these catalysts. The catalysts were mainly prepared by Jan-Yves Ruzicka, but some of the Au/TiO_2 catalysts were prepared by David Anderson, who is also a Ph.D. student in the Golovko group.

Research in photocatalysis is a new research direction for the Golovko group. The photocatalytic chamber was designed and constructed by the Electrical and Mechanical Workshop at the Department of Chemistry of the University of Canterbury. A series of preliminary experiments, presented in Chapter 3, were carried out to establish the experimental methodology and analysis.

Kinetics analysis of some important results is presented in Chapter 4. Reaction progress was monitored by UV-Vis spectroscopy (Cary 100 Bio UV-Visible spectrophotometer "VARIAN").

Research Period and Limitation

The research period was from 21st of February 2010 up to 21st of February 2011. This is the period of MSc (Master of Science) part 2, which consists of conducting research and writing thesis. However, two high-magnitude earthquakes struck the Canterbury region on the 4th of September 2010 and the 22nd of February 2011. These have caused significant limitations to research during and immediately after this period. The laboratory was closed and it took around 2 months after the September earthquake and 3 months after the February earthquake to get back to the laboratory.

It should be noted that other than UV-Visible spectroscopy, the analyses were planned to involve TOC (Total Organic Carbon) analysis and HPLC-MS (High Performance Liquid Chromatography-Mass Spectroscopy). Unfortunately, the two last methods of analysis could not be performed because of technical reasons caused by the two high-magnitude earthquakes. Apart from that, this research is also limited by the time (M.Sc. study period).

Chapter 2 – Catalysts Used in This Study

This chapter presents the general characteristics and synthetic methods of all catalysts used in this study, as listed in Table 5. The aim of presenting this chapter is for information purposes; therefore, there is in-depth discussion on aspects regarding synthesis and characterization of the catalysts.

Table 5: List of catalysts used in this study

No	Code-name of a catalyst	Description
1	P25-TiO_2	commercial TiO_2 Degussa P25
2	e-TiO_2	"custom-made" TiO_2, synthesized by hydrolysis sol-gel method
3	p-TiO_2	"custom-made" TiO_2, synthesized by peroxo sol-gel method
4	c-TiO_2	calcined e-TiO_2
5	3%P25-TiO_2/SiO_2	3% by weight of commercial Degussa P25 TiO_2 loaded on SiO_2, followed by calcinations
6	3%e-TiO_2/SiO_2	3% by weight of e-TiO_2 (synthesized by hydrolysis sol-gel method) loaded on SiO_2, followed by calcination of the immobilized product
7	uc-3%e-TiO_2/SiO_2	e-TiO_2 loaded on SiO_2, without calcination
8	1%Au_{11}/P25-TiO_2-100	Au11 nanoparticles deposited on the surface of P25-TiO_2, with calcination at 100^oC
9	0.3%Au_{11}/P25-TiO_2-100	
10	1%Au_{11}/P25-TiO_2-200	Au11 nanoparticles deposited on the surface of P25-TiO_2, with calcination at 200^oC
11	0.3%Au_{11}/P25-TiO_2-200	
12	1%Au_{55}/P25-TiO_2-200	Au55 nanoparticles deposited on the surface of P25-TiO_2, with calcination at 200^oC
13	0.3%Au_{55}/P25-TiO_2-200	
14	ht-P25-TiO_2	heat-treated (calcinated) P25-TiO_2, as reference for catalysts no.8-13
15	0.5%Au_{55}/SiO_2	Au55 nanoparticles loaded on SiO_2, as reference for catalysts no. 18-19
16	1%Au_{55}/SiO_2	
17	1%Au_{55}/10%P25-TiO_2@SiO_2	Au55 nanoparticles deposited on the surface of TiO_2 which was then loaded on SiO_2
18	1%Au_{55}/10%e-TiO_2@SiO_2	
19	1%Au_{55}/3%e-TiO_2@SiO_2	

2.1 Titanium Dioxide Degussa P-25 (P25-TiO_2) – Industry Standard

The P25-TiO_2 powder utilized in this study was obtained from Chemiplas NZ Limited with the trade name "Aeroxide", and is manufactured by Evonik Degussa GmbH. P25-TiO_2 was selected as one of the catalysts in this study because it is a well-known standard material for photocatalysis, and exhibits a relatively large surface area and high activity. In this study, P25-TiO_2 has been used in all preliminary experiments that require a large amount of catalyst, and in every dye-degradation reaction as a reference. The physical and chemical properties of AeroxideP25-TiO_2 as obtained from Chemiplas NZ Limited are presented in Table 6.

Table 6: Physical and chemical properties of "Aeroxide" P25-TiO_2[viii]

Properties	Unit	Typical value
Specific surface area (BET)	m^2/g	50 ± 15
Average primary particle size	nm	21
Density (20 ^oC)	g/cm^3	3.8
Tamped density* *acc.to DIN EN ISO 787/11, Aug. 1983*	g/L	approximately 130
Moisture* *2 hours at 105^oC*	wt.%	≤ 1.5
Ignition loss *2 hours at 1000^oC, based on material dried for 2 hours at 105^oC*	wt.%	≤ 2.0
pH *in 4% dispersion*	wt.%	3.5 – 4.5
Titanium dioxide**	wt.%	≥ 99.50
Al_2O_3 – content**	wt.%	≤ 0.300
SiO_2 – content**	wt.%	≤ 0.200
Fe_2O_3 – content**	wt.%	≤ 0.010
HCl – content**	wt.%	≤ 0.300
Sieve residue (by Mocker, 45µm) *acc. To DIN EN ISO 787/18, Apr. 1984*	wt.%	≤ 0.050

** The data represents typical value (no product specification)*

*** Based on ignited material*

[viii] All information was obtained from the Product Information given by Evonik Industries

According to Datye *et al.*,[65] The P25-TiO_2 powder is synthesized by hydrolysis of $TiCl_4$ in a hydrogen flame, resulting in a crystalline product consisting of both anatase and rutile, with anatase content varying between 60% and 80%. Figure 11 shows the TEM (Transmission Electron Microscopy) image of the fumed P25-TiO_2 obtained by Datye *et al.* from the manufacturer. The arrows shown in the picture indicate the presence of the lattice periphery of single crystals of TiO_2.

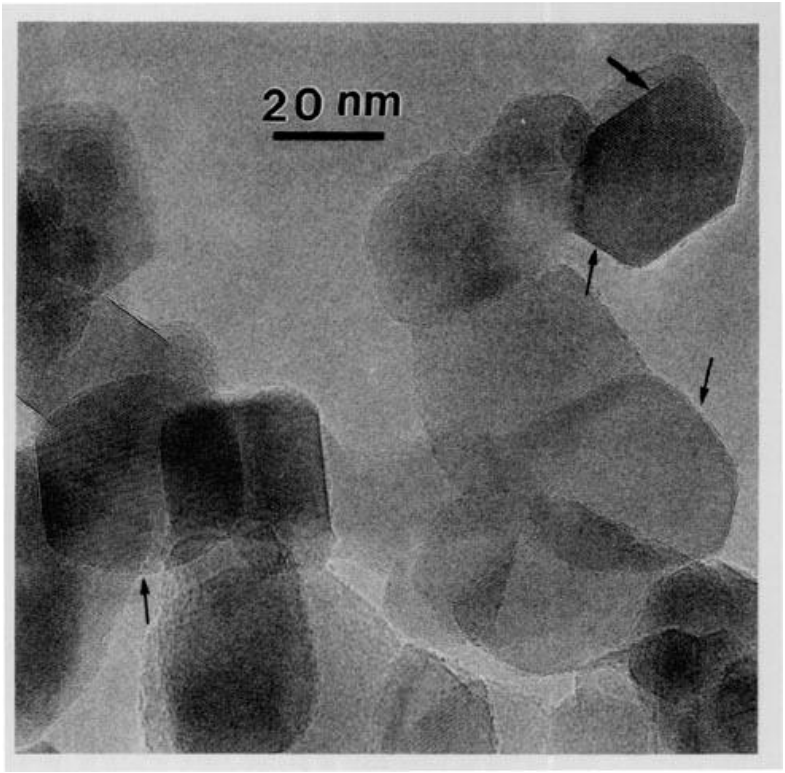

Figure 11: TEM image of the fumed P25-TiO_2[ix]

Characterization on the experimental scale by Ohno *et al.*[66] confirmed Datye's conclusion that the P25-TiO_2 contains anatase and rutile single crystalline particles in a ratio of about 3:1. It was observed that anatase and rutile are present separately in the TiO_2 P-25 powder, they grow on different nuclei and form their own separate agglomerates. Under the conditions present in photocatalytic reactions, the agglomerates were found to decay and thus the anatase and rutile were able to come into contact with each other. The morphology of the isolated anatase and rutile particles are shown by the TEM

[ix] Image was taken from Datye *et al.* ©1995 Academic Press, Inc. [63]

and X-ray diffraction images presented in Figure 12. In addition, a small portion (ca. 0.1%) of amorphous particles was also found as shown by Figure 13.

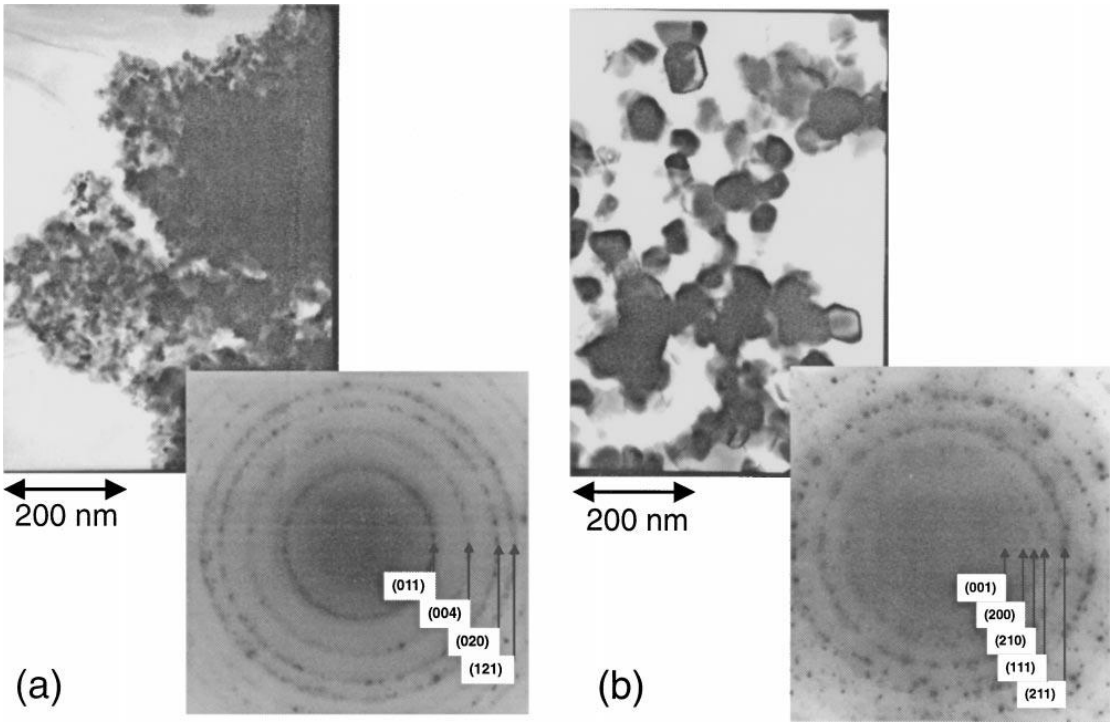

Figure 12: TEM images and electron diffraction patterns of the P25 powder in the regions of (a) the anatase phase and (b) the rutile phase[x]

Ohno *et al.*[66] concluded that the high photocatalytic activity of TiO_2 P-25 is due to the synergistic effect of the mixed-phases of anatase and rutile. Hurum *et al.*[67] further confirmed this conclusion, and observed the charge separation and recombination of mixed-phase TiO_2 P-25 by EPR (Electron Paramagnetic Resonance) spectroscopy. This study emphasizes the point that rutile plays an important role in photocatalytic activity, as it extends the photoactive region of the catalyst into the visible spectrum.

[x] Image was taken from T. Ohno *et al.*@ 2001 by Academic Press [66]

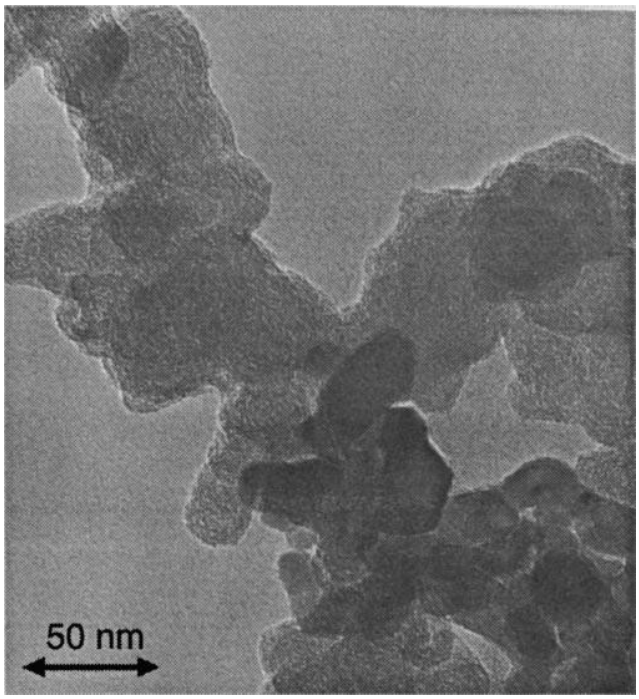

Figure 13: TEM image of the amorphous phase in the mixed-phase TiO_2 Degussa P-25[xi]

2.2 Custom-Made Titanium Dioxide

Three different "custom-made" TiO_2 catalysts were used in this study, synthesized by Jan Yves Ruzicka, in following manners (see Table 5):

1. Hydrolysis of titanium butoxide in ethanol/water (e-TiO_2)
2. Calcination of e-TiO_2 at 500°C (c-TiO_2)
3. Hydrothermal synthesis of TiO_2 nanoparticles from peroxotitanic acid (p-TiO_2)

2.2.1 Hydrolysis Sol-Gel Method

The basic mechanism of TiO_2 synthesis by the hydrolysis sol-gel method (as shown by Scheme 4) is initiated by a nucleophilic substitution of an alkoxy group with a hydroxyl group. The reaction is then followed by condensation reactions producing oxo- and hydroxo- bridges.

[xi] Image was taken from T. Ohno *et al.*@ 2001 by Academic Press [66]

Scheme 4: *Mechanism of hydrolysis of metal alkoxide*[68]

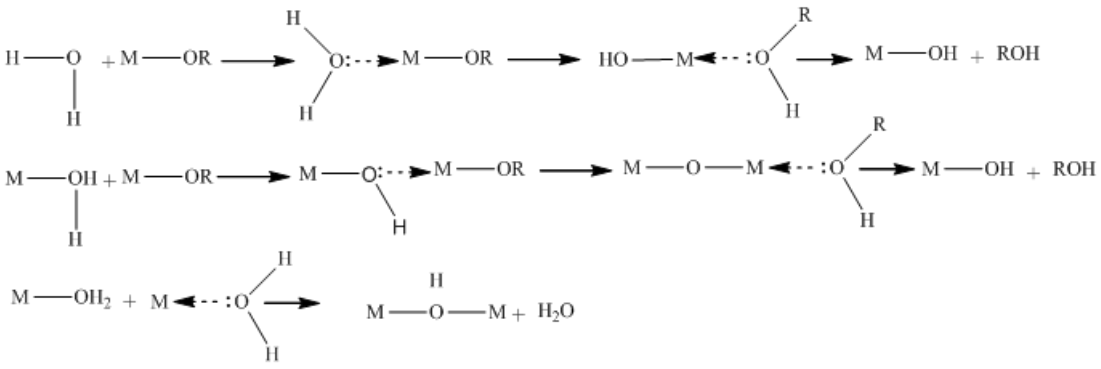

Following the procedure of synthesis given by Golubko *et al.*,[68] titanium (IV) tert-butoxide [$Ti(OBu)_4$] (see Figure 14) was used as a precursor for the synthesis of e-TiO_2. This catalyst was analyzed by TEM and powder X-ray diffraction (PXRD). The TEM images in low and high magnification (obtained by Jan-Yves Ruzicka at University of Canterbury, 200 keV TEM) presented in Figure 15 show the amorphous characteristics of e-TiO_2. This was confirmed by the PXRD graph (obtained by Jan-Yves Ruzicka at IRL, Co X-ray source) shown by Figure 16.

In order to obtain a crystalline product, e-TiO_2 was calcinated (heat-treated) at 500^{o}C for two hours to induce a phase transition. The TEM images of the product (obtained by Jan-Yves Ruzicka at UC, 200 keV TEM), named c-TiO_2, are shown by Figure 17. It is noteworthy that fringes due to the crystalline lattice can be observed in high magnification images (bottom right). The detail procedure of the catalyst preparation developed by Jan-Yves Ruzicka is presented in Chapter 5.

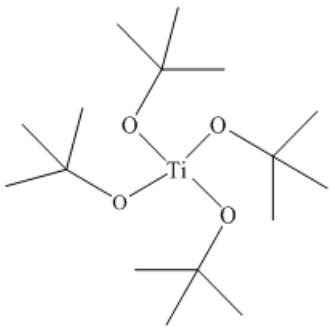

Figure 14: Structure of Titanium (IV) tert-butoxide

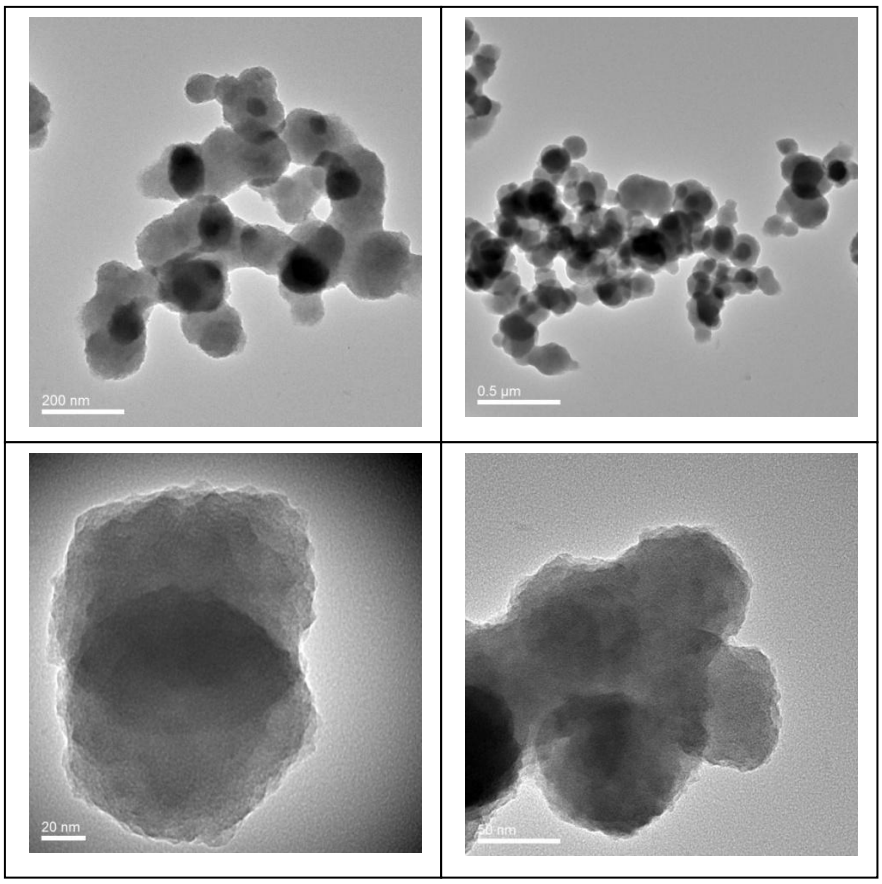

Figure 15: TEM images of e-TiO_2

(obtained by Jan-Yves Ruzicka at University of Canterbury, 200 keV TEM)

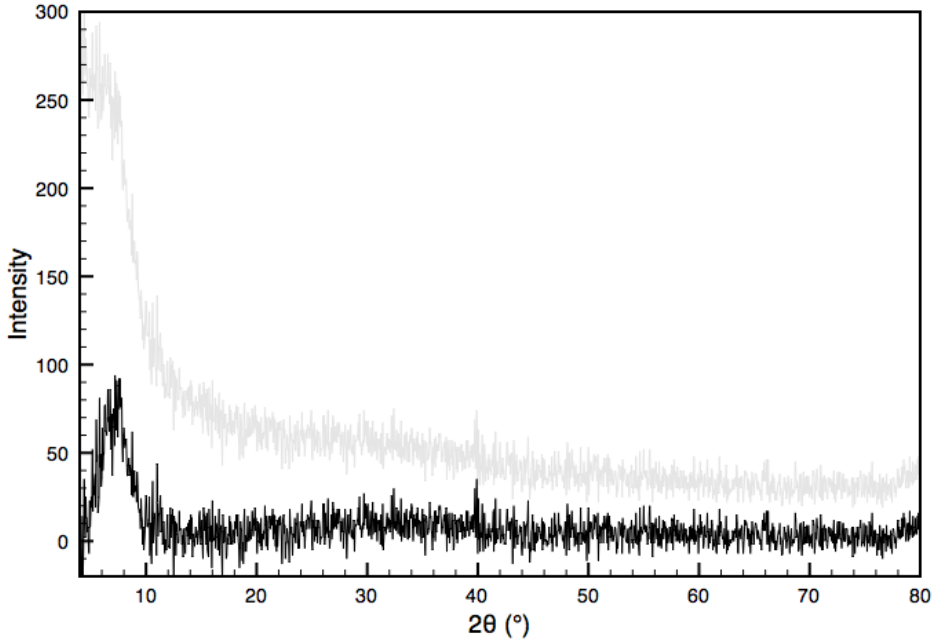

Figure 16: PXRD spectrum of e-TiO_2

(obtained by Jan-Yves Ruzicka at IRL, Co X-ray source)

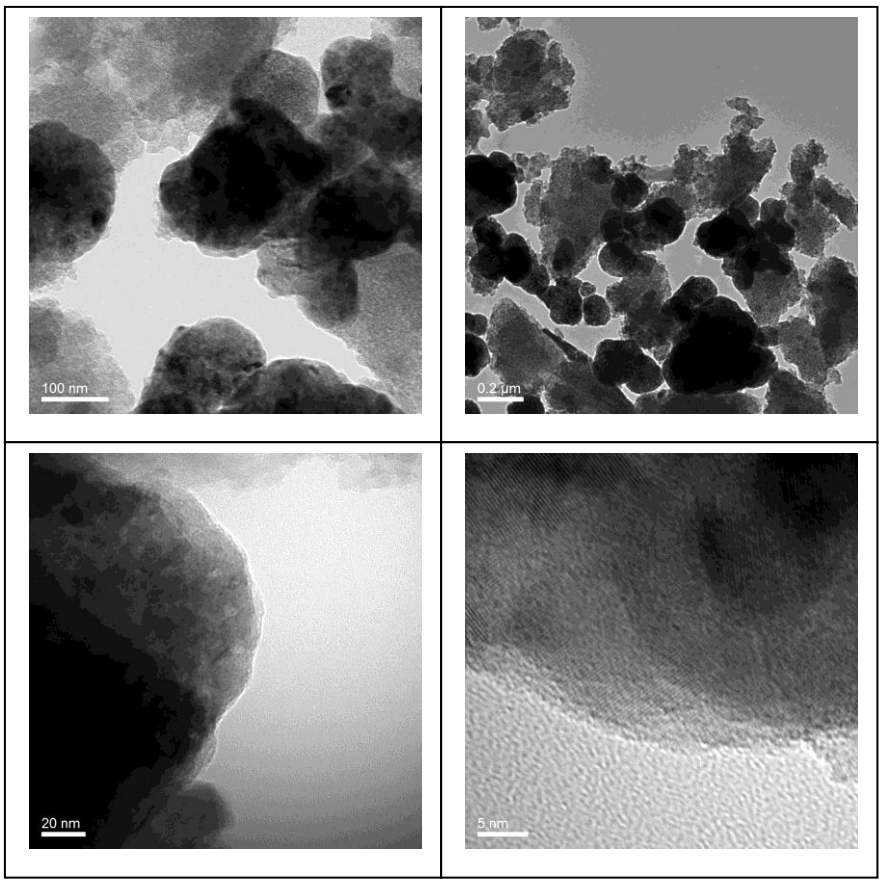

Figure 17: TEM images of c-TiO_2
(obtained by Jan-Yves Ruzicka at University of Canterbury, 200 keV TEM)

2.2.2 Hydrogen Peroxide Based Sol-Gel Method

The ydrogen peroxide based sol-gel method is a modification of the conventional sol-gel synthesis, in which H_2O_2 is added as an oxidizing agent. The resulting TiO_2 solution is more stable than those from the conventional sol-gel method (see Figure 18).[69]

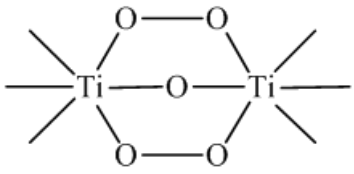

Figure 18: Chemical **s**tructure of p-TiO_2[70]

The nanosized TiO_2 anatase crystals can be produced in a lower temperature regime (hydrothermal conditions) in the case of peroxotitanic pathway compared to the need for high temperature calcinations of amorphous TiO_2 made via the sol-gel method.

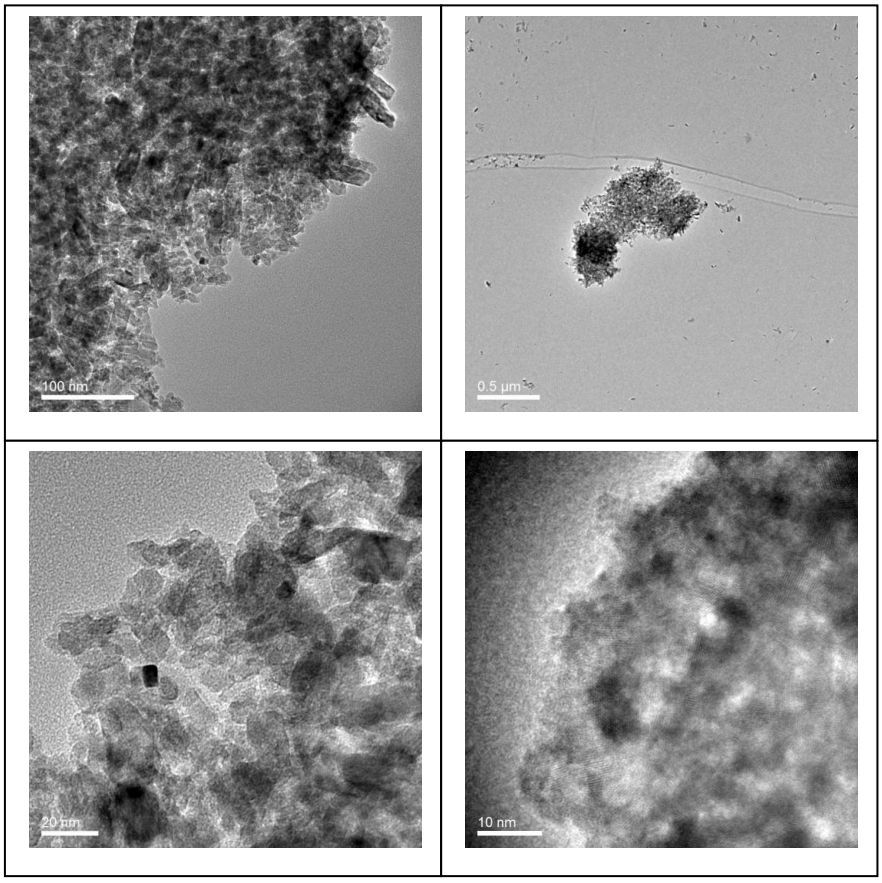

Figure 19: TEM images of p-TiO_2
(obtained by Jan-Yves Ruzicka at University of Canterbury, 200 keV TEM)

The p-TiO_2 was synthesized based on the experiments of Sasirekha *et al*[71]., in which $Ti(OH)_4$ precipitate was formed by adding water to a mixture of titanium alkoxide and ethanol. Titanium peroxide sol (peroxotitanic acid) was then formed after the addition of H_2O_2. Heating the resulting titanium peroxide sol at 80-97^oC gave the peroxo-modified nanosized TiO_2 anatase crystals.[71]

The morphology of the resulting product is shown by TEM images (obtained by Jan-Yves Ruzicka at University of Canterbury, 200 keV TEM) presented by Figure 19. The PXRD spectrum (obtained by

Jan-Yves Ruzicka at IRL, Co X-ray source) shown in Figure 20 confirms the crystalline nature of p-TiO_2, as indicated by peaks around $2\theta = 32^o$.

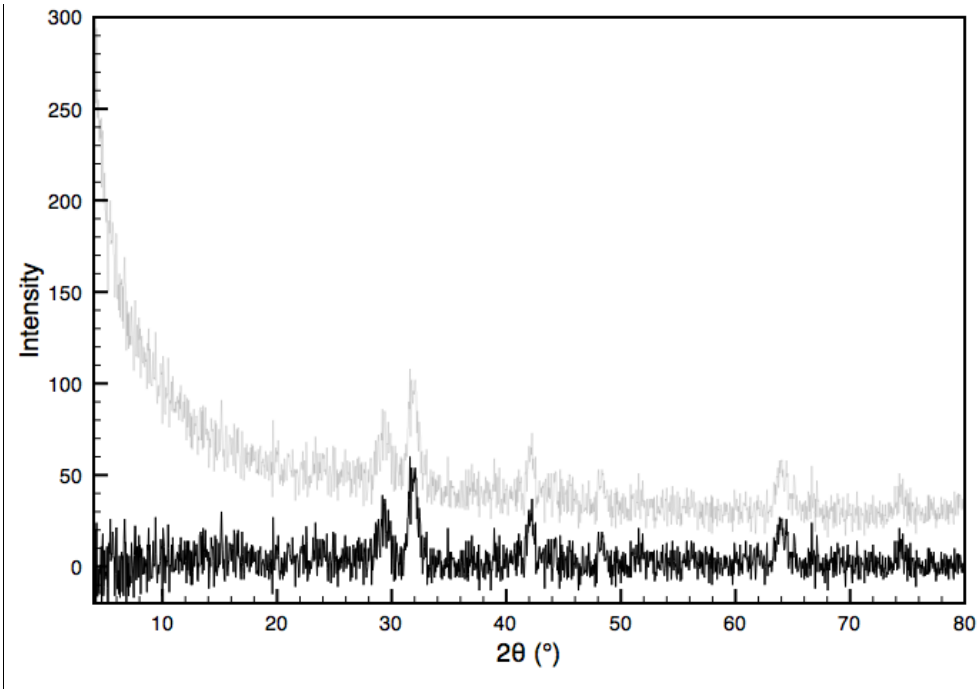

Figure 20: PXRD spectrum of p-TiO_2
(obtained by Jan-Yves Ruzicka at IRL, Co X-ray source)

2.3 Post Synthesis-Modified Titanium Dioxide

One focus of this study was on the modification of titania by other nanoparticles or structures. The following modifications were attempted:

(1) Gold nanoparticles deposited on TiO_2 support (Au/TiO_2);

(2) TiO_2 loaded on SiO_2 support (TiO_2/SiO_2); and

(3) Gold nanoparticles deposited on TiO_2, loaded on SiO_2 support ($Au/TiO_2/SiO_2$). For reference, Au/SiO_2 was also prepared.

Various composition ratios of the catalyst components were prepared, either using the commercial P25-TiO_2 or with e-TiO_2 synthesized in-house.

2.3.1 Au/TiO_2

As described in Chapter 1, gold nanoparticles are incorporated onto the surface of TiO_2 in an attempt to increase the photocatalytic performance of TiO_2. A variety of clusters with gold core sizes less than 1 nm have been successfully synthesized and characterisized by David Anderson. Au_{11} and Au_{55} clusters were selected for this study. Both types of gold nanoparticles were immobilized on the P25-TiO_2 support and then subjected to calcination at different temperatures, i.e. 100^{o}C and 200^{o}C.

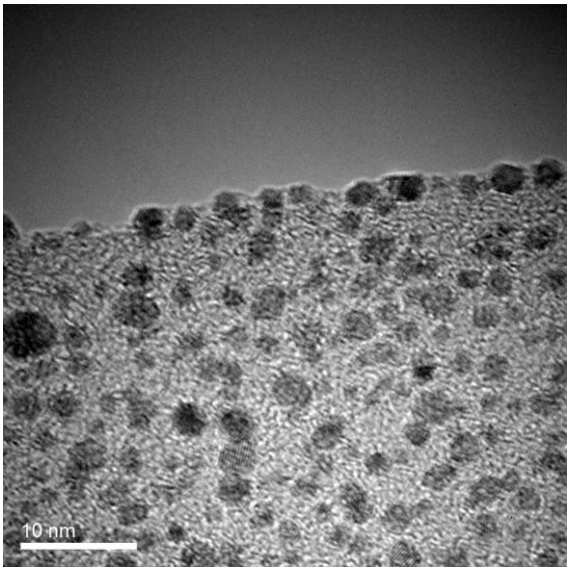

Figure 21: TEM image of Au_{55} clusters on holey carbon film supported on Cu TEM grid (obtained by David Anderson at University of Canterbury, 200 keV TEM)

The Au_{55} and Au_{11} clusters were made using phosphine-stabilized gold nanoparticles as precursors. The methods were adapted from those reported in the literature.[72] The detailed experimental procedures developed by David Anderson are presented in Chapter 5. The Au_{55} cluster was characterized by HR (high resolution)-TEM (see Figure 21, obtained by David Anderson at University of Canterbury, 200 keV TEM)). The average particle size of the Au_{55} cluster was identified (by David Anderson) to be between 1.3-1.6 nm, however, the larger particle size was observed due to sintering of the nanoparticles. The Au_{11} cluster was characterized by X-ray crystallography (obtained by David Anderson, see Figure 22).

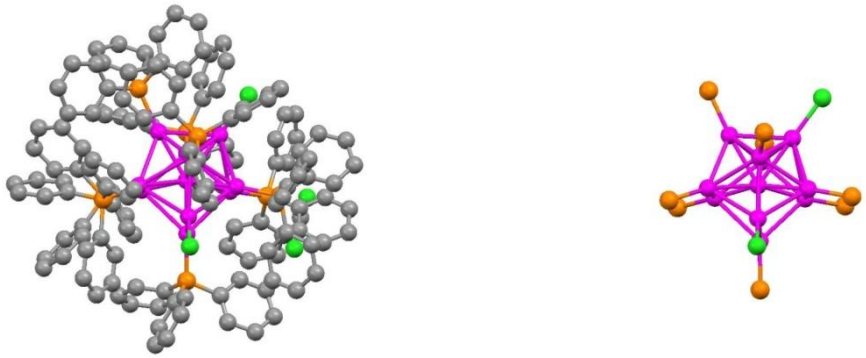

Figure 22: The molecular structure of the Au_{11} cluster (obtained by Davis Anderson using X-ray crystallography)

The catalysts Au/TiO_2 were prepared by David Anderson via the post-synthetic impregnation (deposition) method[19] with 1% and 0.3% loadings by weight for each type of the Au clusters (Au_{55} and Au_{11}). The TEM images of these catalysts are not available at this point.

2.3.2. TiO_2/SiO_2

In this study, the silica gel (SiO_2) support was introduced to the system to provide a means of immobilizing TiO_2 nanoparticles. This was done to minimize the chances of exposure to individual truly small "custom-made" TiO_2 nanoparticles. It is expected that direct contact with TiO_2 through handling or inhalation can be avoided. For reference, the P25-TiO_2/SiO_2 catalyst was also prepared.

The photocatalytic properties of TiO_2 were expected to be preserved because SiO_2 has excellent thermal and mechanical stability, although some studies in the literature[73,74,75] indicate that SiO_2-supported TiO_2 may demonstrate different photocatalytic performance from that of TiO_2 itself. This will be addressed further in Chapter 4.

TiO_2/SiO_2 catalysts were synthesized in 1% and 3% loadings. Here, the loadings refer to the percentage (by mass) of TiO_2. The characterization of these catalysts is not finished at this point.

2.3.3. $Au/TiO_2/SiO_2$

$Au/TiO_2/SiO_2$ catalysts were synthesized in 1%/3% and 1%/10% loadings. Here, the first figure (1%) refers to the percentage of the gold in the TiO_2-Au system (by mass, counting only the gold core of the cluster), while the second figure (3% or 10%) refers to the percentage of the overall catalyst (by mass) that is TiO_2-Au which was supported on SiO_2. Only Au_{55} was used for these studies. The Au_{55} was synthesized (by David Anderson) as described in Section 5.1.3 and immobilized on either P25-TiO_2 or e-TiO_2 supports. For reference, Au/SiO_2 was also prepared to confirm the importance of TiO_2 in this study.

Chapter 3 – Establishment of Experimental Methodology

The preliminary experiments reported in this chapter were designed to establish standardized techniques for reliable analysis of future experiments. In particular, these experiments focused on:

1. Characterization and measurement of dye solutions by UV-Vis spectroscopy: the effects of concentration, calibration curve, dye stability, reproducibility, errors of measurements, baseline correction, and glassware contamination effect on degradation.
2. Experimental methodology: the effect of temperature, sequence of addition of reagent, exposure to light *vs.* experiments in the dark, sampling method, and quenching agents.

All experiments were carried out with one repetition, and a delta (Δ) value (i.e. the difference between average and each individual measurement) is given to reflect the error bars between two measurements.

All catalytic reactions carried out in the preliminary study used commercial "Aeroxide" TiO_2 Degussa P25 as the catalyst.

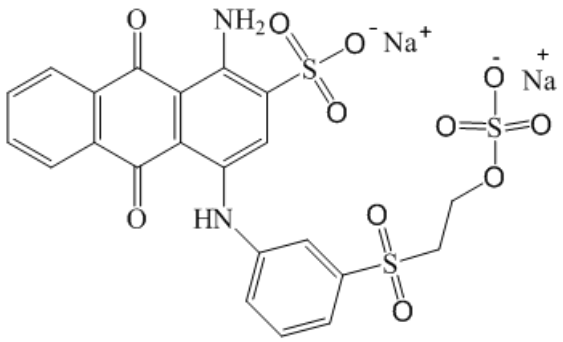

Figure 23: Chemical structure of CI Reactive Blue 19 (FW 626.54 g/mol)

CI Reactive Blue 19 (RB19) was selected as a representative industrial dye. As shown by its chemical structure (Figure 23), the dye is an anthraquinone derivative, which is a commercially valuable bright blue reactive dye in its own right.[24] The dye RB19 is used to dye and print on materials made from cellulosic fibres. It is soluble in water and has excellent fastness to washing because of the strong covalent bonds it forms with the fibres. Repeated measurements of the RB19 solution (five times) by UV-Vis spectroscopy indicated that the average maximum absorption wavelength of the dye falls at (594.00 ±1.26) nm. An example absorption spectrum is presented in Figure 24.

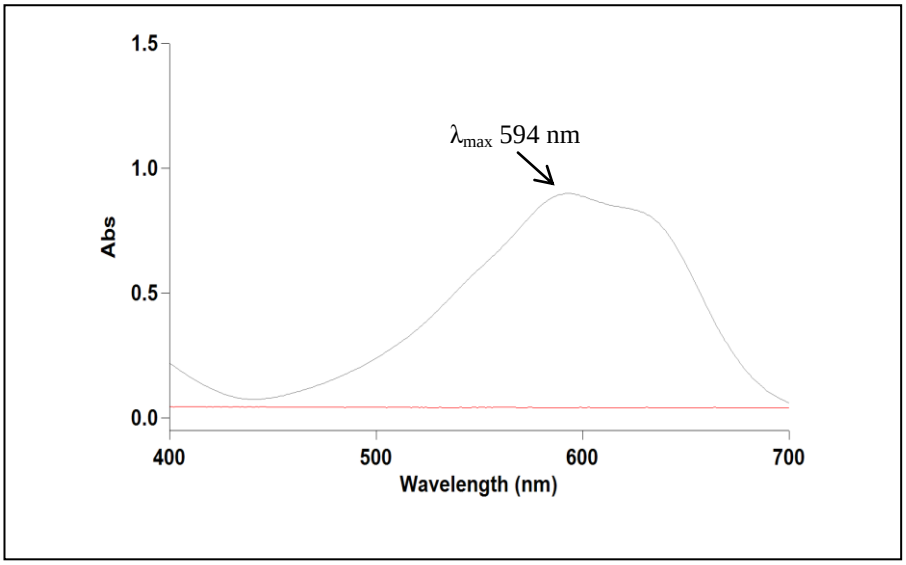

Figure 24: Absorption spectrum of CI Reactive Blue 19 in the visible light region

3.1 Characterization of dye solutions using UV-Visible spectrophotometry

In the visible spectral region, the interaction between matter and electromagnetic radiation shows itself as colour. UV-Visible spectroscopy, therefore, lends itself well to the study of dyes and dye degradation. The relationship between light absorbance and dye concentration is governed by the Bouguer-Lambert-Beer Law shown by *Scheme 5*.[76]

Scheme 5: *The Bouguer-Lambert-Beer Law*

$$\boldsymbol{Log}(\frac{Io}{I})_{\tilde{\upsilon}} = \boldsymbol{Log}\left(\frac{\mathbf{100}}{T(\%)}\right)_{\tilde{\upsilon}} \equiv \boldsymbol{A_{\tilde{\upsilon}}} = \boldsymbol{\varepsilon_{\tilde{\upsilon}}} \boldsymbol{.c.d} \qquad \text{(Eq. 21)}$$

Where; $A_{\tilde{\upsilon}} = Log(\frac{Io}{I})_{\tilde{\upsilon}}$ is the *absorbance*, $T_{\tilde{\upsilon}} = \frac{I}{I_0}$. 100 in % is the *transmittance*, and $\varepsilon_{\tilde{\upsilon}}$ is the *molar decadic extinction coefficient*.

Io and *I* are the intensity of the monochromatic light entering the sample and emerging from the sample respectively; *c* is the concentration of the light-absorbing substance and *d* is the path length of the sample in cm. The functional correlation between intensity and wave number $\tilde{\upsilon}$ is called the "absorption spectrum of a compound".

3.1.1 Dye Concentration, Stability and Reproducibility for Measurement

One limitation of the Bouguer-Lambert-Beer Law is that it only applies to dilute solutions.[76] In these cases, the extinction coefficient ε is independent of the concentration of a substance at the given wave number υ (wavelength λ); in concentrated solutions, ε varies depending on the refractive index of the solution. Due to the limitations imposed by this law, preliminary UV-Vis spectroscopy was performed on solutions of varying concentrations to determine the domain in which ε is constant.

RB19 dye solutions were prepared in two "sets" – the first (A-H) with concentrations ranging between 0.1 g/L (0.16×10^3 mol/L) and 1 g/L (1.60×10^3 mol/L) and the second (I-Q) with concentrations ranging between 0.01 g/L (0.016×10^3 mol/L) and 0.1 g/L (0.16×10^3 mol/L). These dye solutions were then analyzed using a Cary 100 Bio UV-Vis Spectrophotometer. All measurements were taken at the dye's maximum absorbance wavelength of 594.00 nm.

Dye solutions in the series A-H were measured three times – twice immediately after preparation (A_1 and A_2) and once after standing for five hours at room temperature (A_3). Dye solutions in the series I-Q were only measured twice – once immediately after preparation (A_1) and once after standing at room temperature for five hours (A_2). The results of the second and third measurements of these solutions (A-H) showed that the absorbance did not change appreciably over time (< 1% change over 5 hours).

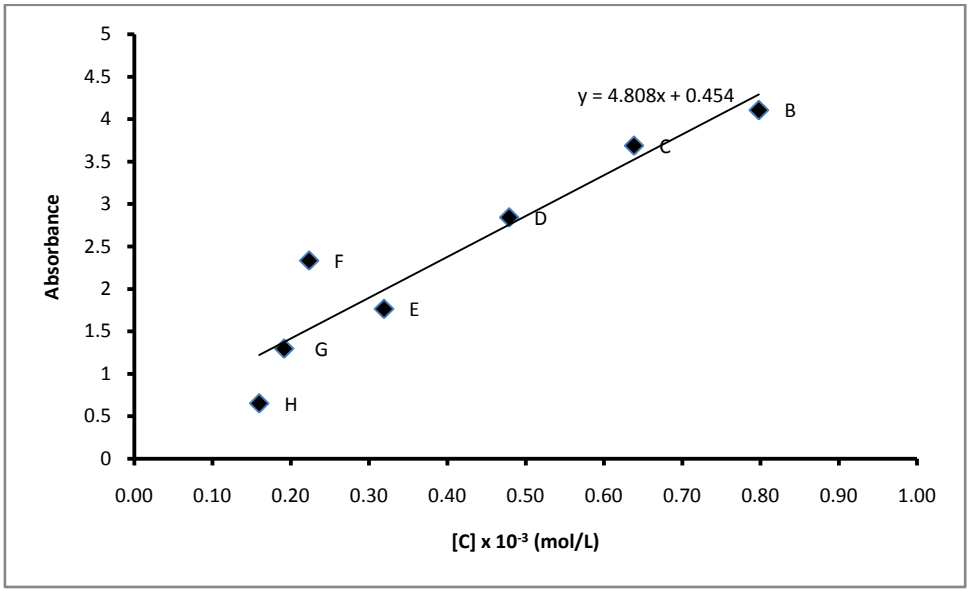

Note: A is missing from this plot (read the following paragraph for explanation)

Figure 25: The non-linearity of concentration v.s. absorbance of CI Reactive Blue 19 (N = 2, errors were reported as Δ)

As shown in Figure 25, at concentration of 1 g/L (1.60×10^3 mol.L^{-1}) (sample A), the solution meets its saturation point. At this point, all light passing through the sample at this wavelength is absorbed, and the actual absorbance cannot be properly measured, and therefore, the sample A is missing from the plot.

At lower concentrations (samples B to H), the absorption spectrum can be detected, but for all samples except H we find that absorbance (Abs) > 1, with inconstant molar absorptivity values (ε). An absorbance of 1 indicates that 90% of the light at this particular wavelength has been absorbed, at which point the extinction coefficient of the substances is believed to be inconsistent.[76] This is shown

by the non-linear relationship between concentration and absorbance for samples B to H on the graph (see Figure 25). The calculated molar absorptivity (ε = extinction coefficient) of these solutions are inconstant, ranging between 0.4×10^4 L/mol.cm and 1.0×10^4 L/mol.cm.

According to the Bouguer-Lambert-Beer Law described earlier, it is important that the absorbance of our samples be in the range 0 < Abs < 1. Therefore, the concentration of dye employed in samples A through H is generally too high for accurate analysis.

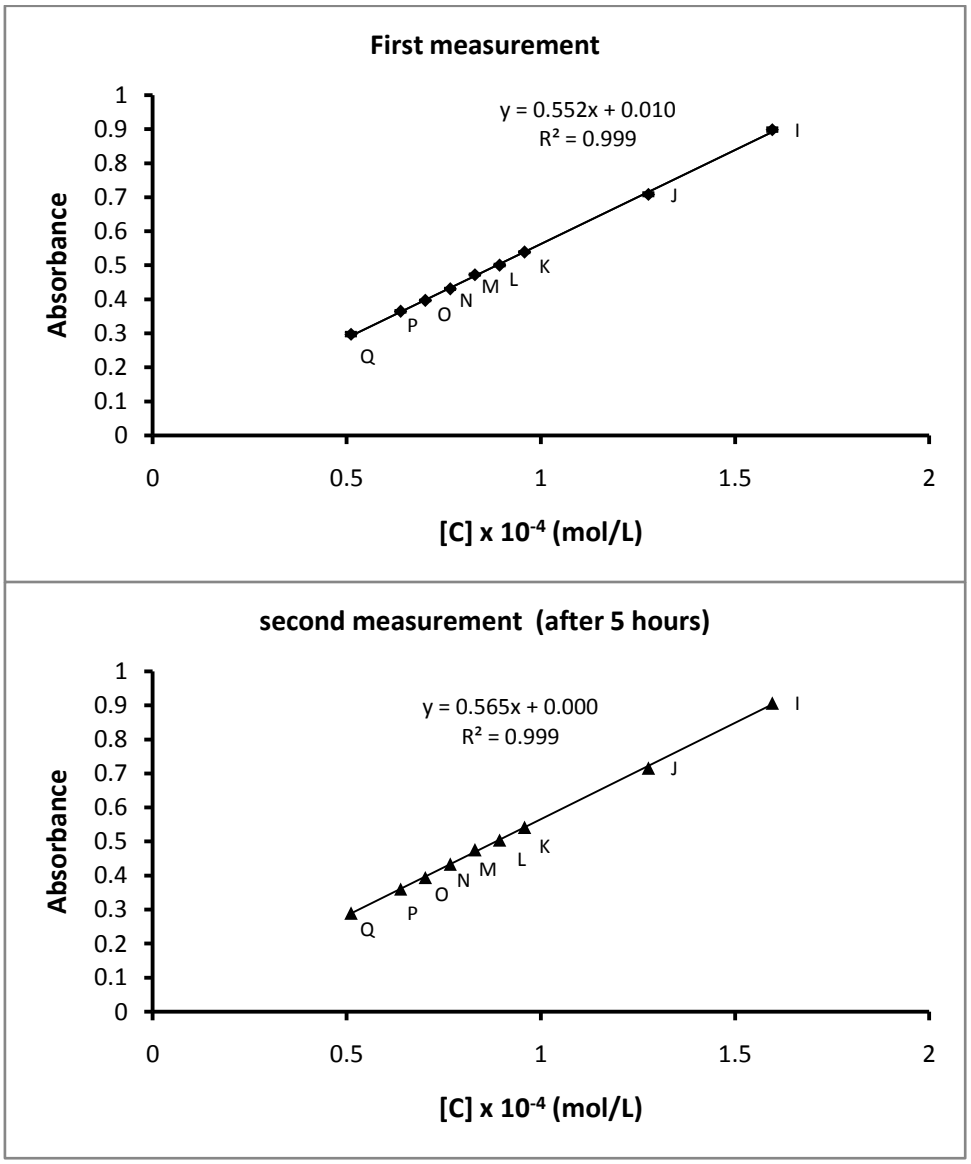

Figure 26: Plots of Calibration (concentration vs. absorbance) of CI Reactive Dye 19 (N = 2, errors are reported as Δ)

Further analysis of RB19 solutions with lower concentrations than those shown in Figure 25 was carried out. These results show that Abs (absorbance) varies between 0 and 1 for this concentration regime (see Figure 26), as desired. The relationship between concentration and absorbance in this range is linear (see Figure 26), which indicates that the Bouguer-Lambert-Beer Law applies and that ε is constant over this range. Calculated ε values of dye solutions at these concentrations remain stable in 0.6×10^4 L/mol.cm.

From this data it was decided that [C] = 0.1 g/L should be used as an initial concentration for all dye solutions used in this study. At this point the initial absorbance would be approximately 0.9: low enough that ε should remain constant as the dye degraded, but high enough that accurate results could be obtained from dye degradation studies.

All errors between measurements were reported to be less than 3% with standard deviations less than 0.1. This suggests that the 5 hour delay between measurements does not significantly affect the results (see the identical graphs of the two measurement results in Figure 26). The fact that $R^2 = 0.99$ is good, but the slope is slightly different (small in %). This indicates that the dye is relatively stable in water. To confirm the reproducibility of these results, a pure dye solution was kept at room temperature for five hours and samples of it measured every hour. These samples appeared to have the same absorbance, with a standard deviation of 4.72×10^{-4} over the range of measurements.

To demonstrate that the UV-Visible apparatus used in our experiments is stable and precise, two dye solutions with 0.16% difference in “as made” concentrations (0.10080 g/L and 0.10064 g/L) were measured by UV-Visible spectroscopy. The difference in absorbance values between the two dyes was reported to be 1.36%. The difference in absorbance (Abs) is significantly greater than the difference (in %) in concentration (g/L). This is possibly due to a standard systematic error.

3.1.2 Baseline correction and impurities

The presence of hydrogen peroxide, which has been used as an oxidizing agent to increase the rate of dye decomposition in some reactions,[62] is another factor that could potentially affect the stability of measurement. Therefore, the comparison between hydrogen peroxide-containing and water-only baselines was taken in every measurement of RB19 containing H_2O_2.

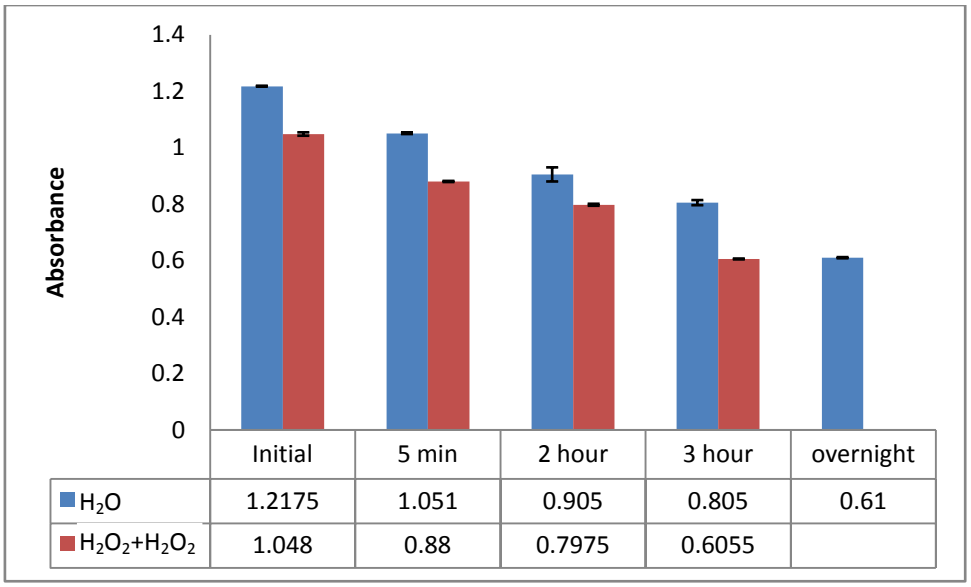

Figure 27: UV-Vis measurement results of RB19 containing H_2O_2 with different baseline corrections (water only and H_2O_2-containing water)
(N = 2, errors are reported as Δ)

Figure 27 represents the UV-Vis measurement results of the RB19 over the time with the two baseline corrections. Here, H_2O_2 was added into the RB19 solution under the constant stirring. Samples were taken as initial (before the addition of H_2O_2), after 5 minutes, 2 hour, 3 hour, and overnight. The errors between measurements with different baseline corrections vary between 0.1% and 0.7%, which is negligible. The results of repeated measurements based on these two different baselines are also essentially identical; with error in every single measurement never more than 0.8%. This is understandable because measurement of the dye solution focuses on the 400-700 nm range and, like water and other organic solvents such as n-heptane or trifluoroethanol, H_2O_2 (with density of 1.110 g/cm^3) is also transparent from ca. 180 nm in the UV-Vis spectral region.[76]

Finally, it is possible that impurities (e.g. from a dirty UV cuvette) may also affect the accuracy of measurements. In order to prevent this, a cleaning method involving detergent and sonication was developed to examine its effect on the elimination of error. However, it was found that this method did not decrease errors as compared to a less rigorous washing routine. It was found that the measurements using either "washed" or "unwashed" cells resulted in the identical values with 0.7% error, so whether the cuvette is rigorously washed or not does not particularly matter.

3.2 Experimental methodology

This section presents the results of TiO_2-catalyzed dye degradation reactions using various different parameters, including the effect of temperature, the presence of oxidant, sequence of reagent addition, exposure to light *vs*. experiments in dark, sampling method and quenching agents. To clarify the terminology in this context, the term "catalytic reaction" refers to any reactions performed in the dark, while all reactions under UV irradiation are termed "photocatalytic reactions". Reaction in the dark had been carried out to elucidate potential for catalytic degradation of dyes by catalysts (TiO_2 and Au/TiO_2) in presence of air/H_2O_2. In order to find a set of standard conditions at which to fix these parameters, a series of preliminary experiments were carried out.

3.2.1 Catalytic reaction

Before starting on photocatalytic reactions (which require special equipment to provide UV irradiation), experiments were performed in the dark. Hydrogen peroxide was used as an environmentally-friendly oxidant as it decomposes to form water and oxygen.[77] Initial reaction conditions were based on the conditions of catalytic oxidation used in the literature for heterogeneous catalysts such as iron oxide[78] and activated carbon:[79] to the best of our knowledge no such studies exist that use TiO_2 as a catalyst for dye degradation in the absence of light.

Table 7: UV-VIS Spectroscopy measurement results (at λ_{max} of 594.00 nm) of catalytic reactions at room temperature (N = 2, errors are reported as Δ)

Time progress (min)	Catalytic reactions			
	"All-in"		*"Step by step"*	
	Absorbance	**% decrease**	**Absorbance**	**% decrease**
	After addition of all reagents		Before addition of H_2O_2	
1			1.151	0.00%
31			1.135	1.37%
61			1.136	1.30%
91			1.131	1.74%
121			1.153	-0.20%
			After addition of H_2O_2	
4	0.488	0.00%	N/A	N/A
60	0.697	-42.92%	0.995	13.52%
120	0.840	-72.24%	0.975	15.27%
180	0.850	-74.34%	0.976	15.22%
Over-night	0.482	**1.14%**	0.854	**25.81%**

All "dark" catalytic reactions were then carried out at room temperature, with parallel reactions performed at 70°C for comparison. All experiments were performed in a three-neck glass round-bottom flask covered in aluminium foil, with continuous stirring (400 rpm), under a constant flow of nitrogen gas (N_2). For the reactions performed at 70°C, the system was connected to a double-jacketed condenser, and silicone oil was used as a heating medium. Detailed conditions and procedures of the experiments are presented in Chapter 5.

For reactions at room temperature, the reagents were introduced to the reactor in the following sequences:

1. "*All-in*": all reagents (dye solution, TiO_2 catalyst, and H_2O_2) were mixed together at the beginning of reaction.
2. "*Step-by-step*": dye solution and TiO_2 powder were mixed first until the adsorption equilibrium was reached. H_2O_2 was then added.

Blank reactions were performed for the dye solution and catalyst only (blank 1) as well as the dye solution and oxidant only (blank 2).

Table 8: UV-VIS Spectroscopy measurement results (at λ_{max} of 594.00 nm) of blank reactions at room temperature (N = 2, errors are reported as Δ)

Time progress (min)	**Blank 1 (RB19 + TiO_2)**		**Blank 2 (RB19 + H_2O_2)**	
	Absorbance	**% decrease**	**Absorbance**	**% decrease**
	Before addition of TiO_2		Before addition of H_2O_2	
1	1.120	0.00%	1.117	0.00%
31	1.142	-1.92%	1.136	-1.69%
	After addition of TiO_2		After addition of H_2O_2	
4	1.133	-1.12%	1.004	10.10%
60	1.131	-0.94%	0.997	10.71%
90	1.127	-0.56%	0.986	11.76%
120	1.125	-0.44%	0.985	11.80%
180	1.128	-0.72%	0.985	11.82%
210	1.131	-0.92%	0.985	11.85%
240	1.136	-1.43%	0.984	11.91%
300	1.143	-2.03%	0.983	11.97%
Over-night	1.086	**3.02%**	0.926	**17.07%**

The UV-Visible spectroscopy data presented in Table 7 demonstrates that complete dye degradation did not occur after running the catalytic reactions with either "*all-in*" or "*step-by-step*" methods. Repetition of the same reactions with both methods gave identical results that the total decrease in absorbance never reached more than 25% after running them overnight. Reaction with the "*step-by-step*" method always resulted in a higher decrease in absorbance than that of the "*all-in*" method.

Similarly, no appreciable colour removal was observed in the case of blank reactions (see Table 8). Repetition of these reactions demonstrated that catalytic reactions containing both catalyst and oxidant always gave a higher decrease in absorbance (but never higher than 25% in 24 hours) than reactions with either catalyst only or oxidant only. This suggests that both catalyst and oxidant

contribute to colour removal through a combination of adsorption and catalytic degradation,[79] but only in the long term, i.e. it takes overnight to get a 25% decrease, compared with the reaction with light that takes a few minutes (see the following section on photocatalytic reaction in this chapter).

3.2.1.1 Adsorption of the RB19 on the P25-TiO_2

The results presented in Table 8 demonstrate that H_2O_2 contributes more to the dye colour removal than the TiO_2 catalyst in the absence of UV light. This suggests that very little colour removal is due to dye adsorption on the P25-TiO_2 surface. To examine the adsorption ability of the P25-TiO_2, a series of experiments was carried out by mixing the catalyst with the RB19 solution at three different concentrations (0.1, 0.08 and 0.06 g/L). The suspensions were constantly stirred at room temperature in dark conditions. Samples were taken and measured 5 minutes after mixing, 1 hour after mixing, and every 30 minutes thereafter. Absorbance of the dye solution without P25-TiO_2 added (t = 0) was also measured.

Figure 28 shows that the absorbance of the dye solution over the five hour period was relatively constant, with the maximum difference between measurements being 0.034. Standard deviations of the given absorbance from the three different concentrations, 0.1g/L, 0.08g/L, and 0.06g/L, are 2.6×10^{-3}, 2.8×10^{-3}, and 2.6×10^{-3} g/L respectively. This data suggests that there was no significant adsorption of RB19 on the surface of P25-TiO_2 observed over 300 minutes, unless the adsorption was instantaneous. The t = 0 reading of the dye solution (without P25-TiO_2) showed that compared to that of the t = 5 minutes, the decrease in absorbance was only 0.07% (from 1.134 to 1.133). This result disagrees with those reported by Lachheb *et al.*[80] that the equilibrium state of adsorption of any dyes with any initial concentrations will occur within 1 hour. Figure 29 shows that the TiO_2 catalyst, when separated from solution by centrifugation, is still white. This suggests no significant amount of dye adsorption on the surface of the TiO_2.

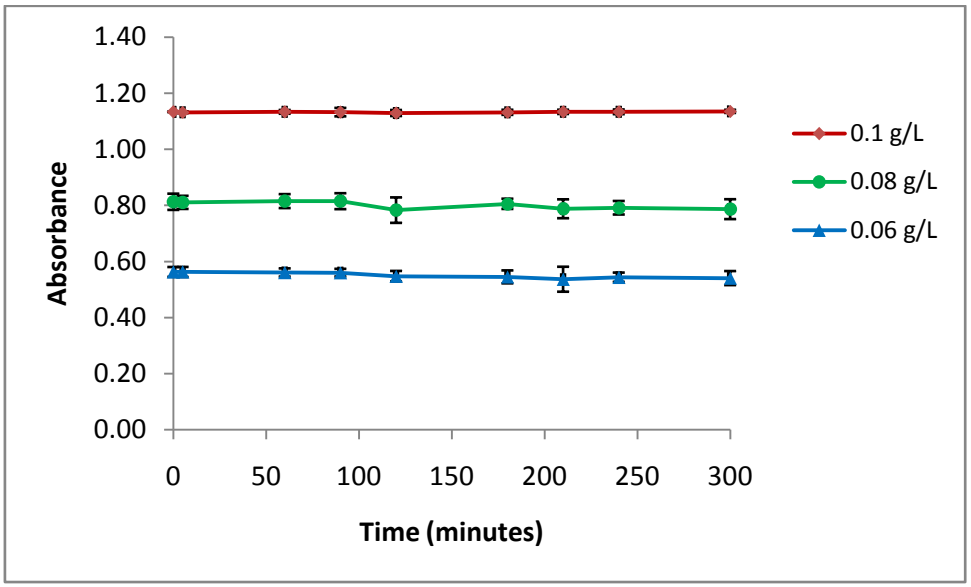

Figure 28: Adsorption profile – in absorbance - of RB19 onto P25-TiO_2

(N = 2, errors are reported as Δ)

Figure 29: Visual appearance of the catalyst after centrifugation (no changes in colour)

Calculation of the estimated total surface area of RB19 indicates that the P25-TiO_2 catalyst has a ≈19 times less surface area than RB19 (0.1 g/L) in the suspension. The surface area of RB19 was calculated using Connoly's analytical algorithms, computing second- and third- order atomic spheres overlaps,[81] with a kind help of Anthony Barros, a visiting student in the Golovko group. The mean of the surface area of one RB19 molecule from 94 conformers applied to the mentioned software was known to be 0.491 x 10^{17} m^2, while the specific surface area of P25-TiO_2 is 50 m^2/g (see Table 6). Detailed calculation is presented in Table 9.

Table 9: Calculation of the surface area of RB19 and P25-TiO_2

RB19	**P25-TiO_2**
Mean of surface area/molecule (from 94 conformers): 0.491 x 10^{17} m^2 Concentration in the solution: 0.1 g/L = 0.16 mmol/L (0.008 mmol in 50 mL solution) Number of molecules in the system: 48.176×10^{17} molecules <u>Total surface area in the system of</u>: 0.1 g/L : 23.66 m^2 0.08 g/L: 18.93 m^2 0.06 g/L: 14.20 m^2	Specific surface area: 50±15 m^2/g Amount in the system: 0.025 g <u>Total surface area in the system</u>: 1.25 m^2

3.2.1.2 Catalytic hydrogen peroxide decomposition

The data presented in Tables 8 and 9, as well as Figure 29, imply that the role of P25-TiO_2 in colour removal is mainly due to its catalytic ability rather than through adsorption of the dye on the catalyst surface. The presence of catalyst may also promote the formation of reactive free radicals from hydrogen peroxide.[82]

Han *et al*.[83] reported that the decomposition of organic compounds through a peroxide oxidation takes place following the mechanism described in *Scheme 6*. In the first step, H_2O_2 is activated to produce ·OH radicals that can oxidize organic compounds (see Eqs. 23 and 24). Next, molecular oxygen is formed through the recombination of ·OH radicals and the subsequent oxidation of organic compounds occurs in the presence of the resulting O_2. Miller *et al.*[82] reported that decomposition of H_2O_2 could to potentially produce several types of free radicals, including hydroxyl (·OH),

perhydroxyl ($HO_2\cdot$), and superoxide ($O_2^{\cdot-}$) groups, but ·OH is believed[82] to be the most reactive species for degradation of organic compounds (including dyes).

Scheme 6: *Possible mechanism of hydrogen peroxide decomposition*[83]

$$H_2O_2 \xrightarrow{\text{catalyst/ T}} 2\ \cdot OH \qquad \text{(Eq. 22)}$$

$$\cdot OH + \text{organic compounds} \xrightarrow{T} CO_2 + H_2O_2 \qquad \text{(Eq. 23)}$$

$$2\ \cdot OH \xrightarrow{T} 1/2O_2 + H_2O \qquad \text{(Eq. 24)}$$

$$O_2 + \text{organic compounds} \xrightarrow{T / P} CO_2 + H_2O \qquad \text{(Eq. 25)}$$

The reactions shown in Eqs. 23 and 24 indicate that the rate of decomposition of organic compounds is mainly dependent upon temperature and the hydroxyl radical concentration, which is controlled by the concentration of H_2O_2. To confirm this assumption, reactions at higher temperature were carried out in our study.

Catalytic reactions at 70°C were performed using the "*step-by-step*" method: dye solution and TiO_2 powder were mixed together for *ca*. 30 minute before heating. Once the solution had equilibrated at 70°C, H_2O_2 was added. Two different blank reactions, one with dye solution and catalyst only (blank 1), and one with dye solution and oxidant only (blank 2), were employed. These blank reactions were set up to be comparable to the main catalytic reaction, and therefore, in blank 1, the catalyst was mixed together with the dye solution at the beginning of reaction, while in blank 2, the oxidant was added to the dye solution after the temperature had equilibrated at 70°C.

Table 10: UV-VIS Spectroscopy measurement results (at λmax of 594.00 nm) of catalytic reactions at 70°C (N = 2, errors are reported as Δ)

Time Progress (minute)	Blank 1 ($RB19 + TiO_2$)		Blank 2 ($RB19 + H_2O_2$)		Catalytic reaction ($RB19 + TiO_2 + H_2O_2$)	
	absorbance	**decrease**	**absorbance**	**decrease**	**absorbance**	**decrease**
	Before heating (dye solution + TiO_2)		*Before heating* (dye solution only)		*Before heating* (dye solution + TiO_2)	
1	1.129	0.00%	1.050	0.00%	1.014	0.00%
31	1.117	1.01%	1.067	-1.57%	1.049	-3.46%
	After heating		*After heating*		*After heating*	
5	1.153	-2.18%	1.058	-0.75%	1.050	-2.76%
30	1.155	-2.31%	1.057**	-0.65%	1.042#	-2.77%
60	1.209*	-7.17%	1.062**	-1.11%	0.742#	26.80%
90	1.210*	-7.22%	0.974**	7.29%	0.696#)	31.38%
120	1.213*	-7.49%	0.966**)	8.04%	0.669#)	33.97%
180	1.159*	-2.66%	0.882**)	16.03%	0.568#)	43.92%
Over-night	1.016*	**9.94%**	0.796**)	**24.17%**	0.020#)	**98.02%**
Note	*temperature has been stable at 70°C		** temperature has been stable at 70°C **) H_2O_2 has been added		# temperature has been stable at 70°C #) H_2O_2 has been added	

The data presented in Table 10 demonstrates that complete dye degradation (98.02% decreases in absorbance) is achieved by the catalytic reaction at 70°C in the presence of H_2O_2 over 24 hours. The results at 70°C show considerably higher activity compared to equivalent reactions performed at room temperature, which only reached 25% decrease in absorbance (see Table 10). In contrast, 25% dye removal was achieved within the first hour of catalytic degradation at 70°C, which confirms that elevated temperature can improve the rate of dye degradation.

The results of the two blank reactions also demonstrate that, in the presence of either only catalyst or only oxidant, dyes are not degraded as efficiently as in the presence of both a catalyst and an oxidant. This suggests that degradation occurs due to the presence of both P25-TiO_2 as a catalyst and H_2O_2 as an oxidizing agent, confirming the mechanism discussed earlier in this section.

3.2.2 Photocatalytic reaction

It should be noted that complete dye degradation, even under the best conditions without exposure to light examined in the study presented in 3.2.1 above, requires a considerable amount of time (*ca*. 24 hours). Several studies have indicated that to obtain the same results without irradiation within a shorter reaction time, higher temperatures and/or pressures are required (150-350^{o}C, 6-17 MPa).[78] Therefore, TiO_2-assisted photocatalytic dye degradation is believed to be a promising alternative due to its ability to remove the dye in a much shorter time frame and at lower temperature.

The photocatalytic chamber used in these studies was designed and constructed in the Golovko group laboratory by the Electrical and Mechanical Workshop at the Department of Chemistry of the University of Canterbury. The chamber consists of:

- a UV light source (500W Xe lamp, $\lambda \leq 380$nm) to allow constant irradiation during the reaction
- a room for the photocatalytic reaction to run with continuous stirring. The reactor's position is fixed, so that the distance between light source and reactor is constant.
- a photometer ["International Light Technologies" (ILT 1700)] to monitor the intensity of light radiated during the reaction, with SED033 detectors, 33 mm^2 silicone detectors for xenon flash lamp (QNDS2 type for spectral range of 326-401 nm and Y/W type for spectral range of 400-700 nm).

The reactor is a quartz tube designed specifically for photocatalytic reactions, which also allows the collection of samples during the reaction. All samples have been ultra-sonicated before the reaction to ensure that the catalyst is well-dispersed, and all solutions have been stirred during the reaction to ensure uniformity of the suspension.

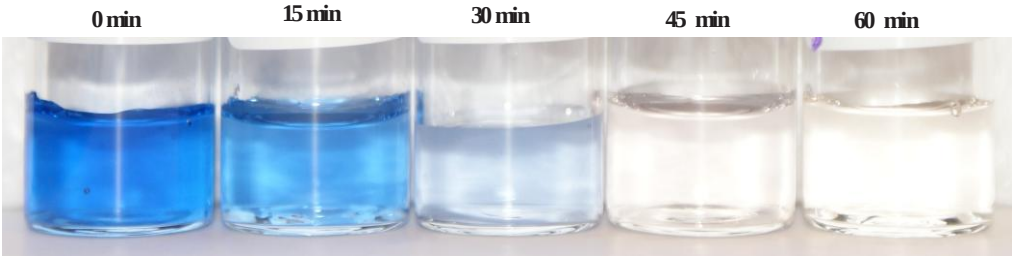

Figure 30: Visual appearance of RB19 solution over the TiO_2-mediated photocatalytic degradation

To check the capability of this equipment, a preliminary TiO_2-mediated photocatalytic reaction was carried out on RB19 solution in the presence of hydrogen peroxide at room temperature. The chemical composition of the system was similar to that of previous catalytic reactions (total of 1.0 g/L P25-TiO_2 and 1.25g/L H_2O_2 in 100 mL of 0.1g/L RB19 solution). An appropriate amount of P25-TiO_2 was added to the RB19 solution, and the suspension was ultrasonicated for 10 minutes. H_2O_2 solution was then added and UV irradiation started. Samples were taken every 15 minutes, and, in 1 hour, all colour had been removed from the solution (see Figure 30). For this reaction, 98% dye removal was achieved in 60 minutes. This is an extremely significant improvement over the catalytic reaction at 70^{o}C.

3.2.2.1 Experimental method

Several different experimental methods were trialled for the photocatalytic reaction, as listed below:

1. Method A (pre-activation): in this method, P25-TiO_2 and H_2O_2 were combined with constant stirring under UV irradiation for 30 minutes, in an attempt to pre–activate the catalyst. The dye solution was then injected into the reactor without stopping UV radiation.
2. Method B (all-in): all reagents were mixed together from the beginning and then immediately subjected to UV irradiation.
3. Method C (adsorption): the catalyst and dye solution were combined, and then left in the dark under constant stirring for 30 minutes to allow any possible adsorption. H_2O_2 was then added and UV irradiation started.

Two blank reactions of dye solutions containing either only a catalyst or only an oxidant under UV radiation have been performed. The composition of reagents used in these reactions was similar to the conditions described above. The detailed procedure for these reactions is presented in Chapter 5.

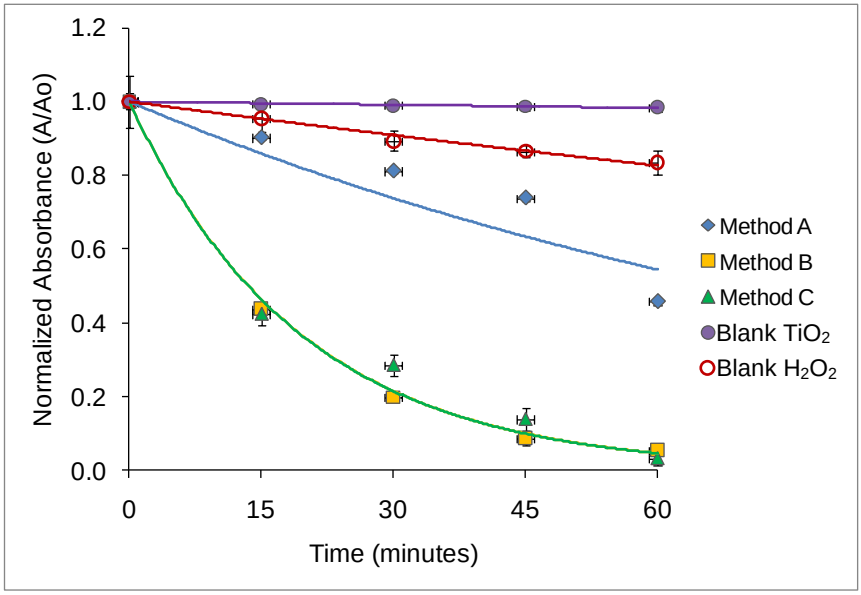

Figure 31: Normalized absorbance *vs.* time on P25-TiO_2-mediated photocatalytic reactions for RB19 with various methods (N = 2, errors are reported as Δ)

Figure 31 presents the plot of normalized absorbance against time for the P25-TiO_2-mediated photocatalytic reaction of RB19 with various methods. The data is presented in normalized absorbance (Abs/Abs_0) to control the difference in initial absorbance caused by standard measurement error and to compare the rate of degradation of the three methods in term of time required from the same point of initial absorbance. The kinetics were also analysed was also done for all photocatalytic reaction with these methods. The fitted curves are shown in Figure 32. Table 11 presents the average rate constants of the reaction with these methods.

It should be noted that the zero minute of method A was determined after the injection of dye solution to the system, i.e. 30 minutes after catalyst pre-activation, thus, the total time required to achieve such a decrease shown in the graphs was actually 120 minutes.

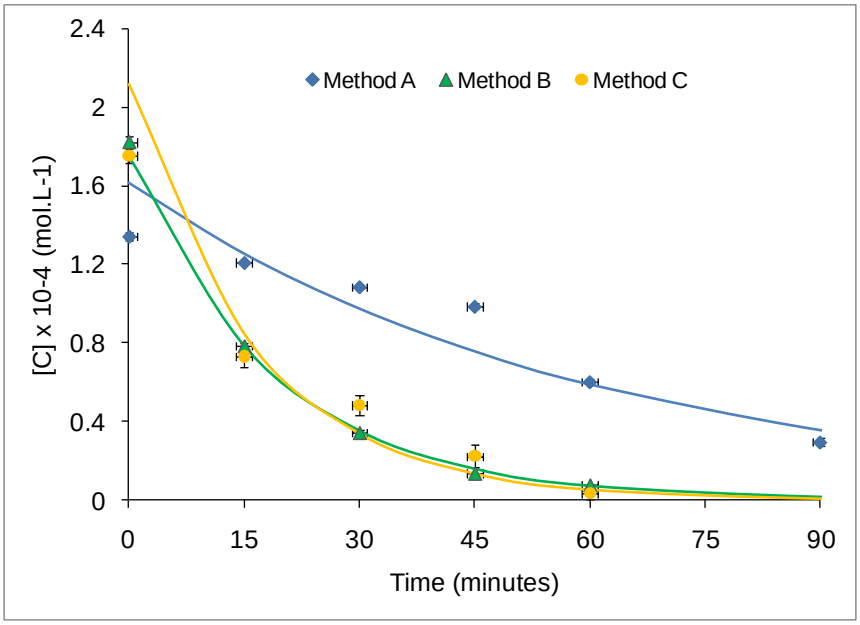

Note: marker data points show the real concentrations, while the lines show the fitted concentration

Figure 32: Kinetics profile of P25-TiO_2-mediated photocatalysis for RB19 with different methods (N = 2, errors are reported as Δ)

It can be seen from the graphs in Figure 31 and 32 that method A (in which TiO_2 is pre-activated under UV irradiation) exhibits a slower rate of dye degradation than the other methods: 78.45% decrease in absorbance was achieved in 120 minutes. This is possibly due to what is known as the "scavenging effect".[83] In the presence of a catalyst and UV light, H_2O_2 can decompose to form reactive radicals as previously discussed (see Scheme 5). At the same time, TiO_2 will produce excited electron-hole pairs upon exposure to UV light, and these electron-hole pairs may proceed to form further reactive radicals (see Schemes 1 and 2). In this case, the hydroxyl radicals decomposed from H_2O_2 can inhibit electron-hole recombination, but can also undergo self-recombination as a competitive reaction (see Scheme 6), and consequently decreases the total amount of radicals available for dye degradation.[83] Therefore, if the dye solution is injected after 30 minutes of pre-activation, the amount of reactive intermediates capable for dye degradation is lower than it would be otherwise. The mechanism of these reactions is detailed later in this chapter in Scheme 6.

Another reason for lack of activity on pre-activated TiO_2 may be the proximity of radicals to the TiO_2 surface. Hydroxyl radicals which form on the TiO_2 surface will obviously end up in close proximity to

the TiO_2,[83] which may encourage scavenging by the catalyst. After the dye is injected into the system, a period of time is required to reach the catalyst surface. Thus, it is understandable that method A gives a slower degradation rate. Moreover, H_2O_2 can adsorb on the TiO_2 and change its surface characteristics that consequently decreases the catalyst activity.[84]

Conversely, methods B and C exhibit similar photocatalytic activity, both higher than method A: in 60 minutes, 95.78% and 98.69% decreases in absorbance were achieved by methods B and C respectively. These results indicate that allowing adsorption before UV radiation does not alter the rate of dye degradation significantly. This agrees with the results obtained from the adsorption study of RB19 on P25-TiO_2 carried out in the previous experiments (see section 3.2.1.1).

The two blank reactions showed a minor decrease in absorbance: in 120 minutes the blank TiO_2 and blank H_2O_2 attained 9.88% and 25.32% dye removal respectively. Again, this suggests that participation of both catalyst and oxidant are important for dye degradation.

Table 11: Average rate constants of photocatalytic reaction with various methods (errors are reported as Δ)

Photocatalytic reaction	Average rate constant (mol/L/s)
Method A	$3.79 \times 10^{-4} \pm 2.89 \times 10^{-4}$
Method B	$8.92 \times 10^{-4} \pm 0.40 \times 10^{-4}$
Method C	$10.16 \times 10^{-4} \pm 2.44 \times 10^{-4}$

The kinetics profile of photocatalytic reactions with these methods presented in Figure 32 shows that method B demonstrates the most reliable kinetics (very well-fitting with the first order character). By method C, the dye degradation was slightly faster than method B, however this method is not well fitted with the first order character: the fitted curve gives a very high intercept (initial concentration), thus the curve is not included in the graph. The relationship between ln[C] *v.s.* t of these methods can be seen in Appendix 1.

3.2.2.2 The effect of catalyst loading and oxidant

It is reported[30,85,86] that catalyst loading will directly affect the rate of dye degradation only up to a certain point; above this point, the rate will plateau and may even decrease. This is hypothetically because of the decrease in the number of active radicals produced by TiO_2 photoexcitation.[62] It seems obvious that the more catalyst is present in the system, the higher the number of active sites available for photodegradation. However, above the optimum concentration, the excess catalyst can inhibit illumination of the sample due to catalyst agglomeration, which effectively reduces the available surface area. Consequently, the degradation rate will decrease. The other possible cause of the reduced photocatalytic degradation rate is absorption of scattered light by the excess of catalyst, which then could increase the optical density in the active site of the catalyst.[87]

Akpan and Hameed[62] reported in their review that based on previous studies on UV-photocatalysis, the optimum catalyst loading varies between 1.5 and 12.5 g/L, while Konstantinou and Albanis[30] observed that the optimum catalyst concentration in their study was in the range of 0.4-0.5 g/L.

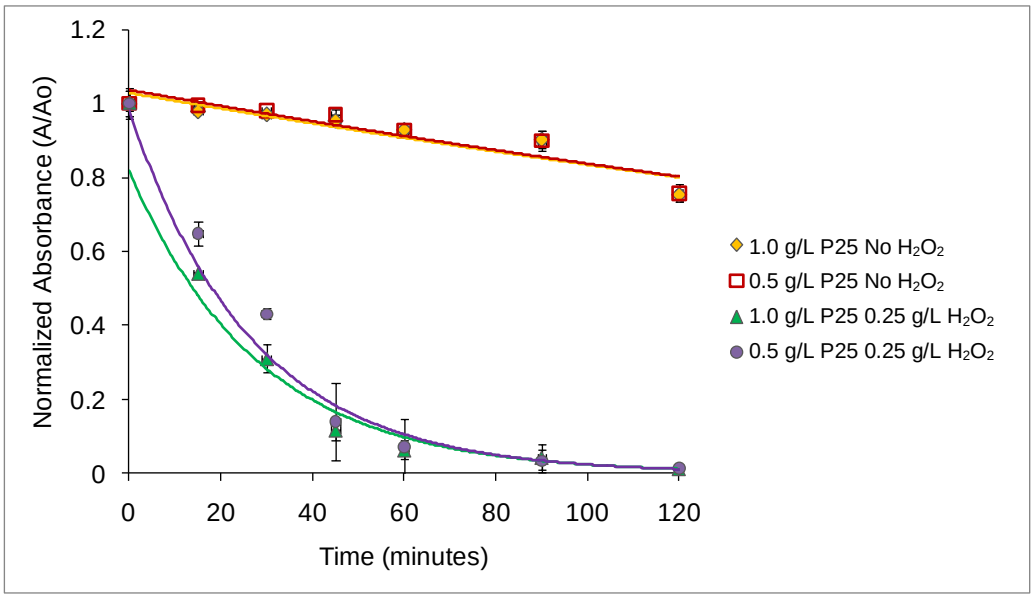

Figure 33: Effect of different catalyst loading
(N = 2, errors are reported as Δ)

Thus, a brief exploration of the effect of catalyst amount on the efficiency of dye degradation was undertaken. From this study, the optimum catalyst concentration cannot be determined because of the limited data. However, it was observed that altering the concentrations of catalyst from 0.5g/L to 1.0g/L, did not appreciably alter the rate of the dye degradation process (see Figure 33). It can be observed that both with and without H_2O_2, photocatalysis results for 0.5 g/L catalyst loading suggest that the rate of dye degradation is not hugely different (*cf.* 100% increase in the amount of the catalyst) compared to 1.0 g/L catalyst loading test which may be supporting the plateau effect in catalyst loading *v.s.* activity observed earlier by others.[30,85,86] This is also confirmed by the rate constants of these reactions (see Table 12). Again, this does not suggest an optimum concentration of the catalyst, however, a 0.5 g/L catalyst loading was designated from this data to be the standard concentration for subsequent work, the reason being that photocatalytic activity will be roughly similar and the method will use less catalyst. Significantly lower amounts of catalysts have not been tested to avoid the necessity to work with extremely small amounts of catalysts in the form of the light power and associated errors (*e.g.* in measuring the weight and weight losses during transfer of the catalyst material).

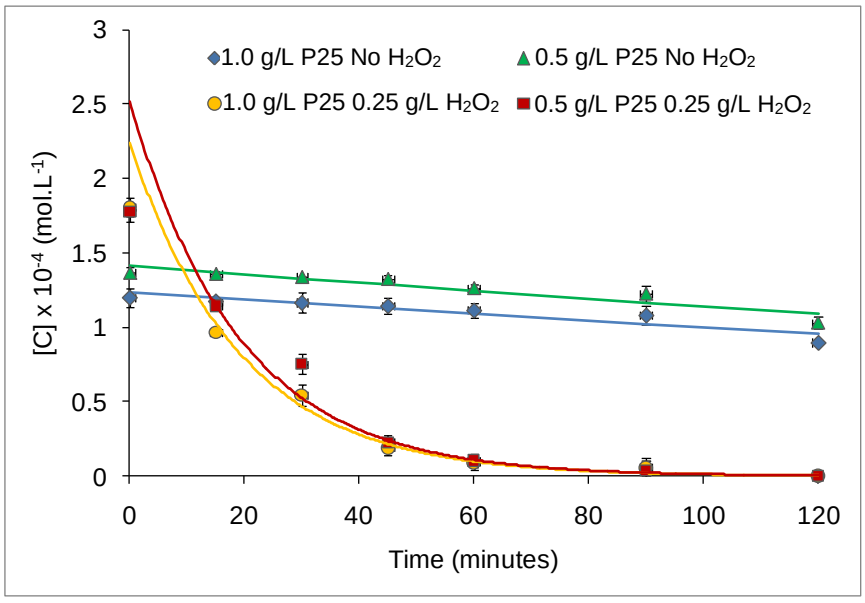

Note: marker data points show the real concentrations, while the lines show the fitted concentration

Figure 34: Kinetics profile of P25-TiO_2 mediated photocatalysis for RB19 with different catalyst concentration (N = 2, errors are reported as Δ)

Kinetics analysis of the reactions presented in Figure 34 suggests that in general, all reactions are well fitted with the first order character. However, in the photocatalytic reaction using 0.5 g/L P25-TiO_2 and 0.25 g/L H_2O_2, the gaps between the actual and fitted concentrations, particularly in 15 and 30 minutes, are quite big. The ln[C] relationships between these reactions can be seen in Appendix 1.

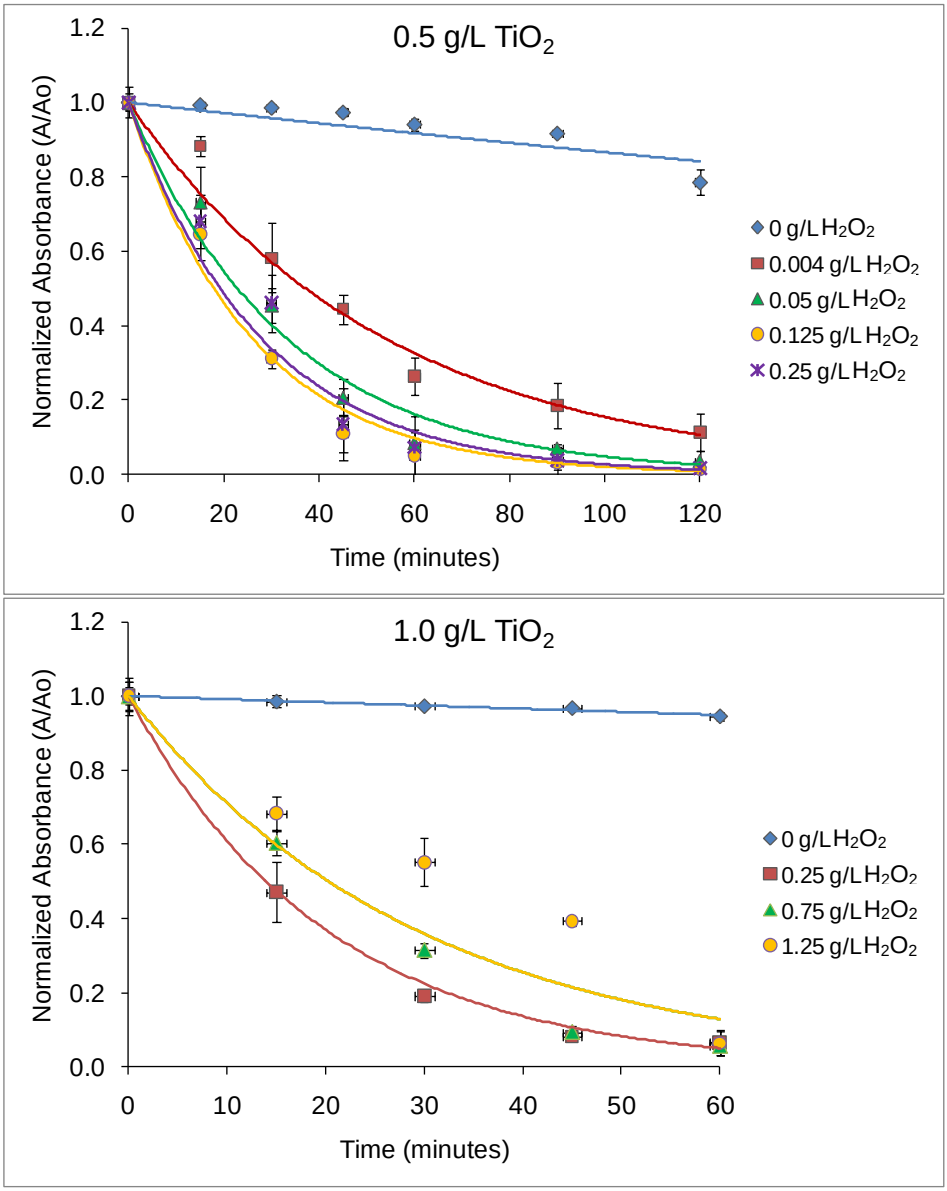

Figure 35: Effect of concentration of H_2O_2 in two different catalyst loading (N = 2, errors are reported as Δ)

Figure 35 also demonstrates that the use of H_2O_2 does indeed greatly influence photocatalytic dye degradation, and without it the degradation will proceed only very slowly. Regarding the concentration of H_2O_2, we found that for higher concentrations of catalyst (1.0 g/L), increasing the amount of H_2O_2 decreased the rate of degradation. This is shown by Figure 35: the normalized absorbance of dye in the reaction with 1.25g/L H_2O_2 is always higher than that of 0.75g/L and 0.25g/L H_2O_2 at any point.

With a lower catalyst loading (0.5 g/L), the three highest concentrations of H_2O_2 (0.05, 0.125, and 0.25 g/L) gave approximately the same end result with slightly lower activity observed for the 0.05 g/L H_2O_2. It is also noted that the lower H_2O_2 concentration (e.g. to 0.004 g/L) results in somewhat slower rate of dye degradation in this case.

Scheme 7: *Effect of the presence of H_2O_2 in photocatalysis*[62]

$$H_2O_2 + O_2^{\cdot} \longrightarrow {\cdot}OH + OH + O_2 \qquad \text{(Eq. 26)}$$

$$H_2O_2 + h\nu \longrightarrow 2{\cdot}OH \qquad \text{(Eq. 27)}$$

$$H_2O_2 + e_{CB} \longrightarrow {\cdot}OH + OH \qquad \text{(Eq. 28)}$$

$${\cdot}OH + H_2O_2 \longrightarrow HO_2{\cdot} + H_2O \qquad \text{(Eq. 29)}$$

$${\cdot}OH + HO_2{\cdot} \longrightarrow O_2 + H_2O \qquad \text{(Eq. 30)}$$

$$TiO_2(h_{VB}^{+}) + H_2O_2 \longrightarrow TiO_2 + O_2 + 2H^{+} \qquad \text{(Eq. 31)}$$

$${\cdot}OH + {\cdot}OH \longrightarrow H_2O_2 \qquad \text{(Eq. 32)}$$

Akpan *et al.*[62] reported that hydroxyl radicals that form from H_2O_2 can act as both strong oxidants and electron scavengers in the photocatalytic reaction. This implies that hydroxyl radicals may cause the inhibition of electron-hole recombination by scavenging electrons from the TiO_2 catalyst (see Eq. 29).

Thus, the presence of H_2O_2 is doubly beneficial to the dye degradation reaction, but, beyond a certain optimum, the rate of the dye degradation reaction is observed to decrease. This is because of the lack of hydroxyl radicals (·OH) and valence band holes (h_{VB}^{+}) that are required are very active for dye degradation. The excess of H_2O_2 can consume both its own radicals and the valence band holes (see Eqs. 31-32), a process that competes with the recombination of ·OH – ·OH (see Eq. 33). Furthermore, the surface of the catalyst can also be modified by the adsorption of H_2O_2, effectively blocking the catalyst's active sites and reducing its photocatalytic activity.

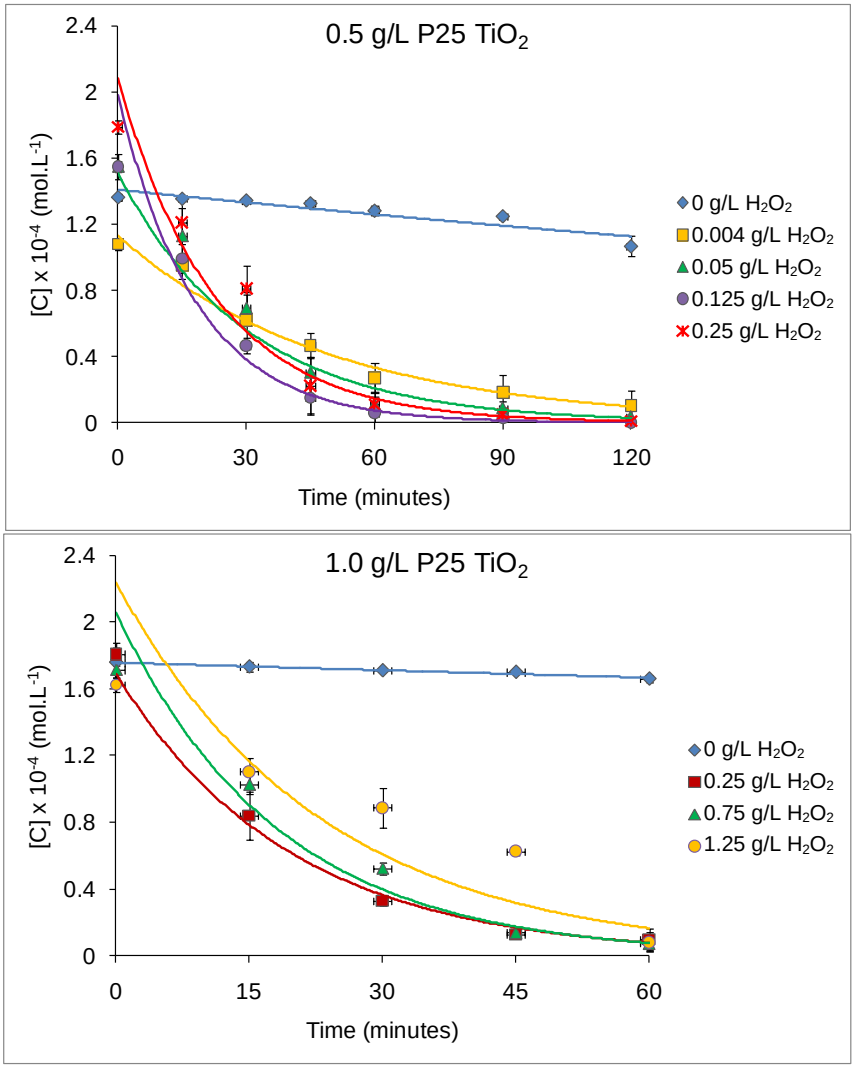

Figure 36: Kinetics profile of P25-TiO_2-mediated photocatalytic reactions for RB19 with different H_2O_2 concentrations (N = 2, errors are reported as Δ)

Kinetics analysis shown in Figure 36 demonstrates that most of photocatalytic degradation of RB19 with different concentrations of H_2O_2 using two different catalyst loadings (0.5 and 1.0 g/L) are well-fitted with the first order character, except the reaction with 1.0 g/L catalyst and 1.25 g/L H_2O_2 that has big gaps at some points. Rate constants of all photocatalytic reactions with different catalyst loadings and H_2O_2 concentrations are presented in Table 12. The relationship of ln[C] *v.s t* of these reactions can be seen in Appendix 1.

Table 12: Average rate constant of P25-TiO_2-mediated photocatalytic reaction with different concentration of catalyst and oxidant (N = 2, errors are reported as 2σ)

Concentration of H_2O_2 (g/L)	**Average rate constant ($mol.L^{-1}.s^{-1}$)**	
	0.5 g/L TiO_2	**1.0 g/L TiO_2**
0.0	$3.63 \times 10^{-5} \pm 9.57 \times 10^{-6}$	$3.56 \times 10^{-5} \pm 1.34 \times 10^{-6}$
0.004	$34.61 \times 10^{-5} \pm 11.92 \times 10^{-5}$	-
0.05	$56.79 \times 10^{-5} \pm 14.72 \times 10^{-5}$	-
0.125	$92.48 \times 10^{-5} \pm 92.40 \times 10^{-6}$	-
0.25	$93.16 \times 10^{-5} \pm 34.19 \times 10^{-5}$	$92.02 \times 10^{-5} \pm 21.35 \times 10^{-5}$
0.75	-	$91.87 \times 10^{-5} \pm 16.09 \times 10^{-5}$
1.25	-	$73.00 \times 10^{-5} \pm 16.63 \times 10^{-5}$

From our data, it is observed that for photocatalytic reactions with 0.5 g/L catalyst loading, the best degradation rate is obtained with a H_2O_2 concentration in the range of 0.05-1.25 g/L. These results do not suggest the optimum amount of H_2O_2 because of the limited number of data points per set in the data series. However, for the subsequent study in this research, 0.05 g/L is used as the standard concentration of H_2O_2, which allows quick catalytic tests with high degree of dye degradation at the reasonably low levels of H_2O_2 (a trade-off between efficiency and reagent consumption).

3.2.2.3 Use of quenching agent and sampling method

This part of study was carried out due to the limitation on usage of the UV-Vis spectroscopy facilities at the Department of Chemistry of The University of Canterbury. Ideally, every sample taken from the reaction would be measured instantly to avoid possible further degradation, especially due to the presence of active species (*e.g.* hydroxyl radicals) formed from H_2O_2 decomposition. However, it could not always be guaranteed that spectroscopy could be carried out immediately.

In an attempt to minimize the effect of any delay between sample extraction and measurement, a study was carried out to pinpoint the effect of treating samples with a quenching agent immediately after collecting them. This quenching agent would be an effective reductive agent,[78,88] that should remove any strong oxidants (e.g. H_2O_2 and radicals) prior to UV-Vis spectroscopy measurement. The tests were performed by running a normal reaction with a modified sample treatment.

Table 13: Effect of the use of quenching agent (instant measurements)

Time (minute)	**Absorbance**		**errors**
	Non-quenched reaction	Quenched reaction	
	Absorbance	Absorbance	
0	0.915	0.858	5.76%
15	0.636	0.591	4.59%
30	0.524	0.531	0.66%
45	0.362	0.278	8.40%
60	0.047	0.045	0.17%

Note: N = 2, errors are reported as Δ

Duplicate samples were taken from the reaction vessel, the catalyst was separated from the suspension by centrifugation as normal (11k rpm, 3 minute), and the filtrate was carefully decanted from the centrifuge vial. One of the two samples was then mixed with quenching agent ($Na_2S_2O_2$, 0.01 g) and both were subsequently refrigerated. After 5 minutes refrigeration, both samples were analyzed by

UV-Vis spectroscopy, and again after 5 hours and 20 hours. The experiment was repeated once to check the reproducibility of the data.

Table 13 shows that the use of quenching agent generally decreases the absorbance of the dye taken from the "instant" (5 minute) measurements, with errors ranging between 0 and 8.5%. The maximum gap of the absorbance (8.5% error) is rather high and would reduce the data quality. Repetition of this test gave an identical result that an attempt to use a quenching agent generally decreases the absorbance of the dye with associated errors in the same range.

Table 14: Effect of delay of measurements

Time (minute)	**Non-quenched reaction**				**Quenched reaction**			
	5 hour delay		**20 hour delay**		**5 hour delay**		**20 hour delay**	
	Abs	% error*	Abs	% error*	Abs	% error*	Abs	% error*
0	0.914	0.10%	0.880	3.58%	0.857	0.09%	0.833	2.44%
15	0.635	0.13%	0.630	0.64%	0.590	0.10%	0.564	2.65%
30	0.524	0.01%	0.408	1.61%	0.053	0.10%	0.515	1.64%
45	0.362	0.02%	0.339	2.29%	0.278	0.01%	0.257	2.09%
60	0.045	0.11%	0.068	-2.13%	0.044	0.11%	0.026	1.88%

*% errors are compared with the absorbance from instant measurements presented in Table 13 (non-quenched reactions)

Table 14 shows that after 5 hours, even simple refrigeration of the samples effectively prevents further dye degradation. It can be seen from the table that compared to the absorbance taken from the "instant" measurement, both quenched and non-quenched samples, give only small errors (below 0.13%). However, measurement after 20 hours shows appearance of somewhat significant deviation compared to the measurements immediately after sampling.

These results show that if there is a delay between sample extraction and measurement, colour removal can be halted simply by refrigeration. However, if the delay is for more than 5 hours, errors may be introduced to the subsequent data. Even after 20 hours, the error in measurement is still small ($\leq 3.58\%$), and would generally be still acceptable.

3.3 Summary

From our study, it can be concluded that TiO_2-assisted photocatalytic dye degradation proved to be a significantly improved process over catalytic reactions carried out in the dark at room temperature and at 70 ^{0}C. On the basis of the results obtained from this preliminary study, the experimental methodology for subsequent studies has been established.

Photocatalytic dye degradation is carried out using the "*all-in*" method, in which all reagents are mixed together before the UV light irradiation. 5-10 minutes of ultrasonication of the TiO_2 suspension in the dye solution precedes H_2O_2 addition. Adsorption in the dark before the light radiation is not necessary, but it is better to do this to ensure that the most important mechanism towards dye degradation is the photocatalytic reaction. Thus, the reactor is left in the dark under constant stirring for 15 minutes.

RB19 is used as the standard type of dye with 0.1 g/L (0.160 mmol/L) initial concentration to obtain the best results for UV-Vis spectroscopy measurements. The composition of the other reagent is as follows: 0.5 g/L catalyst TiO_2 and 0.05 g/L H_2O_2 (1.471 mmol/L).

Samples are taken every 30 minutes starting from the -15 minute (i.e. at the mixing of TiO_2 and dye solution, fifteen minutes before start of irradiation). The standard reaction period is 120 minutes, although in some cases, a shorter or longer period may be used. Centrifugation (11k rpm, 3 minutes) is applied to every sample before UV-Vis measurements to separate the catalyst from the dye solution. In the case that measurement cannot be made immediately, the sample is refrigerated until the end of the day (no more than 5 hours) when all samples can be run (minimizing errors). The use of a quenching agent is not recommended.

UV-Vis spectroscopy is only the most basic method of analyzing dye degradation. The method merely provides data on colour removal, and does not allow the determination of intermediates or products

produced by the dye degradation reaction. Therefore, other methods of analysis (such as total organic carbon analysis, gas or liquid chromatography and mass spectroscopy) are recommended in order both to reinforce the data obtained by UV-Vis spectroscopy and to provide more information on the system. Unfortunately, as is detailed in the following chapter, all results of photodegradation experiments presented herein are based entirely on UV-Vis spectroscopy results because of both time limitations and the disrupting effect of two large earthquakes in the Canterbury region that occurred during this study (as mentioned in Chapter 1). Therefore, further analysis is recommended as further work (see Chapter 6).

With regards to UV-Vis spectroscopy, analysis is performed by measuring the absorbance at the dye's maximum wavelength. Water is used as the measurement reference (baseline correction) for the dye solution. Every sample should be analysed twice in order to ensure reproducibility, but this is not an absolute requirement as our study has already shown by analysis by UV-Vis spectroscopy analysis to be highly reproducible.

Chapter 4 – Photocatalytic Dye Degradation

This chapter presents the photocatalytic dye degradation results obtained with various TiO_2-based catalysts as listed in Table 5 (Chapter 2). CI Reactive Blue 19 (RB19) was used as the standard dye in these experiments, although other dyes were used in some cases. The dyes CI Disperse Yellow 211, CI Acid Red 42, CI Basic Blue 41, CI Basic Yellow 67, and Methylene Blue, have been used at different points in this study. Figure 37 presents the chemical structure of these dyes, except CI Basic Yellow 67, the structure of which is not disclosed in the Colour Index.

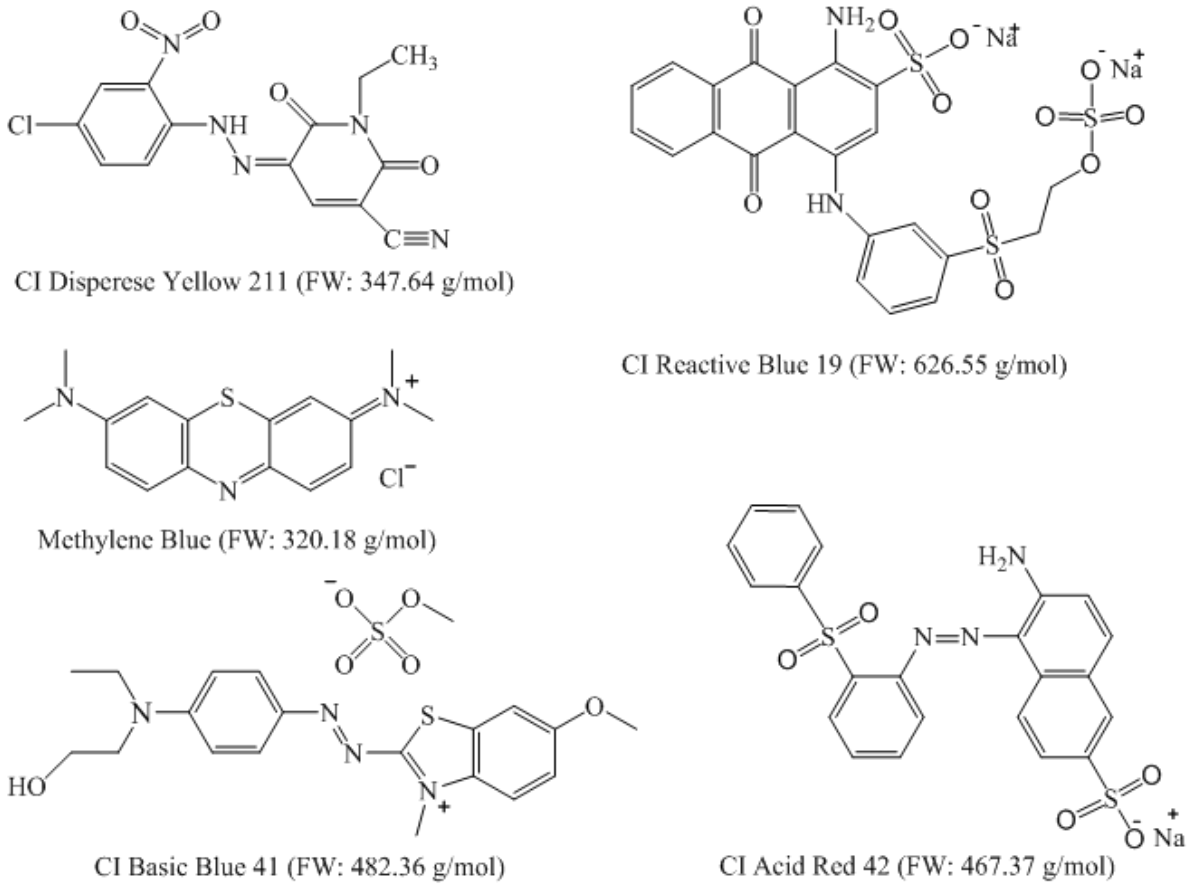

Figure 37: Chemical structure of dyes used in this study

All experiments discussed in this chapter were repeated once, and the data presented in the results are the average of the two data sets. The error bars were calculated as Δ (the difference

between the average and each individual measurements). The kinetics of the reactions were analyzed when applied, by fitting the data into the first order kinetics: $\frac{dC}{dt} = kC$, and therefore $C_t = C_0 e^{-kt}$, where C_t is concentration at time t (mol/L), C_0 is initial concentration (mol/L), and k is the rate constant (mol/L.s).

Concentration of the dyes was converted from their absorbance values using the constant extinction coefficient of each dye (in pure water). Deviations in the values of C_0 in the series reflect small differences between specific photocatalytic test runs (pH adjustment, amount of H_2O_2, *etc*.), which gave rise to slightly different absorbance values even though the amount of dye used was aimed to be the same. To obtain precise and corrected (for the conditions) values of C_0, the linear regression of each dye must be obtained under specific experimental conditions, which would have been too time-consuming for this time-limited study.

4.1 Effect of pH on P25-TiO_2-based photocatalytic reaction

Preliminary studies in this work showed that it was possible to achieve almost total degradation of RB19 dye using the commercially-available P25-TiO_2 as a photocatalyst and UV light. Our initial studies focused on how pH and type of dye affected the rate of degradation when using P25-TiO_2 as a UV photocatalyst.

4.1.1 Effect of initial pH in photocatalytic degradation of RB19

To study the effect of pH on photodegradation of RB19, a series of experiments were carried out with following different initial pHs:

(1) acidic (pH 2-3);

(2) neutral (pH 7);

(3) basic (pH 9-10); and

(4) natural (pH 4.5-5, i.e natural pH of the dye - TiO_2 suspension, without adjustment)

Initial pH here means pH of the dye and TiO_2 suspension, to which the pH adjustments were performed. No buffer was added to these systems, and at the end of reaction, the pH was found to consistently decrease:

Initial pH	2-3	4.5-5	7	9-10
Final pH	1.5-2	2.5-3.5	5-6	7-8

For reference, the pH and absorbance of pure RB19 were measured alongside every sample. From these measurements, it was found that the average pH of the pure dye solution was relatively stable at 5-6. The average absorbance of a control dye solution stored in the refrigerator was at all times stable in the range of 0.85701-0.85712 with a standard deviation of 5×10^{-5}.

The same batch of dye was used in all experiments in order to maintain consistency. Sodium hydroxide (NaOH, 0.5 M) and acetic acid (CH_3COOH, 0.35 M) were used to adjust the pH. pH adjustments were performed on the dye solution/catalyst mixture before H_2O_2 addition, and the initial absorbance was measured after the H_2O_2 addition.

Figure 38 presents the plot of absorbance against time of RB19 photocatalytic degradation for various different pH ranges. It can be seen from the graphs that the initial absorbance of the dyes decreases following pH adjustment. For pH 7 and 9-10, the initial absorbance decreases by 20% and 9.36% respectively. A drastic decrease of 66.95% is shown by the dye with pH adjustment to 2-3, but without H_2O_2 addition it is found that the decrease is only 31.97%. These results indicate that initial absorbance of the dye solution is sensitive to the pH and that RB19 dye degradation appears to be fastest under natural pH (4.5-5) as inferred from the rate of change of absorbance.

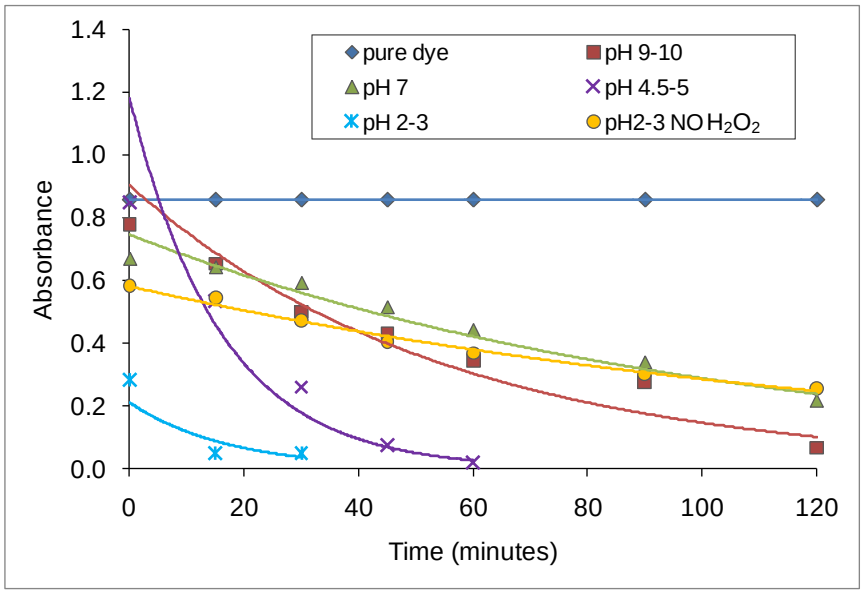

Figure 38: Plot of absorbance v.s. time of P25-TiO_2-mediated photocatalytic degradation of RB19 in various different initial pH ranges (N = 2, errors are reported as Δ)

The acid-base properties of the system can influence the ionisation state of the catalyst surface, as well as that of the dye.[89] For TiO_2, the presence of H^+ or OH^- ions in solution changes the charge of the TiO_2 surface *via* protonation or deprotonation of Ti-OH groups (see Eqs. 34-35) giving rise to positively charged surface under acidic conditions and a negatively charged surface under basic conditions. The *point of zero charge* (pzc) of P25-TiO_2, e.g. value of pH at which the surface is uncharged, is located at pH 6.8.[89] Therefore, at pH lower and higher than 6.8, the adsorption of the dye molecules on the P25-TiO_2 will change due to the changes in charge of the TiO_2 surface.[90]

$$\text{pH} < \text{pzc:}\quad Ti{-}OH + H^+ \longleftrightarrow TiOH_2^+ \qquad \text{(Eq. 26)}$$

$$\text{pH} > \text{pzc:}\quad Ti{-}OH + OH^- \longleftrightarrow TiO^- + H_2O \qquad \text{(Eq. 27)}$$

Changes to the chemical structure and the charge of the dye itself (due to protonation or deprotonation *etc*.) under various pH conditions must be also taken into account when considering the interaction of the dye molecules with the charged surface of TiO_2. For example, RB19 is a reactive dye with a vinyl sulphone-based reactive system. It possesses a ββ-sulphatoethylsulphone group [see compound (a) in

Scheme 8], which is considered the most important commercial vinyl sulphone masking group.[26] Under basic pH conditions, this group may eliminate sulphuric acid to form a vinyl sulphone [compounds (b) and (c) in Scheme 8]. The polarization of the groups's carbon-carbon double bond by the strong electron-withdrawing sulphone group creates a positively-charged terminal carbon atom, which in turn can react with hydroxyl groups, hydroxide ions, water or other negatively-charged species.[91,92]

Under a similarly basic pH, TiO_2 will exhibit a negatively charged surface. Therefore it is likely that interaction will occur between the TiO_2 surface and the dye molecule. However, the presence of H_2O_2 must be taken into account as well. H_2O_2 can potentially produce free radicals such as hydroxyl (·OH), perhydroxyl (HO_2·), and superoxide ($O_2^{\cdot-}$), which may influence efficiency of the interaction between the dye and the catalyst surface, as free radicals are more reactive and mobile in the solution than the particles of a catalyst. To the naked eye there was no change in the colour of the catalyst when it was removed from the system (see for example Figure 29). However, this does not necessarily indicate that there was no adsorption of RB19 on the surface of P25-TiO_2. It is believed that a very small amount of dye could be adsorbed yet be undetectable by the eye.

Scheme 8: reaction of β-sulphatoethylsulphone under basic pH

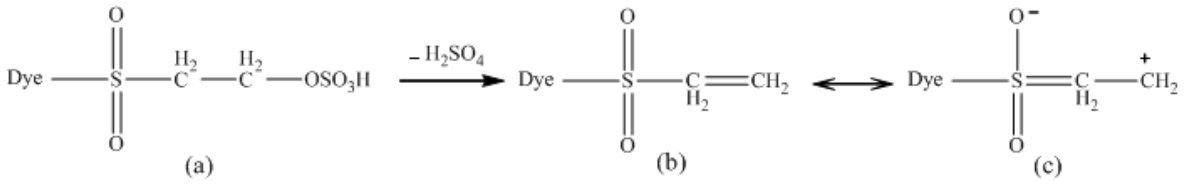

At natural pH, the presence of the hydrogen peroxide does not affect adsorption. At this pH, the RB19 dye is much more stable and thus the formation of the positively charged carbon described by Scheme 8 does not occur.

Under acidic condition (pH 2-3), the decrease in initial absorbance is likely to be due to the change in the conjugation system of the dye molecule; this is due to the interaction between H^+ ions and oxygen atoms in the dye molecule. Furthermore, the presence of hydrogen peroxide leads to enhancement of decolorization because more hydroxyl radicals are expected to form under acidic pH conditions.[93] Some studies have reported that there is siginificant adsorption of the dye on the catalyst under acidic pH, especially in the range of 1-3, that can be observed visually.[93] However in our study there was no observable change in the catalyst colour, although this does not tell exactly that there was no significant adsorption of the dye on the surface of the catalyst.

Table 15: Decrease in absorbance of RB19 after UV photocatalysis at different initial pH ranges

Initial pH	Decrease in absorbance	Radiation time
2-3	94.15%	30 minutes
2-3 (no H_2O_2)	69.96%	120 minutes
4.5-5	97.68%	60 minutes
7	74.90%	120 minutes
9-10	92.15%	120 minutes

Changes in absorbance of RB19 (*cf.* initial absorbance of the pure dye solution in water) of RB19 after UV photocatalysis at different initial pH are summarized on Table 15. It can be seen from Table 15 that the fastest colour removal (decrease in absorbance) was exhibited by the reaction performed with pH 2-3 with addition of H_2O_2. However it should be noted that the initial absorbance (even before the start of UV irradiation) was already very low, which indicates that the decrease in absorbance takes place *via* mechanisms other than photodegradation. The photocatalytic system at natural pH gave a decrease in absorbance of 97.68% after 1 hour of irradiation, with no significant decrease in absorbance before radiation, as was shown by other systems. These results indicate that at natural pH (4.5-5), colour removal is almost exclusively caused by some photocatalytic mechanisms.

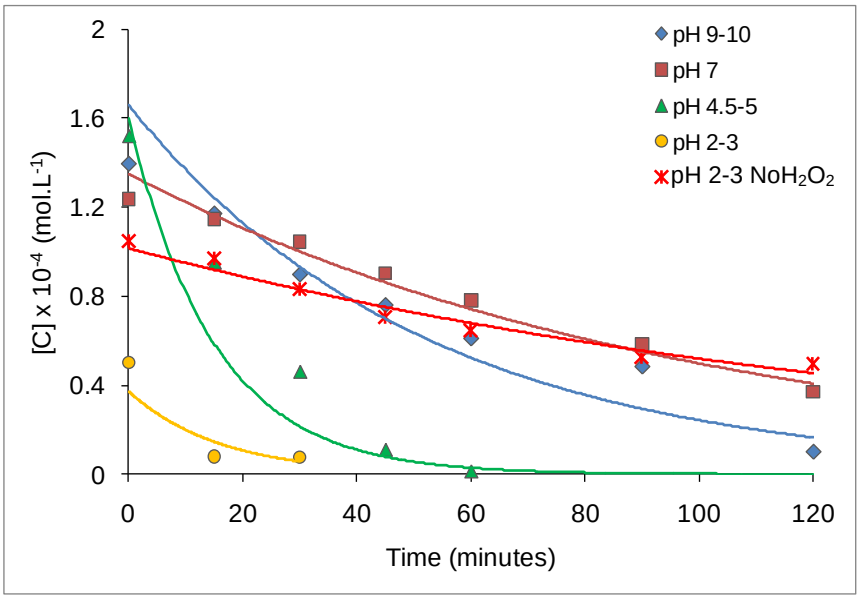

(the marker data points are the average concentrations at each time, while the lines are the fitted concentration to the first order kinetics. N = 2, errors are reported as Δ)

Figure 39: The kinetics profile of TiO_2-mediated photocatalytic degradation of RB19 with different initial pH ranges.

Table 16: Average rate constant of RB19 photodegradation at various different pH ranges

pH	Average rate constant (mol/L.s)
9-10	$3.20 \times 10^{-4} \pm 0.02 \times 10^{-6}$
7	$1.66 \times 10^{-4} \pm 7.79 \times 10^{-6}$
4.5-5	$1.3 \times 10^{-5} \pm 6.0 \times 10^{-8}$
2-3 (no H_2O_2)	$1.1 \times 10^{-5} \pm 2.0 \times 10^{-7}$

*errors are reported as Δ

The kinetics analyses of these reactions presented in Figure 39 shows that all reactions are well fitted with by first order kinetics models. The exception is reaction at pH 4.5-5 that indicates the gaps between the actual and the fitted concentrations are quite big at some data points. The average rate constants are listed in Table 16. The rate constant of reaction at pH 2-3 is not analyzed because of the limited data given by this reaction. Relationships between ln[C] *vs.* t of these reactions are presented in Appendix 1.

4.1.2 Effect of process pH and natural pH on photocatalytic degradation of different dyes

It has been previously mentioned that the application of reactive dyes in industrial applications generally occurs at basic pH. Therefore, although dye removal seems to be most efficient at low pH, this does not correspond with conditions found in industry. To further investigate dye removal under industrially relevant conditions, P25-TiO_2-assisted photocatalytic reactions were carried out on two other dyes, Acid Red 42 (AR42) and Disperse Yellow 211 (DY211), at natural and real process pH. Methylene Blue was also included in the experiments, but the results are discussed separately in the following sub-section due to differing reaction conditions.

Table 17: Mean process pH and typical wastewater pH for dyes used in this study[94,95]

Dye	Natural pH	Mean process pH	Typical wastewater pH
RB19	5.0-5.5	10-11	9-10
AR42	5.0-5.5	2-4	3-4
DY211	6.0-6.5	5-6	6-7

It should be noted that wastewater discharge from textile mills will generally consist of waste from several different wet processes, each with its own pH. A single dyeing operation cannot represent the real characteristics of the wastewater, including pH. Therefore, the mean process pH in these experiments is defined as the typical pH of wastewater discharged from a single operation using a particular type of dye. The mean process pH, typical wastewater pH, and natural pH for various dyes is presented in Table 17. Here, pH adjustments were done to the dye solution before addition of the TiO_2 catalyst to mimic the industrially relevant conditions.

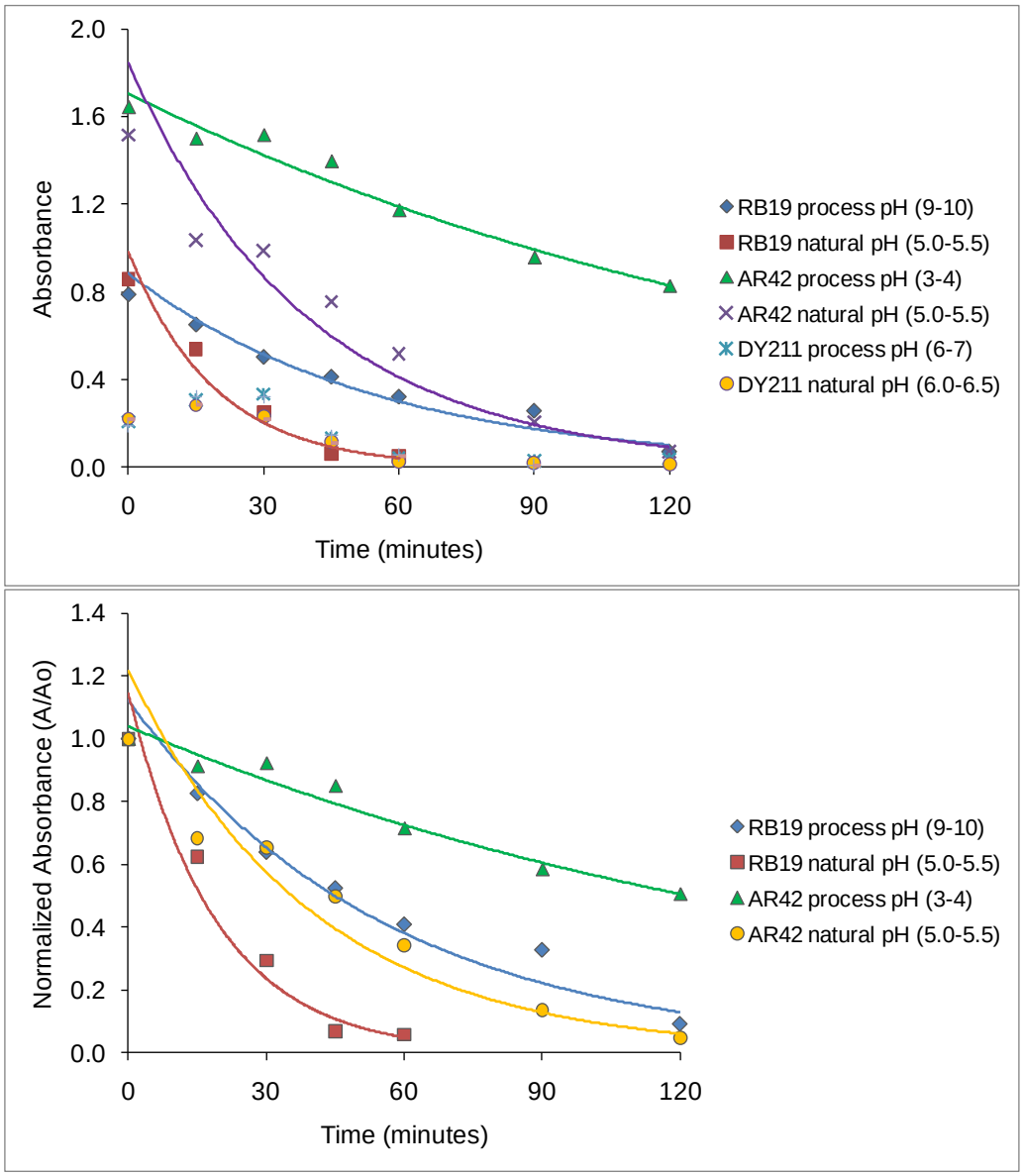

Figure 40: P25-TiO_2-mediated photocatalytic degradation of various dyes at their process and natural pH in absorbance (above) and normalized absorbance (below)
(N = 2, errors are reported as Δ)

Figure 40 presents the plot of absorbance and normalized absorbance against time of the photocatalytic degradation of various dyes (RB19, AR42, and DY211) at their process and natural pH. The plot of normalized absorbance is presented to provide information of the rate of decrease in absorbance against irradiation time in terms of the same initial absorbance.

Figure 40 shows that photodegradation on TiO_2 is a generally effective method for the removal of colour from RB19 and AR42 under both natural and process pH. In contrast, DY211 shows drastically

different activity when subjected to photocatalytic degradation. Before UV irradiation, all DY211 systems show colour removal of greater than 90%, and after two hours of irradiation this level reaches more than 99%. In other words, photodegradation is not an appropriate method to remove the colour of DY211 because it removes less than 10% of its colour. Further discussion about this type of dye is presented separately in the following sub-section.

As described earlier, the concentration of the dyes was converted from their absorbance values using constant extinction coefficient of each dye in pure water. With pH adjustments, it is possible to obtain deviations of the concentrations because of these different conditions. However, the resulting converted concentrations are still substantially comparable with their absorbance (see Figure 41). Average rate constants for the reaction of each dye at these two different pH ranges are presented in Table 18. The linear relationship between ln[C] and time of these reactions can be seen in Appendix 1.

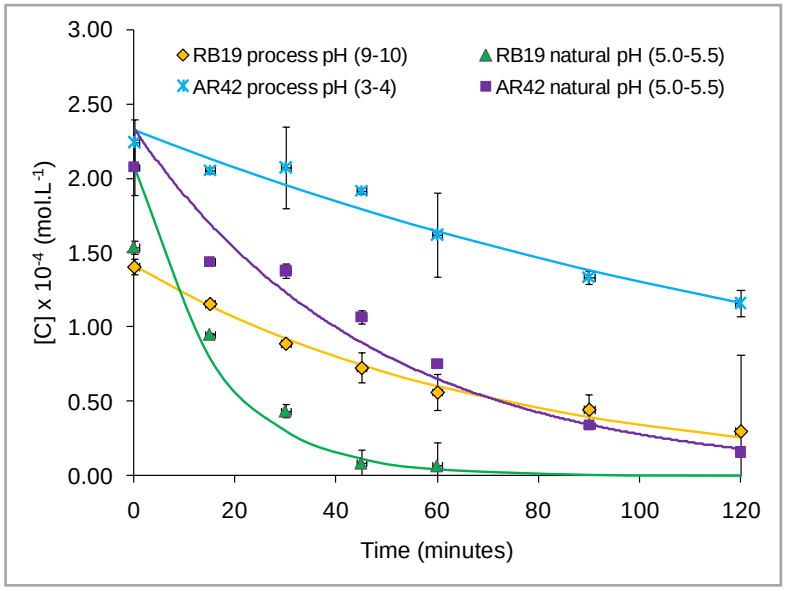

Figure 41: Kinetics profile of TiO_2-mediated photocatalytic degradation of different type of dyes (RB19 and AR42) based on process and natural pH
(N = 2, errors are reported as Δ)

The graphs of RB19 and AR42 photodegradations shown in Figure 40 and 41indicate that degradation at natural pH is more efficient than those at process pH. The least efficient colour removal is in the

case of photocatalytic reaction under acidic pH (3-4, the process pH of AR42). Under this pH, the TiO_2 surface would be positively charged and AR42 in its dissociated form is positively charged as well, thus, adsorption of the dye on the surface is hindered, and the photocatalytic mechanism of the dye on the TiO_2 surface is much reduced.

As well as the effects discussed in the previous section, the pH of the system may also affect the formation of hydroxyl radicals on the TiO_2 surface. These radicals are formed due to the reaction between hydroxide ions (OH^-) and positive holes.[83] At pH > 6, hydroxyl radicals are believed to be the main oxidation species in solution because, at this pH level, it is easier to produce hydroxyl radicals by oxidizing more hydroxide ions on the catalyst surface. However, inhibition of the ·OH formation is also possible under basic conditions because of a Coulombic repulsion between the negatively charged catalyst surface and the hydroxide anions.

Table 18: Average rate constants of photodegradation of RB19 and AR42 at process and natural pH values

Dyes	**Average rate constants ($mol.L^{-1}.s^{-1}$)**	
	at process pH	**At natural pH**
RB19	$2.37 \times 10^{-4} \pm 2.0 \times 10^{-8}$	$10.7 \times 10^{-4} \pm 6.0 \times 10^{-8}$
AR42	$9.6 \times 10^{-5} \pm 1.60 \times 10^{-6}$	$3.54 \times 10^{-4} \pm 3.63 \times 10^{-6}$

*errors are reported as Δ

On the other hand, at pH < 6, it is positive holes that are considered to be responsible for the photooxidation process. This mechanism could lead, for example, to the reductive cleavage of azo bonds in AR42 by electrons from the conduction band of the TiO_2 catalyst. Low pH may also result in the aggregation of TiO_2, a phenomenon that will result in reduced photo absorption and a subsequent decrease in activity.[83]

Each dye behaves differently in response to alteration of the system pH;[96] for this reason one cannot use the results from a study of the pH-dependence of one dye as a template for other dyes.

Additionally, colour removal does not necessarily correspond to dye removal, and other analytical methods such as TOC or GC-MS should be used to confirm dye degradation and to identify the exact species resulting from the colour removal process.

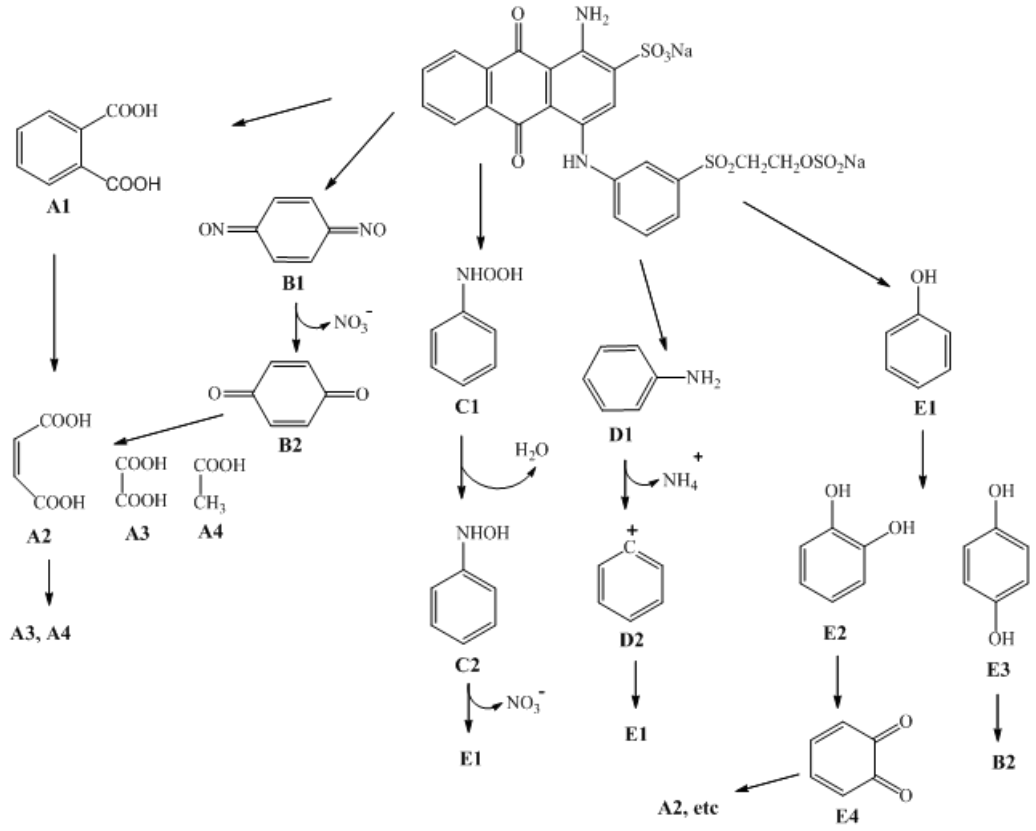

Figure 42: Possible photo-oxidation pathways of RB19 by the hydroxyl radicals resulting from photocatalysis[93]

Figure 42 shows all possible pathways of photo-oxidation of RB19 by the hydroxyl radicals formed in photocatalysis as suggested by He *et al.*[93] It was reported that other than the desirable mineralization products (CO_2, *etc.*), the possible by-products of RB19 by photodegradation include butenediacid, oxalic acid, acetic acid (A4), phenol (E1), and benzo-1,4-quinone (B2). In addition, the possible photodegradation pathways of AR42 are presented in Figure 43. Possible byproducts include 2-naphthol, 2-hydroxy-1,4-naphthoquinone, phthalic acid phthalimide, fumaric, sussinic, maleic, and

malonic acids, in addition to the main mineralization products. It is reported that with a longer radiation time, these by-products can be mineralized.[30]

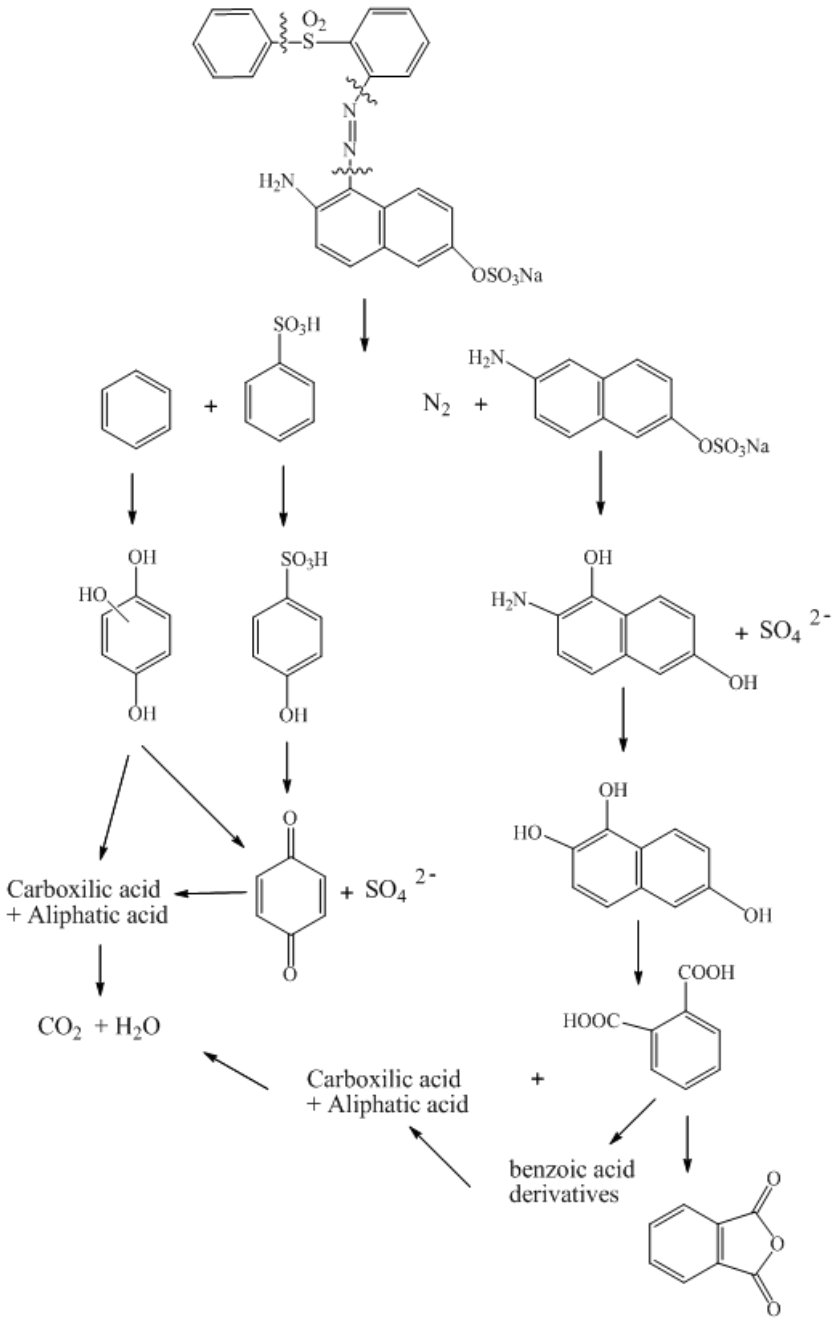

Figure 43: Possible photocatalytic pathways of AR42[30]

4.1.3 Disperse dye

As mentioned previously, DY211 is not suitable dye for degradation by photocatalysis because it adsorbs very efficiently onto the surface of the catalyst TiO_2. It was observed that TiO_2 catalyst extracted from the dye solution was yellow-coloured (see Figure 44), further confirming the adsorption of dye on the catalyst surface. Figure 45 shows that absorbance decreased to less than 0.4 before irradiation. It could be that catalytic degradation has occurred in the dark, however the yellow appearance of the centrifuged catalyst suggests that adsorption is the main reason for colour removal.

Figure 44: The visual appearance of catalyst precipitate from DY211 solution after centrifugation

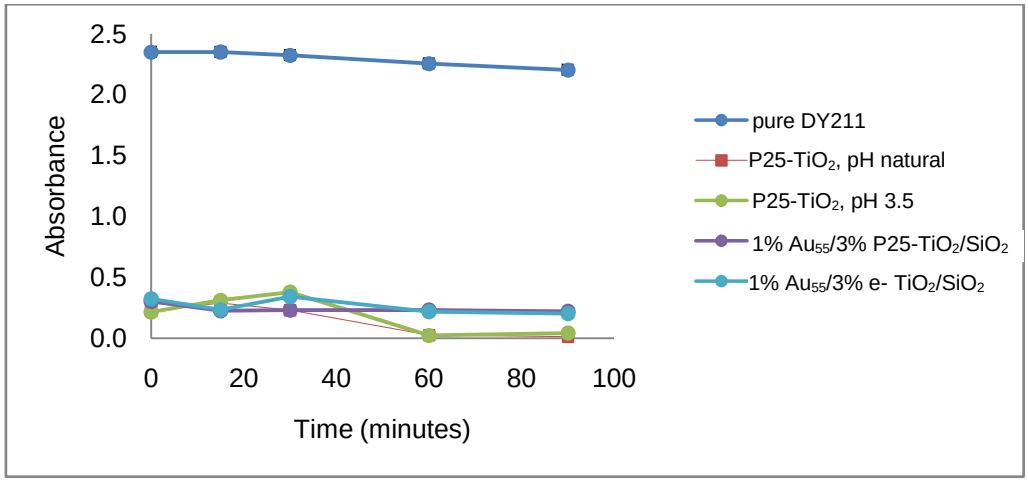

Figure 45: Photocatalytic performance of Disperse Yellow 211 (N = 2, errors are reported as Δ)

These results suggest that photocatalytic degradation is an inappropriate method for the destruction of DY211 because adsorption processes at the surface of TiO_2 beat photocatalytic reactions for these dyes. This conclusion can be extended to any and all disperse dyes due to their hydrophobicity. As shown by the chemical structure of DY211 (see Figure 37), this dye possesses polar groups that are more typical for hydrophobic substances and can interact with the catalyst surface through hydrogen bonding, dipole-dipole interaction, or dispersion forces.[97]

4.1.4 Basic dyes

Basic dyes merit their own subsection in this chapter as several basic dyes (e.g. methylene blue, basic blue 41, basic yellow 67) demonstrate appreciably different photodegradation profiles to other dyes. Firstly, they tend to adsorb significantly on the TiO_2 surface, reaching equilibrium approximately 30 minutes after introduction (as shown in Figure 46); second, these dyes were susceptible to degradation even in the absence of H_2O_2, especially at neutral pH. A summary of the photodegradation studies performed on basic dyes is given in Figure 47.

The majority of research on basic dyes in this study was performed upon the dye methylene blue, which is widely used in photocatalytic procedures in the literature.[63,80, 98] The other dyes, such as basic blue 41 and basic yellow 67, were selected for comparison with methylene blue. Due to the high absorbance of these dyes, their initial concentrations for photodegradation studies were an order of magnitude lower than those of studies on other dye groups.

Figure 46 shows the adsorption profile of methylene blue on P25-TiO_2 in the absence of UV irradiation. It can be seen that adsorption equilibrium is reached after approximately 30 minutes under these conditions (natural pH, no H_2O_2, no UV). These findings agree with those quoted in the literature,[63] although some studies report that it takes longer to reach equilibrium.[98] In order to ensure

that dye adsorption does not affect the photodegradation profile, all systems were stirred in darkness for 30 minutes before irradiating with UV light.

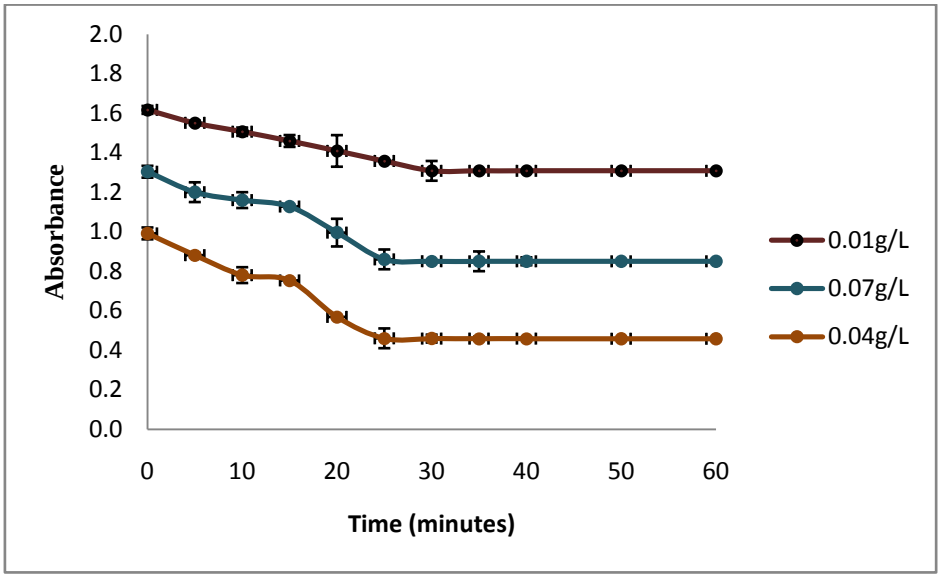

Figure 46: Adsorption profile of Methylene Blue on P25-TiO_2 at natural pH (N = 2, errors are reported as Δ)

As can be seen from their chemical structures (see Figure 37), the organic component of the basic dyes will be positively charged in solution. This cationic charge will allow them to adsorb easily on the surface of the TiO_2 catalyst. This was observed in the case of methylene blue photodegradation, in which TiO_2 removed from the system was blue-coloured.

Figure 47 shows the photocatalytic performance of the TiO_2 catalyst against the three basic dyes in various conditions. Here, the graph is presented as absorbance and normalized absorbance. The kinetics of these reactions was not analyzed because of the irregular results as shown on the graph. Also, the concentration of BY67 cannot be calculated because of undisclosed information about the chemistry of this dye. Rapid decrease in absorbance is shown by system A, C, D, and F since the initial time.

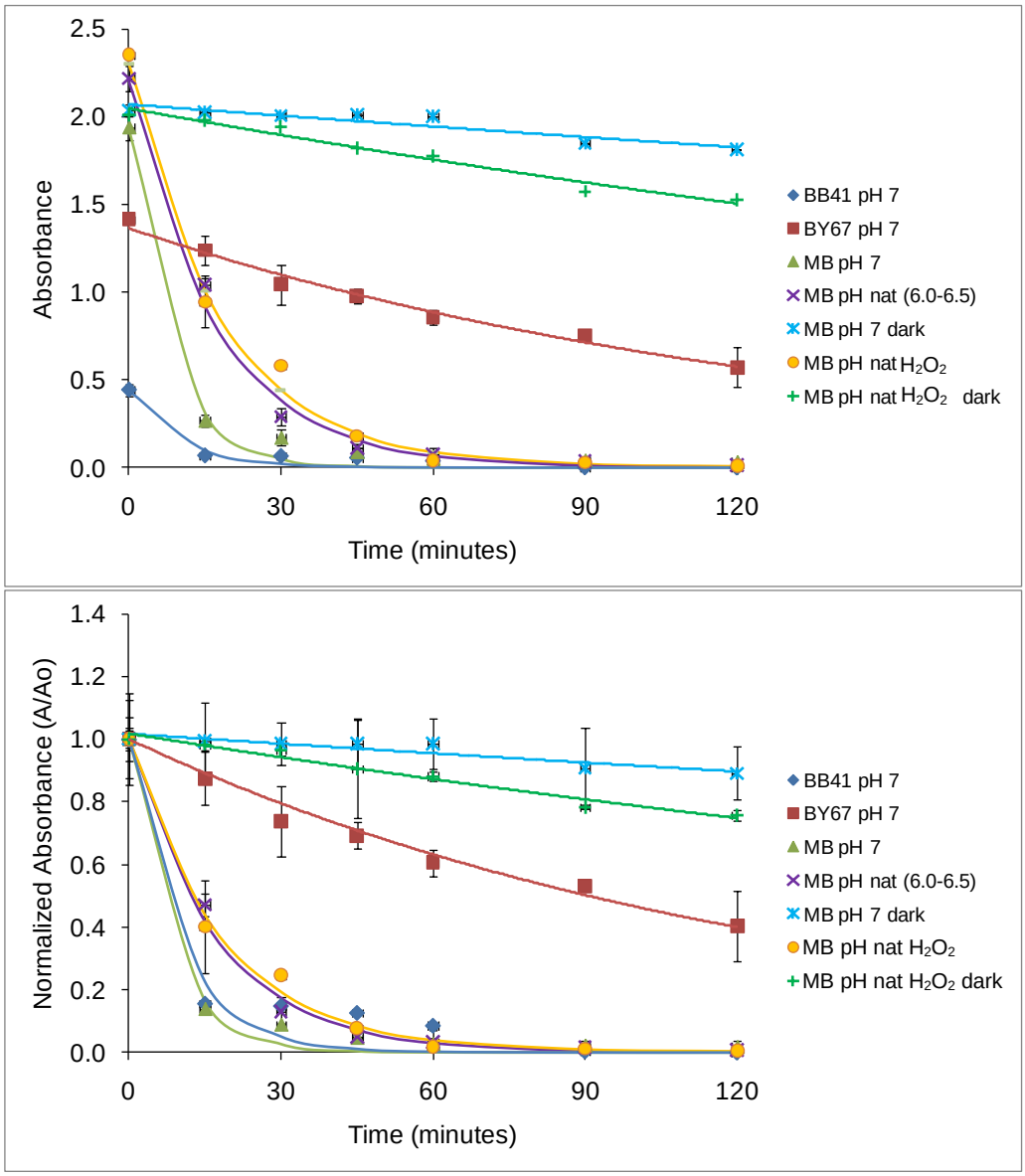

Figure 47: Photocatalytic performance of MB, BB41, and BY67 in various conditions, in absorbance (above) and normalized absorbance (below), N = 2, errors are reported as Δ

Figure 47 shows that methylene blue degrades quickest at pH 7 in the absence of H_2O_2 (system C). Under these conditions, the dye solution experiences 97% colour removal after 60 minutes of UV irradiation. The colour of the TiO_2 catalyst was observed to be light blue after centrifugation. The degradation profile of the system is similar to those exhibited by systems F (MB, natural pH with H_2O_2) and A (BB41, pH 7 without H_2O_2), In contrast, the dye BY67 shows a considerably different degradation profile under the same conditions compared to systems A and C. Three systems show a

sharp drop in absorbance within the initial 15 minutes of irradiation time, a similar trend to the profiles seen in the degradation of the disperse dye DY211. Studies of MB without UV illumination show very little decrease in absorbance, which indicates that photodegradation is the main mechanism for the colour removal process.

These results demonstrate that pH plays an important role in the degradation of the basic dyes. Under natural pH conditions (6-6.5) and without H_2O_2, colour removal of MB on P25-TiO_2 reaches only 73% after 105 minutes of irradiation, in contrast to the results obtained at pH 7. By comparing systems C and D as well as F and G, it can be seen that the hydroxyl ions formed at the higher pH and the hydroxyl radicals formed from H_2O_2 synergistically enhance the dye degradation of methylene blue. The possible photodegradation products of MB can be seen in Table 4 (Chapter 1).

4.2 Photocatalytic tests of custom-made TiO_2 and TiO_2/SiO_2

This section presents the results of photocatalytic degradation of RB19 using three different forms of TiO_2 synthesized by Jan-Yves Ruzicka (a Ph.D. student in our group): e-TiO_2, c-TiO_2, and p-TiO_2, as well as 1% loading of these on the SiO_2 support. In this section, smaller masses of catalyst and oxidant were used than previously. While the dye solution was prepared at the same concentration as for the other experiments (0.1 g/L, 0.160 mmol/L), the amount of catalyst used was five times less than the standard conditions used previously, i.e. 0.1 g/L of pure TiO_2 and 10 g/L of TiO_2/SiO_2 (which is equal to 0.1 g/L pure TiO_2). The amount of H_2O_2 was also scaled down two-fold, i.e. 0.025 g/L instead of 0.05 g/L. For reference, reactions with P25-TiO_2-based catalysts were included under the two different conditions.

4.2.1 Photocatalytic tests of custom-made TiO_2

Figure 48 presents the plots of the absorbance of RB19 versus irradiation time with various catalysts. It is shown by the graph that despite its amorphous nature, e-TiO_2 shows the highest activity for the

photodegradation of RB19: 95% decrease in the concentration of the dye solution after irradiation at 2 hours. This is 1.25 times faster compared to the results in the case of the commercial P25-TiO_2 (under the same conditions).

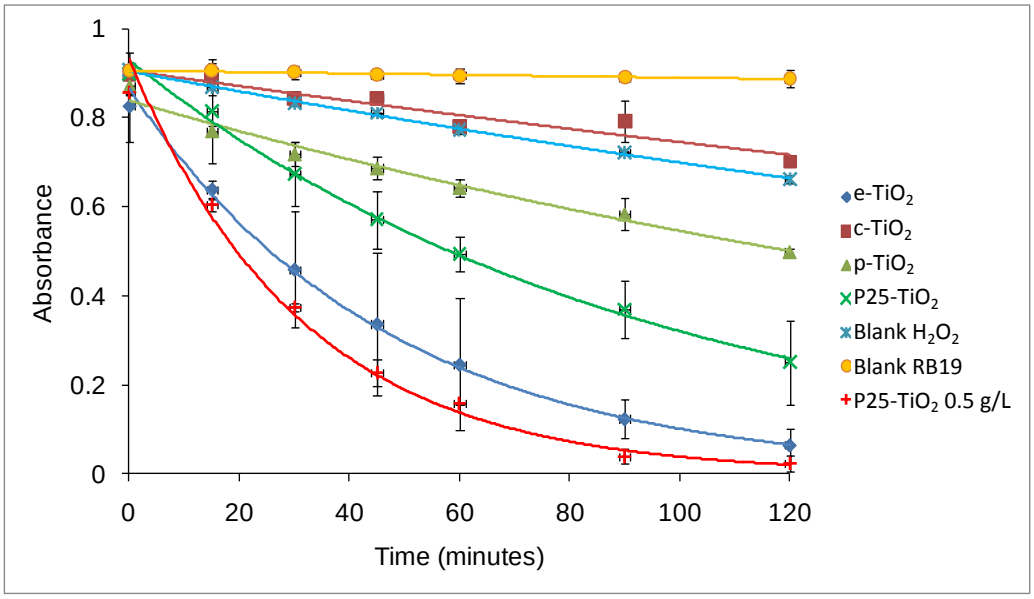

Figure 48: Plot of absorbance against time of photocatalytic degradation of various TiO_2 catalysts for RB19 (N = 2, errors are reported as Δ)

Based on the graph in Figures 48 and 49, the catalysts activity can be ordered as follow: e-TiO_2 > P25-TiO_2 > p-TiO_2 > c-TiO_2. The average rate constants of these reactions are presented in Table 19. Considering merely the crystallinity of the catalysts used, these results are inconsistent with other reports on TiO_2 photocatalytic activity.[64,99] The crystalline c-TiO_2 and p-TiO_2 should exhibit higher activity to dye degradation than the amorphous e-TiO_2, as photocatalytic activity mainly depends on the particular phase or phase combination(s) and crystallinity. High activity is typically shown by crystalline products, preferably with an anatase:rutile phase composition ratio similar to that of the commercial P25-TiO_2, i.e. 80:20.[64] However, crystallinity is not the only factor that affects photocatalyst activity: size, shape, and number of active sites also play a part.[99]

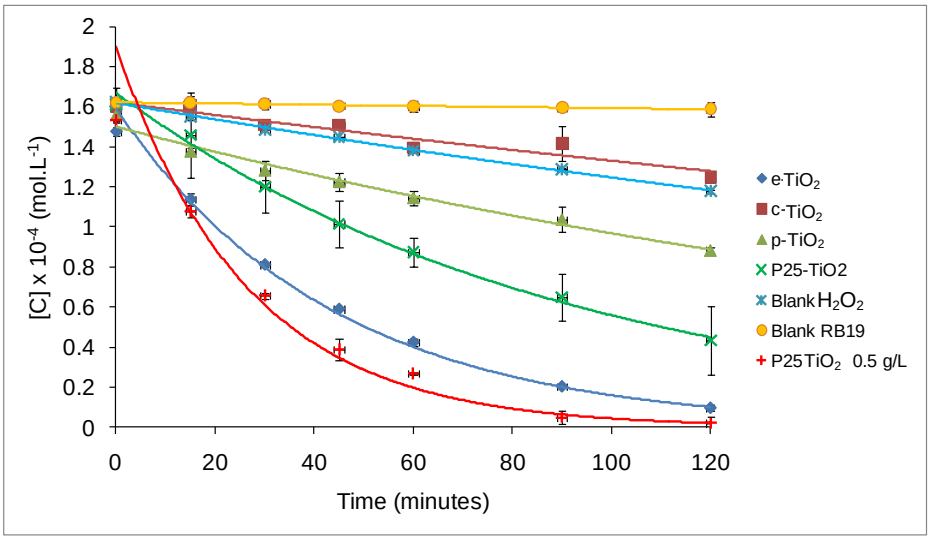

*marker data points represent the real concentration during the reaction, while lines represent the fitted concentration with the first order reaction, N = 2, errors are reported as Δ

Figure 49: Kinetics profile of TiO_2-mediated photocatalytic degradation of RB19 with various TiO_2 catalysts

In the case of the results shown in Figures 48 and 49, it is believed that the amorphous (see Figures 16 and 17) e-TiO_2 exhibits a considerably larger surface area than other TiO_2 catalysts used in the photodegradation study. This is probably due to the porosity in the particle, which has been previously observed in TiO_2 catalysts prepared by this method.[68,100] When e-TiO_2 is calcinated, the nanoparticles become crystalline (as confirmed by TEM and pXRD of c-TiO_2) but the pores would disappear as the nanoparticle reforms, resulting in a lower surface area. Therefore, while it might be a more active per unit of surface area, the total surface area itself decreases, which may explain the lower everall photocatalytic efficiency per unit of mass.

Table 19: Average rate constant of TiO_2-mediated photocatalytic degradation of RB19 with various TiO_2 catalysts

Catalysts	**Average rate constants ($mol.L^{-1}.s^{-1}$)**
e-TiO_2	$3.88 \times 10^{-4} \pm 1.03 \times 10^{-5}$
c-TiO_2	$3.30 \times 10^{-5} \pm 3.64 \times 10^{-6}$
p-TiO_2	$7.30 \times 10^{-5} \pm 3.50 \times 10^{-6}$
P25-TiO_2	$1.83 \times 10^{-4} \pm 1.34 \times 10^{-5}$
P25-TiO_2 (0.5g/L)	$6.50 \times 10^{-4} \pm 2.21 \times 10^{-5}$
Blank H_2O_2	$4.40 \times 10^{-5} \pm 1.93 \times 10^{-6}$

*errors are reported as Δ

The results of scanning ion occlusion spectroscopy (SIOS) using the Izon qNano nanoparticle sizing device (obtained by Jan-Yves Ruzicka) confirmed that the mean particle size of e-TiO_2 (463 ± 80 nm) is larger than that of c-TiO_2 (293 ± 50 nm), which is to be expected if calcination causes pore collapse.

The kinetics profiles of photocatalytic reactions using these catalysts presented in Figure 49 shows that all reactions are well-fitted with by the first order kinetics model. The average rate constants of these reactions are presented in Table 19, while the linear relationships between ln[C] against time (t) can be seen in Appendix 1.

4.2.2 Photocatalytic tests of custom-made TiO_2 supported on SiO_2

TiO_2 is immobilized on SiO_2 for two purposes: to help disperse the nanosized TiO_2 particles, and to immobilize them onto a macroscopic support to improve catalyst recyclability and reduce safety concerns due to exposure to free nano-sized particles. It is hypothesized that the photocatalytic activity of TiO_2 supported onto SiO_2 could increase because of the increase in the effective positive charge of the Ti atom.[75] Gao, *et al.*[73] reported that the SiO_2 surface may provide additional surface area on which the dye can be adsorbed and can degrade, resulting in a synergistic effect when combined with TiO_2. The photodecomposition of organic pollutants was believed to occur on the SiO_2 sites because of the hydrophilicity and adsorption ability of SiO_2 surface. Organic pollutants are adsorbed by SiO_2, and the photogenerated intermediates diffuse into the SiO_2 sites.

Instead it is found that photodegradation of RB19 with 1% (by mass) TiO_2 on SiO_2 (see Figure 50) shows that in all cases, the pure catalysts show a markedly greater photocatalytic activity (per unit mass of TiO_2 photocatalyst) than their SiO_2 immobilized equivalents. The maximum decrease in absorbance achieved after 2 hours of UV irradiation is only 34.98%. Here, compared to the other custom-made photocatalysts used in this study, p-TiO_2 on SiO_2 exhibits the highest activity. The

kinetic profiles and the average rate constants of these reactions are presented in Figure 51 and Table 20.

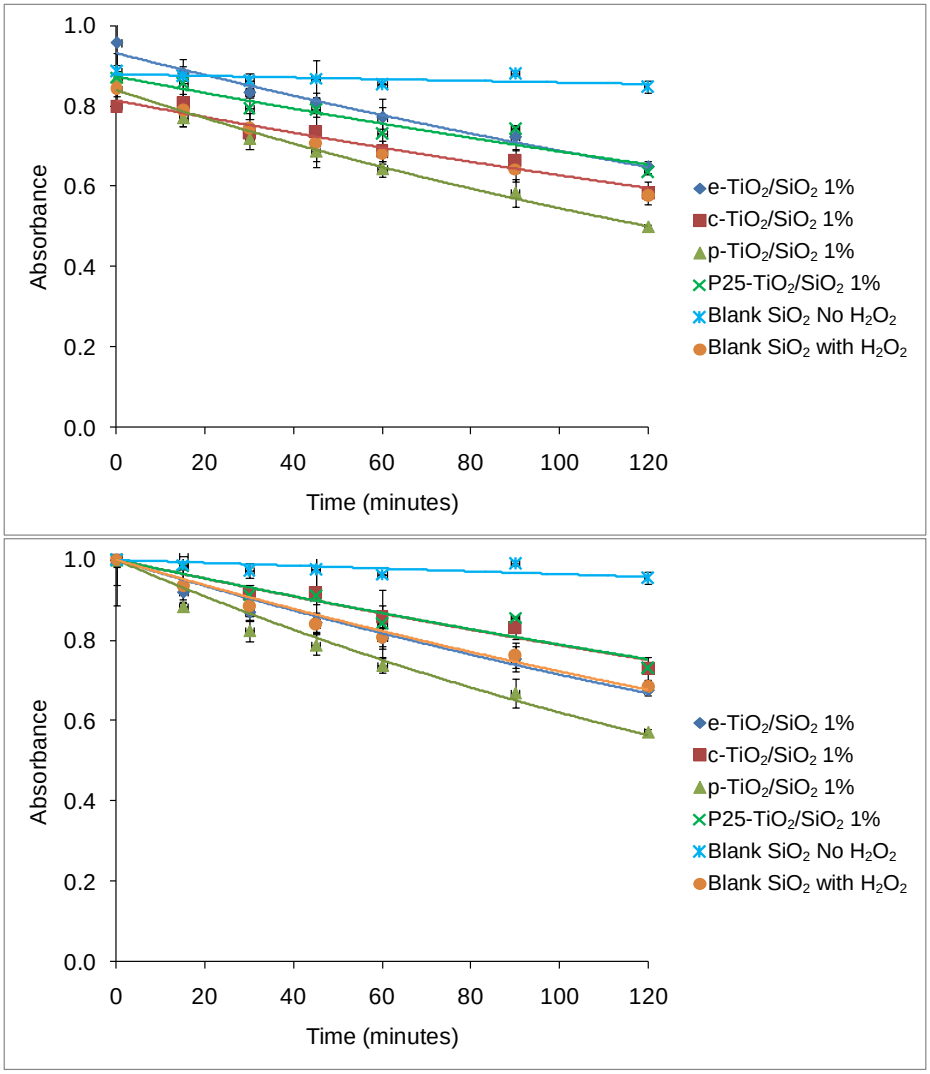

Figure 50: Photocatalytic degradation of RB19 with various 1%TiO_2/SiO_2 catalysts, in absorbance (above) and normalized absorbance (below), N = 2, errors are reported as Δ

One possible reason for the lower observed photocatalytic activity of the supported catalysts may be the extremely low TiO_2:SiO_2 ratio, as SiO_2 is not photoactive (see Figure 50). Excess SiO_2 may in fact inhibit photodegradation, reducing catalyst activity. It may be that at extremely low TiO_2 loadings a significant proportion of it could be hindered from UV light by the SiO_2, while at higher loadings, more of the TiO_2 would be residing on the outer surface of TiO_2 exposed to light. Anderson *et al.*[74] reported that the efficiency of photodegradation of the organic pollutants is highly dependent on the

ratio between TiO_2 and SiO_2, and found that the highest activity was reported when the catalyst was comprised of 30% TiO_2. This is further confirmed by our results presented in Figures 52 and 53. With a higher loading of TiO_2 (3%) on SiO_2 support, the efficiency of photocatalytic degradation per mass unit of catalyst is higher than that of the 1% loading. The decrease in absorbance of dye solution achieved when using the 3% e-TiO_2/SiO_2 is almost comparable with results obtained using the pure e-TiO_2. It might be that with higher loadings of TiO_2, closer to the 30% mark suggested by Anderson *et al.*[74] the photocatalytic activity of TiO_2 supported on SiO_2 could exceed that of pure TiO_2.

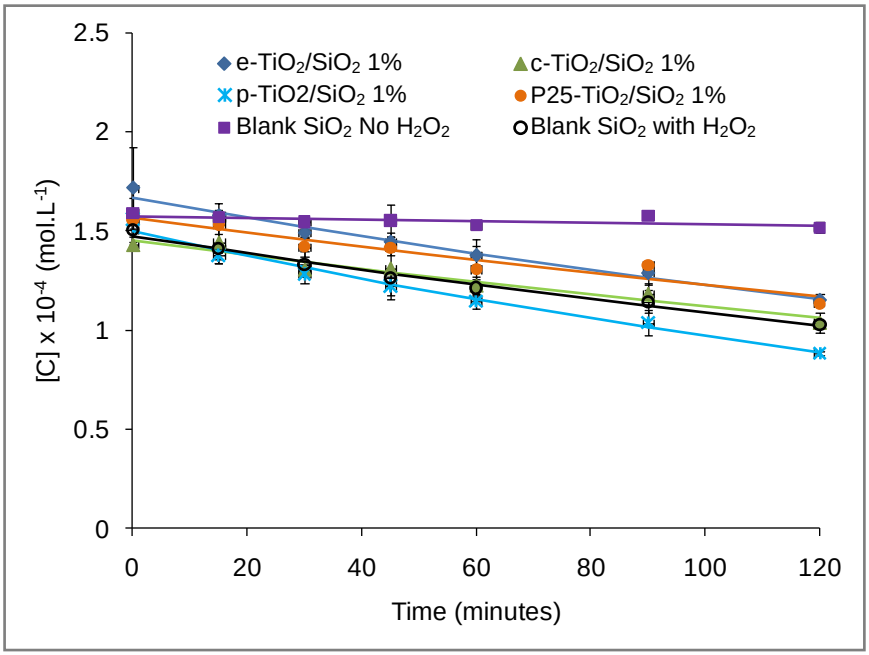

*marker data points represent the real concentration during the reaction, while lines represent the fitted concentration with the first order reaction, N = 2, errors are reported as Δ

Figure 51: Kinetics of SiO_2-supported TiO_2-mediated photocatalytic degradation of RB19 (1% loadings)

Figures 52 and 53 present the comparison between natural and process pH on photodegradation of RB19, in absorbance and normalized absorbance as well as concentration *versus* time respectively. In all cases, photodegradation at process pH (9-10) occurs faster than at natural pH (3.5-4.5). This is presumably because huge positively charged surfaces of SiO_2 are available and should be attracting negatively charged organic parts of RB19, speeding up diffusion to the TiO_2 active centers. This is inconsistent with the results of pH effects discussed earlier in this chapter (see Section 4.1.2), but may

stem from the altered acid-base properties of the TiO_2/SiO_2 catalyst. At higher pH, the catalyst surface is negatively charged, making it easier to produce hydroxyl radicals by oxidation of hydroxyl ions present in excess. These radicals will then help with dye oxidation. Here, the possible inhibition of hydroxyl radical formation due to Coulombic repulsion between the hydroxyl ion and the negatively (overall) charged surface is less of the problem because of the increase in the effective positive charge of Ti atoms on the TiO_2/SiO_2 catalyst. Thus, in these cases, the photocatalytic activity at process pH (9-10) is higher than at natural pH (3.5-4.5). Additionally, the natural pH of TiO_2/SiO_2 (in suspension) is more acidic than TiO_2.

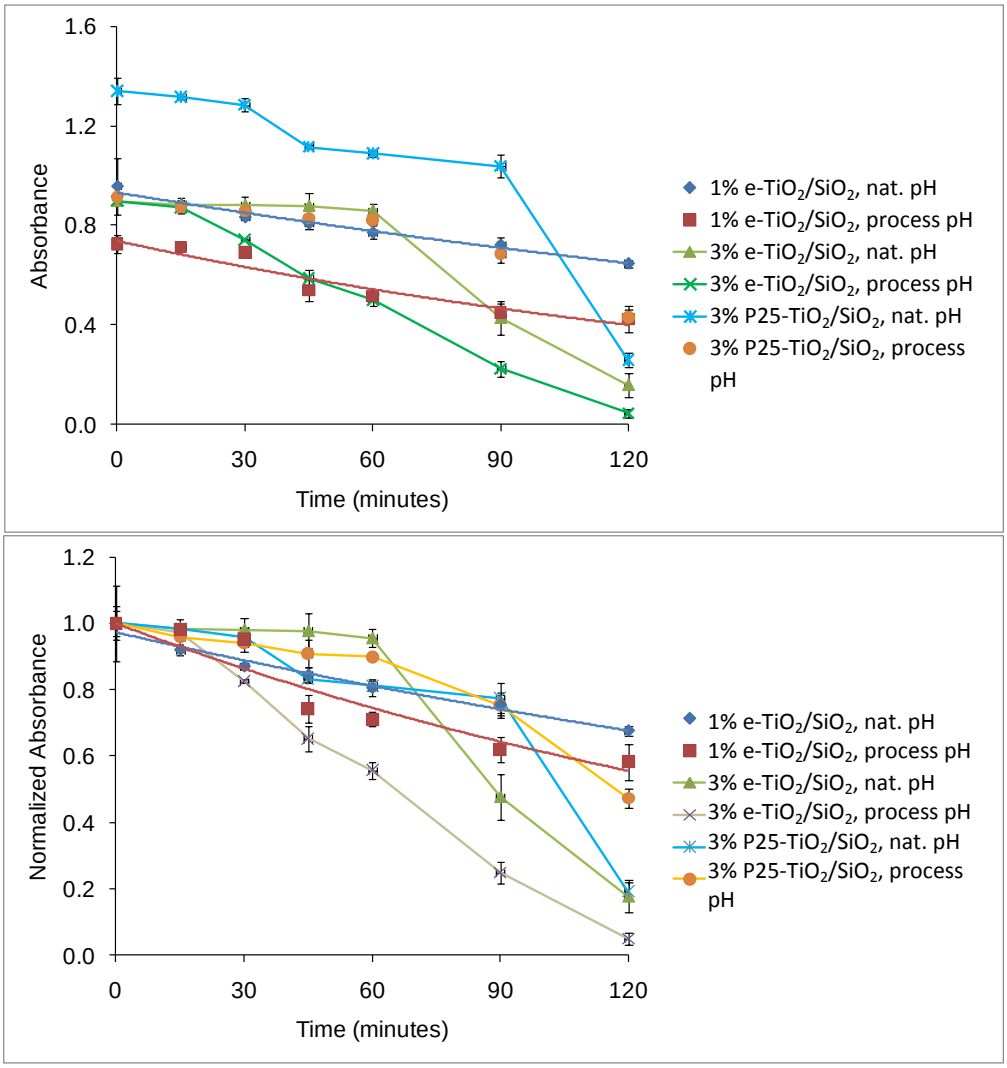

Figure 52: Photocatalytic degradation of RB19 with various TiO_2/SiO_2 in process pH (9-10) and natural pH (3.5-4.5), N = 2, errors are reported as Δ

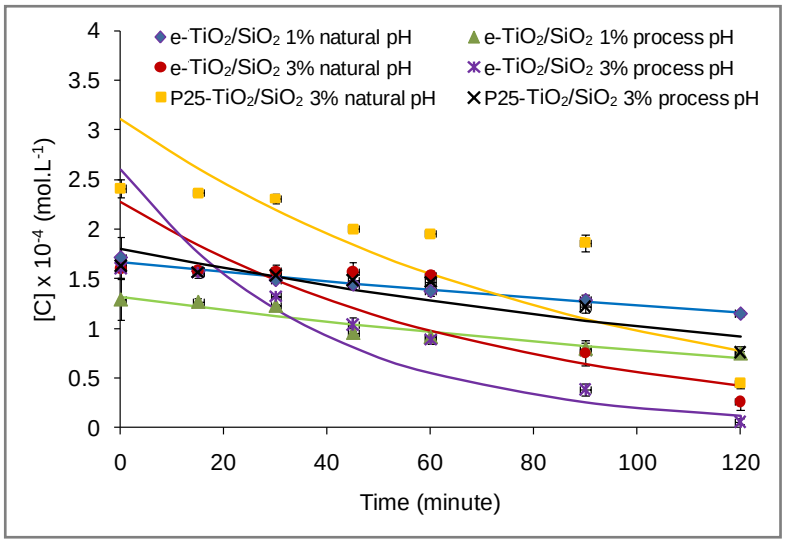

*marker data points represent the real concentration during the reaction, while lines represent the fitted concentration with the first order reaction.

Figure 53: Kinetics profile of photocatalytic degradation of RB19 using various TiO_2/SiO_2 under process (9-10) and natural (3.5-4.5) pHs (N = 2, errors are reported as Δ)

Table 20: Average rate constant of photodegradation of RB19 with various SiO_2-supported TiO_2 in 1% loading

Catalyst	Average rate constant ($mol.L^{-1}.s^{-1}$)
1%e-TiO_2/SiO_2	$5.11 \times 10^{-5} \pm 5.87 \times 10^{-6}$
1%c-TiO_2/SiO_2	$4.40 \times 10^{-5} \pm 1.82 \times 10^{-6}$
1%p-TiO_2/SiO_2	$7.31 \times 10^{-5} \pm 3.50 \times 10^{-6}$
1%P25-TiO_2/SiO_2	$8.53 \times 10^{-5} \pm 1.18 \times 10^{-4}$
Blank SiO_2 (no H_2O_2)	$4.0 \times 10^{-6} \pm 1.60 \times 10^{-6}$
Blank SiO_2	$5.06 \times 10^{-5} \pm 8.79 \times 10^{-5}$

*errors are reported as Δ

Figure 51 shows that all photocatalytic reactions using various 1%TiO_2/SiO_2 catalysts are well-fitted by the first order kinetics model, while the kinetics profile of photocatalytic reactions presented in Figure 53 shows that only 1% e-TiO_2/SiO_2 under process and natural pH only are well-fitted with by the first order kinetics model. The average rate constants of these reactions according to the first order kinetics are presented in Tables 20 and 21. It is important to stress that in all the experiments comparing theperformance of pure and supported TiO_2, the amount of active ingredient (TiO_2) was

kept constant in all catalytic tests by scaling amounts of the materials used. Thus, higher efficiency observed in the test run using 3% TiO_2/SiO_2 is not due to the three times greater amount of TiO_2 compared to the test run using 1% TiO_2/SiO_2 – the total amount of TiO_2 was the same in both runs.

Table 21: Average rate constant of photodegradation of RB19 with various SiO_2-supported TiO_2 in 1% and 3% loadings at natural (3.5-4.5) and process pH (9-10)

Catalyst	Average rate constant ($mol.L^{-1}.s^{-1}$)
1%e-TiO_2/SiO_2, natural pH	$5.11 \times 10^{-5} \pm 5.87 \times 10^{-6}$
1%e-TiO_2/SiO_2, process pH	$8.69 \times 10^{-5} \pm 2.45 \times 10^{-5}$
3%e-TiO_2/SiO_2, natural pH	$2.36 \times 10^{-4} \pm 5.00 \times 10^{-5}$
3%e-TiO_2/SiO_2, process pH	$4.33 \times 10^{-4} \pm 4.57 \times 10^{-5}$
3%P25-TiO_2/SiO_2, process pH	$1.93 \times 10^{-4} \pm 5.39 \times 10^{-6}$
3%P25-TiO_2/SiO_2, process pH	$9.46 \times 10^{-5} \pm 6.54 \times 10^{-6}$

*errors are reported as Δ

It can be seen from the all results that catalysts based on e-TiO_2 always exhibit higher activity than ones based on c- and p- TiO_2, reflecting the importance of surface area. Interestingly, e-TiO_2 also shows higher activity than the commercial P25-TiO_2 in all cases in this study (*i.e.* pure and supported on SiO_2).

4.3 Photocatalytic test of Au/TiO_2-catalyzed dye photodegradation

In an attempt to enhance the photocatalytic activity of TiO_2, gold clusters have been immobilized on the catalyst surface. As mentioned in Chapter 2, the TEM images of these catalysts are not available at this stage due to the unavailability of the machine caused by the earthquake during the study period. However, the change of the colour of the catalysts indicated the presence of gold cluster in the catalyst system. Gold clusters may act as electron traps, accumulating photoexcited electrons, preventing electron-hole recombination, and improving photocatalytic activity of the TiO_2 catalyst.[18]

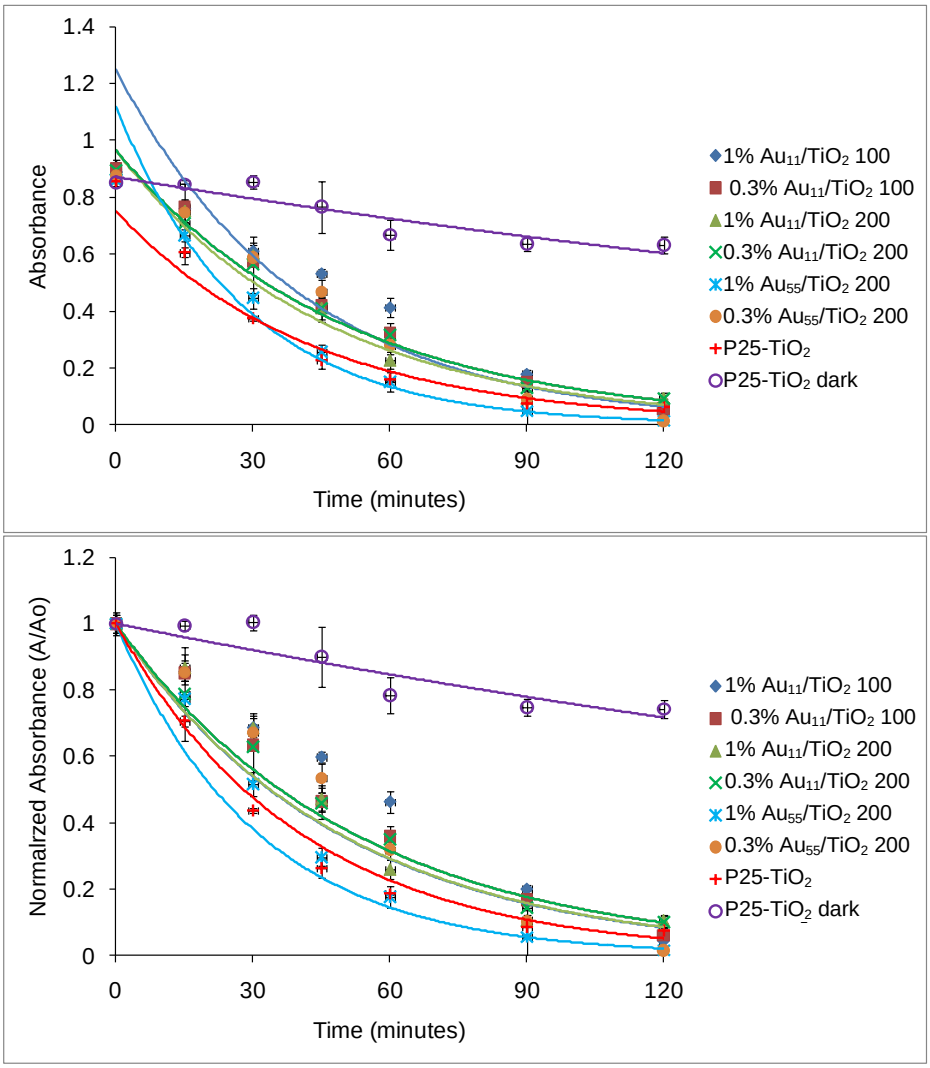

Note: 100 and 200 shown in the name of the catalysts represent the calcinations temperature

Figure 54: Photocatalytic performance of various Au/TiO_2 catalysts for degradation of RB19 (N = 2, errors are reported as Δ)

In this study, Au/P25-TiO_2 catalysts synthesized by members of the Golovko group (David Anderson kindly provided the Au nanoparticles while Jan-Yves Ruzicka kindly fabricated the catalysts) were tested as photocatalysts for the degradation of RB19 dye by UV light in the presence of H_2O_2. Several catalysts were synthesized with different gold cluster sizes (Au_{11} and Au_{55}), gold loadings (1% and 0.3%), and the calcination temperatures (100 and 200 °C). Specific details of the catalyst fabrication are reflected in the catalyst code-name. Blank reactions (P25-TiO_2 without gold) were carried out both under UV irradiation and in the dark. The amount of reagent added in all cases was similar to the

amounts used in the study of pure TiO_2: 0.1 g/L RB19 in aqueous solution, 0.5 g/L catalyst (either Au/TiO_2 or pure TiO_2), 0.05 g/L H_2O_2. All reactions were run under natural pH (*ca.* 4.5-5.5).

Table 22: Decrease in absorbance of RB19 during the Au/TiO_2-assisted photocatalysis

time (min)	Decrease in absorbance of RB19							
	$Au_{11}/P25\text{-}TiO_2$ (100°C calcination T)		$Au_{11}/P25\text{-}TiO_2$ (200°C calcination T)		$Au_{55}/P25\text{-}TiO_2$ (200°C calcination T)		Blank P25-TiO_2(without heat-treatment)	
	1%	0.3%	1%	0.3%	1%	0.3%	UV	Dark
0	0.00%	0.00%	0.00%	0.00%	0.00%	0.00%	0.00%	0.00%
15	15.33%	15.06%	14.75%	27.27%	23.70%	15.07%	30.57%	
30	32.49%	35.70%	32.83%	41.02%	50.37%	33.40%	56.84%	
45	41.02%	52.68%	51.13%	52.53%	72.36%	48.16%	75.85%	
60	55.44%	65.73%	75.31%	64.74%	84.88%	69.87%	82.45%	17.80%
90	81.54%	85.41%	88.87%	88.67%	98.62%	90.70%	91.62%	
120	97.48%	96.63%	89.92%	90.13%	100%	100%	93.44%	0.54%

Overall kinetics profiles of $Au\text{-}TiO_2$-mediated photocatalytic dye degradation for RB19 are presented in Figure 55. These results show that overall, gold cluster immobilization improves the photocatalytic activity of $P25\text{-}TiO_2$. The greatest activity is shown by 1% Au_{55}/TiO_2 200 (1% Au_{55} on TiO_2, calcinated at 200 °C), with a 98.62% decrease in concentration of RB19 after 90 minutes. This is 7% more than is achieved by pure $P25\text{-}TiO_2$ under the same conditions, in terms of total % decrease achieved under the same time (see Table 22). After 120 minutes, complete degradation (100%) is achieved by the 1% and 0.3% $Au55/TiO_2$. The average rate constants of these reactions are presented in Table 23. Here, higher catalytic activity of Au_{55} on TiO_2 compared to pure $P25\text{-}TiO_2$ under the same conditions is clearly evident as the rate is *ca.* 100% higher in the case of gold-containing catalyst (see Table 23). These results indicate that the mechanisms suggested in the literature[17,18, 19] as shown by Eqs. 34-37 are responsible for the increase in photocatalytic activity.

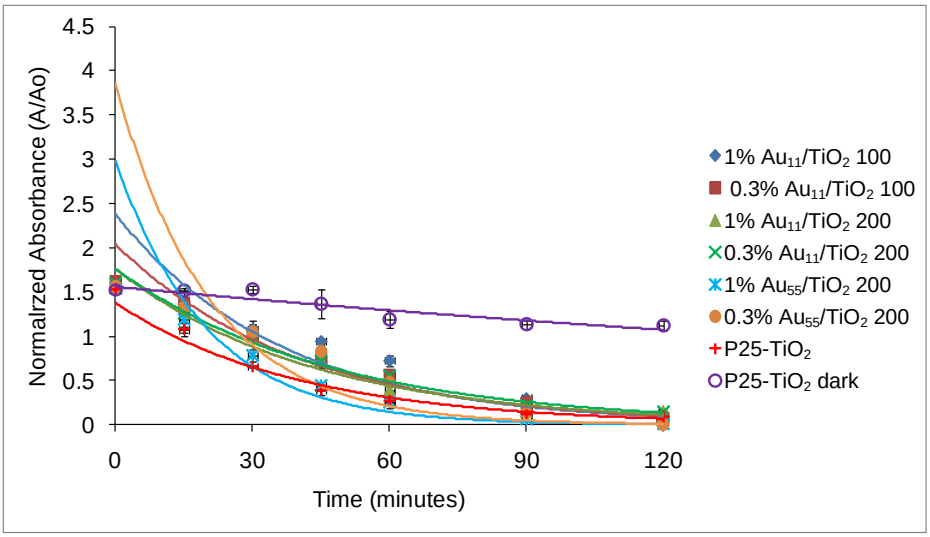

*marker data points represent the real concentration during the reaction, while lines represent the fitted concentration with the first order reaction, N = 2, errors are reported as 2σ

Figure 55: Photocatalytic activity of Au/TiO_2-mediated photocatalytic dye degradations

$$\text{Au-TiO}_2 \xrightarrow{h\nu} \text{Au-TiO}_2(e_{CB}^-) + \text{Au-TiO}_2(h_{VB}^+) \qquad \text{(Eq. 35)}$$

$$\text{Au-TiO}_2(h_{VB}^+) + \text{dye} \longrightarrow \text{degradation product} \qquad \text{(Eq. 36)}$$

$$\text{Au-TiO}_2(e^-) + \text{Au} \longrightarrow \text{Au-TiO}_2 + \text{Au}_{surf}(e^-) \qquad \text{(Eq. 37)}$$

$$\text{Au-TiO}_2(e_{CB}^-) / \text{Au}_{surf}(e^-) \longrightarrow \text{reduction reaction} \qquad \text{(Eq. 38)}$$

The main mechanism of RB19 degradation is believed to be through the hydroxyl radical-mediated oxidation resulting from the photoexcitation of TiO_2 (see Scheme 1 and 2).[19] Gold nanoparticles on the TiO_2 surface can behave as trapping sites for the photoexcited electrons, leading to localised negative charge (Eqs. 36 and 37). This charge separation becomes more efficient due to the surface barrier between TiO_2 and Au, which can then prevent undesired electron-hole pair recombination.[101]

$$H_2O_2 + e^- \longrightarrow \cdot OH + OH^- \qquad \text{(Eq. 39)}$$

$$H_2O_2 + h_{VB}^+ \longrightarrow HO_2\cdot + H^+ \qquad \text{(Eq. 40)}$$

The presence of H_2O_2 is believed to enhance the efficiency of dye photodegradation, although its presence can also reduce dye degradation efficiency by scavenging electrons and holes (see Eqs 38 and 39).[17] However in this study it was found that the presence of H_2O_2 generally enhanced the photodegradation ability of catalysts, suggesting that photodegradation enhancement occurred in preference to electron-hole scavenging.

Quite an opposite view on the possible mode of action of gold nanoparticles at the TiO_2 surface was suggested by Dozzi *et al*.[19] It was argued the gold nanoparticles could actually retard or prevent dye photodegradation. Valence band holes can act as strong oxidizing intermediates, capable of forming hydroxyl radicals by oxidizing water adsorbed on the surface of the TiO_2 particle. These radicals are an important species for dye degradation, but are also able to oxidize the gold on the surface of TiO_2 into the +1 oxidation state. The oxidized gold then can be reduced back using the photogenerated conduction band electrons, effectively reducing the localized concentration of hydroxyl radicals and also promoting electron-hole recombination.[101]

Table 23: Average rate constant of photodegradation of RB19 with various Au/TiO_2 catalysts

Catalyst	**Average rate constant ($mol.L^{-1}.s^{-1}$)**	
	0.3% Au loading	**1% Au loading**
$Au_{11}/P25\text{-}TiO_2(100\ ^0C)$	$4.21 \times 10^{-4} \pm 1.07 \times 10^{-4}$	$4.56 \times 10^{-4} \pm 5.73 \times 10^{-5}$
$Au_{11}/P25\text{-}TiO_2(200\ ^0C)$	$3.56 \times 10^{-4} \pm 2.07 \times 10^{-5}$	$3.84 \times 10^{-4} \pm 0.09 \times 10^{-5}$
$Au_{55}/P25\text{-}TiO_2(200\ ^0C)$	$8.14 \times 10^{-4} \pm 1.16 \times 10^{-4}$	$8.63 \times 10^{-4} \pm 2.40 \times 10^{-4}$
$P25\text{-}TiO_2$	$4.17 \times 10^{-4} \pm 5.17 \times 10^{-5}$	

*errors are reported as Δ

Furthermore, gold nanoparticles of a smaller size can be even more reactive.[19] This could possibly explain the results obtained in the photocatalytic tests using Au_{11}/TiO_2, which demonstrate lower activity than Au_{55}/TiO_2 in all cases. Due to the higher surface area, Au_{11} clusters will be more active than Au_{55} clusters, and thus provide more sites for H_2O_2 recombination. However, it is possible that

larger gold particles could result from aggregation of Au_{11}. An HRTEM and XPS study of the catalysts is needed to clarify this; unfortunately, this is not yet finished.

The data presented in Table 22 demonstrates that each set of conditions gives a different dye degradation rate, suggesting that all factors (gold cluster type, gold loading, and calcination temperature) affect the catalytic activity of the sample. The plots of ln[C] *vs.* time of these reactions can be seen in Appendix 1.

4.3.1 Recyclability of the catalyst

In order to be truly industrially relevant, a catalyst must be recyclable. It should be possible to re-use the catalyst after separating it from the product mixture in further photodegradation reactions without an appreciable drop in activity. To examine the recyclability of the catalysts, a set of experiments was performed using 1% Au_{11}/P25-TiO_2 100:

A: Photocatalytic degradation for RB19 with the same procedure and regular sampling, as in the previous catalytic tests.

B1: Same setup as A, but without regular sampling (to avoid loss of the catalyst). At the end of the reaction, the catalyst was recovered as fully as practically possible for further use.

B2: photocatalytic degradation for RB19 as outlined in A, using the catalyst recovered in B1, with regular sampling as usual.

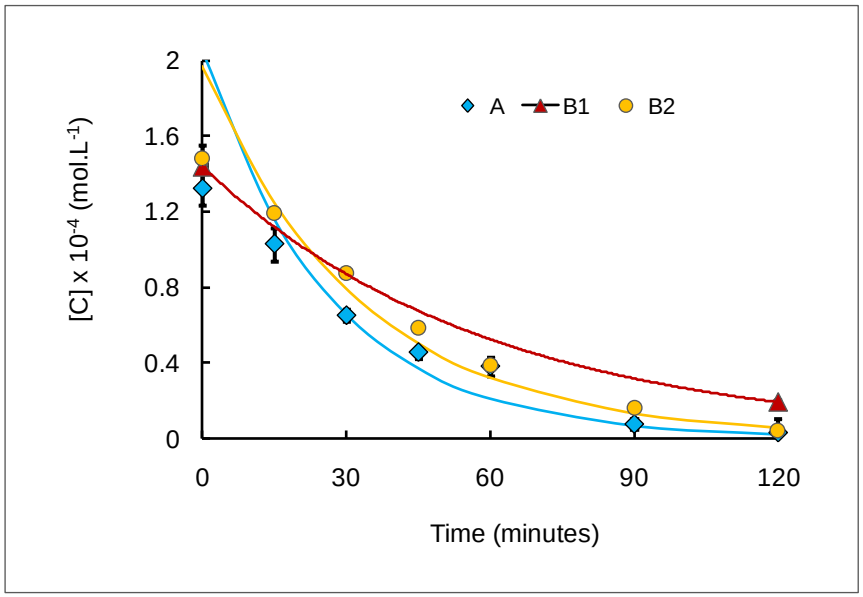

*marker data points represent the real concentration during the reaction, while lines represent the fitted concentration with the first order reaction, N = 2, errors are reported as Δ

Figure 56: Recyclability of 1%Au_{11}/TiO_2

Figure 56 clearly confirms excellent recyclability of the catalyst 1% Au_{11}/TiO_2 100. While other catalysts were not studied for recyclability due to the time limitation, the result obtained in the case of 1% Au_{11}/TiO_2 100 catalyst is quite encouraging.

4.3.2 SiO_2-supported Au/TiO_2 ($Au/TiO_2/SiO_2$)

This sub-section presents the photocatalytic performance of Au_{55}/e-TiO_2/SiO_2 catalysts for the photodegradation of RB19. This particular catalyst was prepared based on previous results that demonstrated both e-TiO_2 and Au_{55}/P25- TiO_2 were active photodegradation catalysts. Au_{55} nanoparticles have been deposited on the e-TiO_2 support (1% of Au by weight), which was then immobilized on SiO_2 support (3% of TiO_2 by weight).

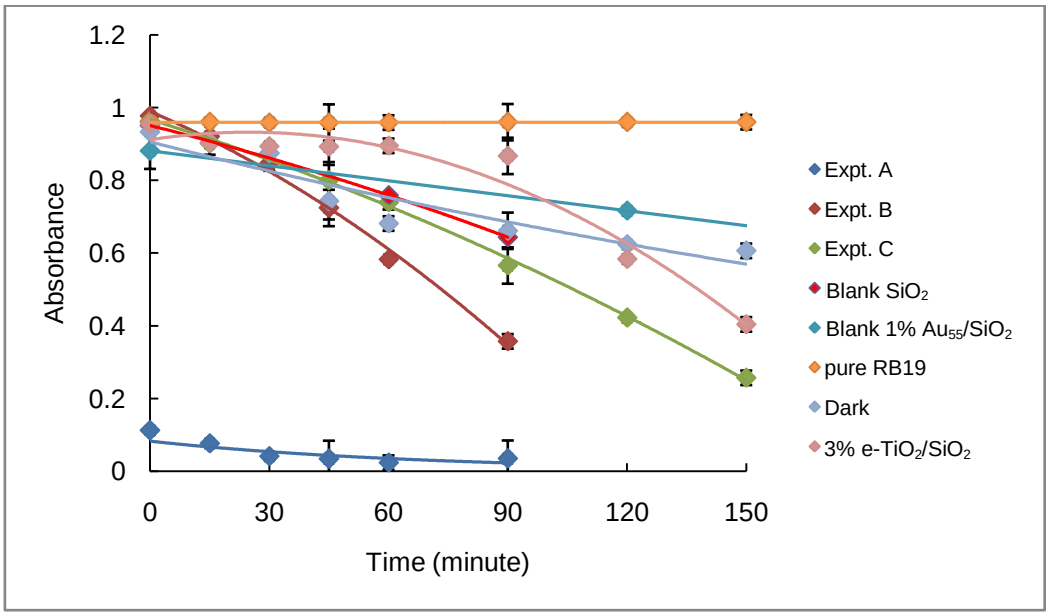

Figure 57: Photocatalytic performance of RB19 with 1%Au_{55}/3%e-TiO_2/SiO_2

(N = 2, errors are reported as Δ)

In the first experiment using 1%Au_{55}/3%e-TiO_2/SiO_2, a dramatic decrease in absorbance of the dye solution (more than 95%) was observed before UV irradiation, indicating that a high proportion of the dye had been adsorbed on the catalyst surface (see expt. A in Figure 57). To confirm this result, repeats of the experiment using the catalyst from the same batch were carried out (see expt. B and C in Figure 57). As shown by the graph, for experiments B and C there was no significant adsorption of dye on the catalyst surface in the time between dye addition and UV irradiation. While dye degradation is observed for these two systems, complete degradation is never achieved, even after 150 minutes irradiation. These results suggest that experiment A can be considered an abnormality, possibly caused by heterogeneity in the Au/TiO_2 dispersion when it was immobilized on SiO_2. In experiments B and C, it is assumed that the photocatalytic degradation is the main cause of colour removal, but there is also the possibility that colour removal is due to dye adsorption (without degradation) on the catalyst surface during the photocatalysis process. This can be tested by comparison of the results of experiments B and C with that of a SiO_2 blank carried out under UV irradiation. This system shows a similar photodegradation profile to that shown by experiment C. As

SiO_2 is known to be UV inactive, this suggests that the main cause of colour removal in this system is dye adsorption rather than dye degradation.

To test the abovementioned assumption, a series of experiments were carried out to examine the adsorption ability of this catalyst. Three different initial concentrations of RB19 in aqueous solution were prepared. The catalyst 1% Au_{55}/3% e-TiO_2/SiO_2 from the same batch as before was added to each dye solution. No H_2O_2 was added to the mixtures. The mixtures were left in the dark with constant stirring, with regular samplings until 150 minutes had passed.

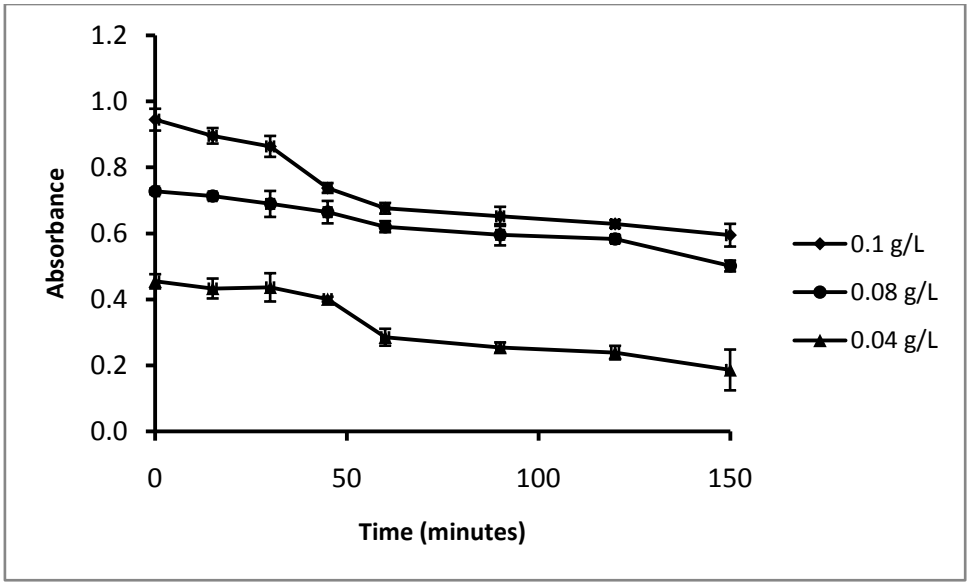

Figure 58: Adsorption profiles of RB19 on 1%Au_{55}/3%e-TiO_2/SiO_2

(N = 2, errors are reported as Δ)

The results presented in Figure 58 show that after 45 minutes, considerable adsorption tends to occur in the three systems. While systems appear to reach adsorption equilibrium relatively quickly, further adsorption is observed at or past 120 minutes. These results confirm the high adsorption affinity of photoactive TiO_2 in the catalyst. The adsorption profile of RB19 on blank SiO_2 under the same conditions presented in Figure 59 shows that pure SiO_2 does not give significant adsorption at any concentrations of the dye.

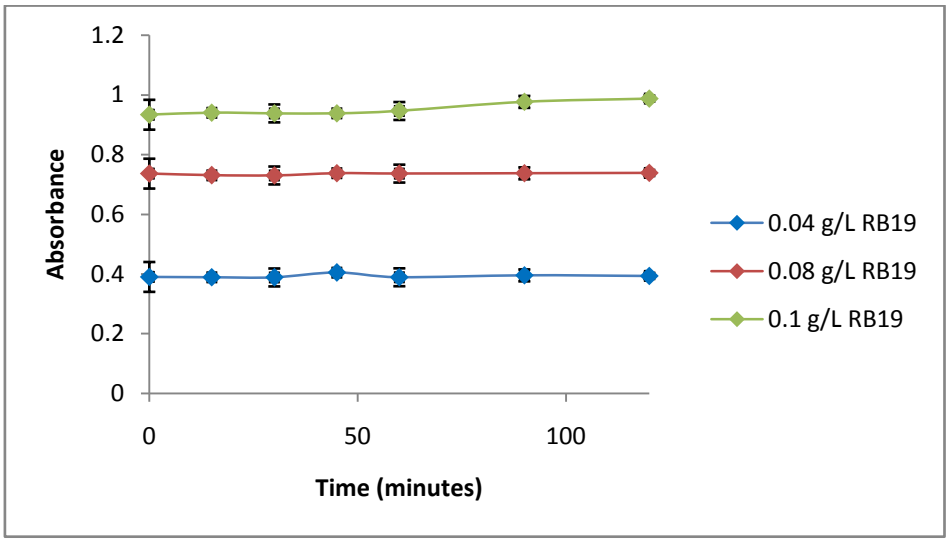

Figure 59: Adsorption profiles of RB19 on pure SiO_2

(N = 2, errors are reported as Δ)

As discussed earlier, TiO_2 is the main component of the catalyst system contributing to the photocatalytic activity, either when it acts as support for gold nanoparticles or when it is immobilized on an SiO_2 support. Therefore, the amount of TiO_2 loading is expected to play a vital part in the photocatalytic activity of the catalyst.

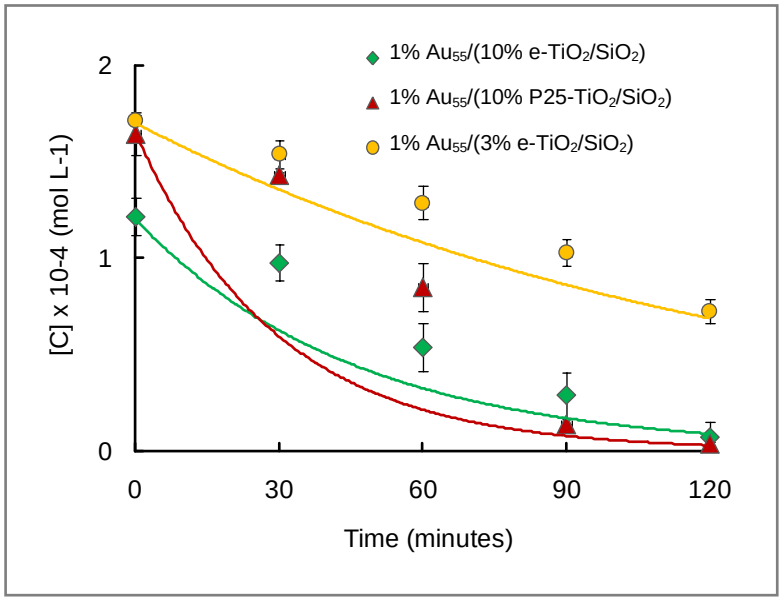

Figure 60: Effect of different TiO_2 loadings on SiO_2-supported Au_{55}/TiO_2-assisted photocatalysis of RB19

(N = 2, errors are reported as Δ)

Table 24: Average rate constants of photocatalytic degradation of RB19 using Au/e-TiO_2/SiO_2 with different loadings of e-TiO_2 (N = 2, errors are reported as Δ

Catalyst	Average rate constants ($mol.L^{-1}.s^{-1}$)
1%Au_{55}/10%e-TiO_2/SiO_2	$4.55\times10^{-4} \pm 2.18\times10^{-4}$
1%Au_{55}/10%P25-TiO_2/SiO_2	$7.19\times10^{-4} \pm 6.74\times10^{-5}$
1%Au_{55}/10%e-TiO_2/SiO_2	$1.50\times10^{-4} \pm 6.99\times10^{-6}$

The photocatalytic degradation of RB19 shown in Figure 60 demonstrates that with higher TiO_2 loading, the photocatalytic activity of the catalyst increases. The amount of catalyst added to these systems was equivalent to the amount of TiO_2 as was done to the other photocatalytic reactions (*i.e.* equivalent to 10% by weight of TiO_2). Here, the role of gold is also not clear because of the many variables that may affect the system. Further studies are required to assess the importance and efficiency of immobilizing an Au/TiO_2 catalyst on SiO_2 support. The average rate constants of these reactions are presented in Table 24.

Chapter 5 – Experimental

This chapter presents the experimental procedures carried out during this study, including photocatalytic reactions using various catalysts, catalytic reactions at room temperature and 70 ^{o}C, adsorption studies, and characterization of the dye solutions using UV-Vis spectroscopy. This study did not focus on the synthetic procedures behind the production of TiO_2, however, procedures for synthesis of the catalysts used are presented at the last part of this chapter.

As mentioned in Chapter 3, the term "catalytic reaction" is used in this study to refer to all reactions carried without exposure to UV irradiation (*i.e.* in the darkness), while reactions under UV irradiation are referred to as "photocatalytic reactions". All catalytic and photocatalytic reactions have been carried out at least twice, to test the reproduceability of each experiment. All data collected in this way have been averaged and reported with an uncertainty of *delta* (Δ, the difference between average and each individual measurement).

5.1 Materials and apparatus

The P25-TiO_2 (made by Degussa/Evonik) catalyst was obtained from Chemiplas NZ Ltd., while the other synthesized catalysts were prepared by Jan-Yves Ruzicka and David Anderson, both Ph.D. students in the Golovko group. All dyes used in this study were obtained from the Laboratory of Physical Chemistry of Dyeing, Department of Textile Chemistry at the Institute of Textile Technology in Bandung, Indonesia. The chemical structures of the dyes used in this study are presented in Figure 37 (Chapter 4). Milli-Q purified water was used to dissolve the dyes. Hydrogen peroxide (H_2O_2) was the only oxidant used in all experiments. Sodium hydroxide (NaOH, 0.5M) and acetic acid (CH_3COOH, 0.35M) were used for pH adjustment.

Photocatalytic reactions were carried out in a custom-built photocatalytic chamber made by mechanical and electrical workshops at the Department of Chemistry, University of Canterbury (see

Figure 61), which used a 500W Xe lamp ($\lambda \leq 380$nm) to provide UV irradiation. Water and nitrogen gas flow were used to cool the system during irradiation. Reagents were placed in a quartz tube reaction vessel designed for photocatalytic reactions, and the vessel was placed at a fixed distance (20 cm) from the light source. Sample collection was performed during photocatalysis *via* a syringe equipped with a long needle which could be inserted into the reaction vessel from outside the chamber for this purpose. Typically, 1.5 mL of reaction mixture/suspension was collected with a cycle of filling/emptying the syringe 3 times before collecting a final aliquot. All these procedures were performed without interruption to stirring and UV-irradiation. An "ILT 1700" photometer (International Light Technologies) with SED033 detectors, *i.e.* 33 mm^2 silicone detectors for xenon flash lamp (QNDS2 type for spectral range of 326 – 401 nm and Y/W type for spectral range of 400 – 700 nm) was used to monitor the intensity of the light.

Room temperature catalytic reactions were carried out in a 250 mL three-neck round bottom flask, with stirring provided by a Teflon-coated magnetic stirrer. The flask was carefully wrapped in aluminium foil to prevent ambient light from affecting the "catalytic" reaction. Reactions were performed under an atmosphere of nitrogen gas; the setup is shown in Figure 63. A similar setup was used for catalytic reactions at 70 ^{o}C, with heating provided by an oil bath, and the evaporation being prevented by use of a double-jacket condenser (see the setup in Figure 64).

An "Elmasonic" ultrasonicator and "Eppendorf" centrifuge were used for sonication (5-10 minutes) and centrifugation (11k rpm, 3 minutes).

A Cary 100 Bio UV-Vis spectrophotometer was used to measure the absorption of dye solutions using two 1 cm polished quartz cuvettes, one for the sample solution and one for the background correction using water. For quantitative comparison of reactions, the absorbance was taken at the maximum absorbance wavelength of the dye.

5.2 Photocatalytic reactions

5.2.1 Preparation of reaction mixtures

For all photocatalytic reactions involving non-basic dyes, dye solutions were prepared with concentrations of 0.1 g/L. Basic dye (MB, BB41, and BY67) solutions were prepared with concentrations of 0.01 g/L due to their high comparative absorbance. Table 25 lists the details of the dyes used, including concentrations in mol/L and maximum absorbance wavelength.

The standard concentration for "pure" (unsupported) catalysts used in this study was 0.5 g/L; the exception to this was for experiments with custom-made TiO_2 (as discussed in Section 4.2.1), which used catalyst concentrations of 0.1 g/L. For both TiO_2-SiO_2 and Au/TiO_2-SiO2 catalysts, concentrations were calculated to give a total TiO_2 concentration of 0.5 g/L. Finally, the standard amount of H_2O_2 was 0.05 g/L ($1.471x10^{-3}$ mol/L).

Table 25: Details of the dyes

Dyes	FW ($g.mol^{-1}$)	C ($mol.L^{-1}$)	λmax (nm)*
CI Reactive Blue 19 (RB19)	626.55	$1.60x10^{-4}$	594.00 ± 3.16
CI Acid Red 42 (AR42)	467.37	$2.14x10^{-4}$	512.00 ± 3.16
CI Disperse Yellow 211 (DY211)	347.64	$2.88x10^{-4}$	499.20 ± 2.24
Methylene Blue (MB)	320.18	$3.12x10^{-5}$	664.00 ± 0.00
CI Basic Blue 41 (BB41)	482.36	$2.07x10^{-5}$	605.60 ± 2.74
CI Basic Yellow 67 (BY67)	unknown	unknown	454.80 ± 4.18

*maximum wavelength of the dye taken from at least 5 times measurements

Errors were reported as 5*STDEV (5×standard deviations)

5.2.2 Procedure

Reagents (catalyst and dye solution) were mixed in a quartz tube reaction vessel. The mixture was sonicated for 5-10 minutes, followed by the addition of H_2O_2. When required, the pH of the resulting suspension was adjusted between sonication and addition of H_2O_2.

The suspension was then left in the chamber (see Figure 61) in the dark with constant stirring; for basic dyes, stirring in the dark was performed for 30 minutes, for all other samples 15 minutes was sufficient. This allowed dye adsorption to reach equilibrium before UV irradiation started. The first sample was taken just after mixing the dye solution and the catalyst.

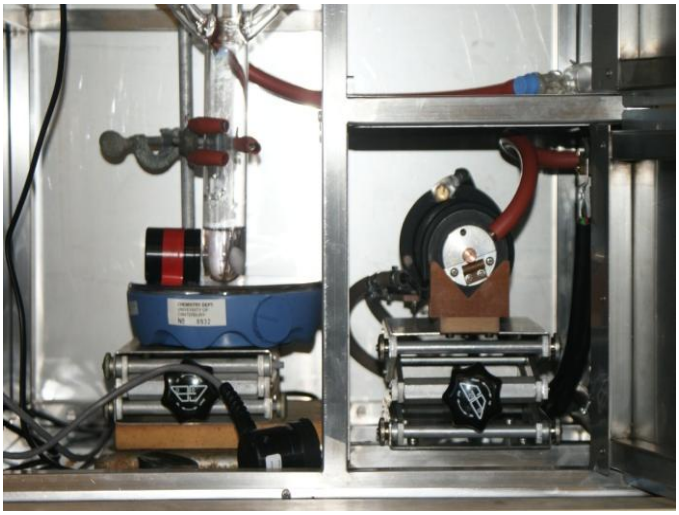

Figure 61: Photocatalytic chamber in the laboratory of the Golovko group

Figure 62: The photometer ILT 1700

During UV irradiation, the flux (W/cm^2) light radiation in the chamber was monitored by the ILT 1700 photometer (see Figure 62).

5.3. Catalytic reaction at room temperature and 70 °C

Catalytic reactions have been carried out in the preliminary stage of this study (during construction of the photocatalytic set-up). RB19 was the only dye used for these reactions. The dye concentration was the same as that of a standard photocatalytic reaction, but the catalyst and oxidant were added in different amounts as detailed in Chapter 3.

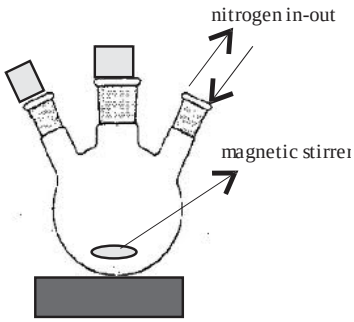

Figure 63: Experiment setup for catalytic reaction at room temperature
(the flask was entirely covered by aluminium foil)

Catalytic reactions at room temperature were performed in a round-bottom flask with a constant nitrogen gas flow (see Figure 63). For the "*all-in*" method, all reagents were mixed at the beginning of the reaction, and then stirred constantly. For the "*Step-by-Step*" method, the catalyst was first mixed with dye solution. A sample was taken after 1 minute of stirring and then measured by UV-Vis spectroscopy. Subsequent samples were collected every 30 minutes. Stability was assumed to be achieved when the absorbance of the solution remains constant over 2-3 samples (see the data in Table 10 at 31, 61, and 91 minutes). At this point it was assumed that adsorption equilibrium had been reached, although in further studies it was found that no equilibrium state was observed for RB19. H_2O_2 was added after the adsorption equilibrium had been reached. Catalyst-only and oxidant-only blank reactions in dye solution were also carried out.

Catalytic reactions at 70 °C were also carried out in darkness with the experimental setup shown in Figure 64. The catalyst was mixed with the dye solution, and the solution was assumed to have reached adsorption equilibrium after 30 minutes based on adsorption data collected at room temperature. Heating was started after adsorption equilibrium was reached, *i.e.* 30 minutes after catalyst addition to the dye solution. H_2O_2 was added after the temperature had equilibrated at 70 °C. Two blank reactions were also carried out: catalyst-only (no oxidant) and oxidant-only (no catalyst).

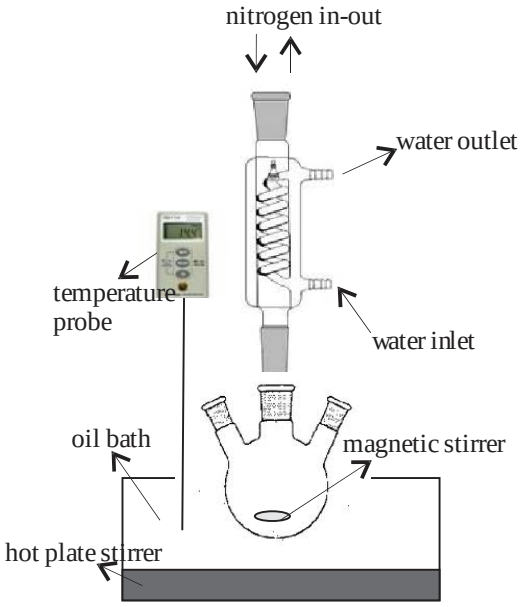

Figure 64: Experiment setup for catalytic reaction at 70 °C

(the three-neck round bottom flask was entirely covered by aluminium foil)

5.4 Adsorption study

As discussed in Chapters 3 and 4, the adsorption study was performed with a focus on particular dyes and catalysts. In a typical adsorption study, the dye solution was prepared at three (or more) different concentrations, to which catalyst was then added. The mixture was sonicated for 5-10 minutes to ensure the formation of a homogeneous suspension. The suspension was then stirred constantly in the dark (similarly to the catalytic reactions). Samples were taken at regular intervals.

5.5 Measurement of dye solution with UV-Vis spectroscopy

All samples from both catalytic and photocatalytic reactions were analysed by UV-Vis spectroscopy. Absorbance measurements were taken at the maximum absorbance wavelength of each dye. To determine the maximum absorbance wavelength of a dye, five dye solutions of different concentrations (typically ≤ 0.1 g/L) were prepared and then analysed by UV-Vis spectrometry. Each sample solution was measured twice, and the average wavelength of maximum absorbance was taken. The final determination of the maximum wavelength was taken from the average of the five averaged wavelengths. The error of this measurement was reported as 5 standard deviations of the data.

For kinetic analysis, the concentration of dye solutions was calculated from the calibration curve of each dye. To make the calibration curve, 10 different dye solutions of varying concentrations were prepared. Concentrations were picked to give absorbance values of between 0 and 1. All samples were then analysed by UV-Vis spectrometry: a plot of absorbance against concentration should then give a linear relationship. From this it was possible to calculate the constants *a* and *b* by linear regression to satisfy the equation $A = ac + b$, where A is the absorbance of the sample and c the concentration of the dye solution.

5.6 Synthesis of Catalysts (procedures)

5.6.1 Preparation of custom-made photocatalysts e-TiO_2 and c-TiO_2

Titanium butoxide ($Ti(OBu)_4$, 0.4M) and distilled water (6M) were dissolved in equal volumes of ethanol to give a two solutions in which the concentration of $Ti(OBu)_4$ and H_2O were 0.2M and 3M respectively. These two solutions were mixed, and the resultant solution immediately turned opaque white. This solution was stirred rapidly under nitrogen for four hours. According to previous literature results,[68] 95% of the titanium butoxide originally present in solution had reacted by this stage.

If the product was required as a powder, the solvent would then be evaporated by heating under reduced pressure and the resulting solid was washed with water and dried. If the resulting product was required as a sol (*e.g.*for immobilisation on SiO_2 support or deposition of gold nanoparticles on TiO_2) it may be left in solution.

The catalyst c-TiO_2 was produced by calcining powder e-TiO_2 at 500 $^{\circ}$C for two hours to induce crystallization.

5.6.2 Preparation of p-TiO_2

In a typical synthesis, titanium **tert**-isopropoxide (TTIP, 1.8g) was added to ethanol (3.6 mL) with stirring. Distilled water (40 mL) was added and white titanium hydroxide [$Ti(OH)_4$] was formed. The mixture was stirred for 10 minutes before being washed with water. The precipitate was recovered by centrifugation and redispersed in distilled water (180 mL). Hydrogen peroxide (H_2O_2, 2.31 g of 50% w/w solution in water) was added dropwise with vigorous stirring resulting in formation of a yellow opaque solution. The solution was stirred for an hour, after which time the transparent yellow peroxotitanic acid sol had formed. The sol was heated at 97 $^{\circ}$C under reflux for 24 hours, and over this time the opaque white titanium dioxide suspension was formed. The solid product was recovered using centrifugation (5000 rpm, 10 minutes) and washed several times with water and ethanol, before being dried.

5.6.3 Synthesis of Au_{55} Cluster $[Au_{55}(PPh_3)_{12}Cl_6]$[72]

A solution of tetrachloroauricacid (1g, 2.54 mmol) in milli-Q water (60 mL) was stirred vigorously for 5 minutes. Toluene (60 mL) was added to the stirred solution, followed by tetraoctylammonium bromide (1.40g, 2.56 mmol). There was an immediate colour change where the aqueous layer became colourless and the organic layer developed a red colour. After 5 minutes, triphenylphosphine (2.3g, 8.76 mmol) was added to the stirred biphasic solution. Upon addition of the triphenylphosphine the

organic layer turned cloudy white. After 10 minutes of vigorous stirring, a solution of freshly dissolved sodium borohydride (2.0g, 5.29 mmol) in Milli-Q water was rapidly added to the reaction mixture. The aqueous and organic layers were separated and the organic layer was washed 3 times with 100 mL of deionised water. The organic layer was separated, filtered to remove precipitates, and evaporated to dryness under flowing nitrogen. The crude product was dissolved in chloroform (40 mL), and pentane (300 mL) was added to precipitate the product. The suspension was filtered through a fritted funnel to collect the solid, crude nanoparticles. The product was then washed with the following solvent combinations to remove the excess tetraoctylammonium bromide:

- 2 x 100 mL hexanes followed by 100 mL 2:3 MeOH : H_2O
- 2 x 100 mL hexanes followed by 100 mL 1:1 MeOH : H_2O
- 100 mL hexanes

If a large amount of tetraoctylammonium bromide remained, the product was washed with 1:1 MeOH : H_2O followed by hexanes. Next the product was washed on the same frit with the following solvent combinations to remove $Au(PPh_3)Cl$:

- 2 x 150 mL 3:1 pentane : chloroform
- 2 x 150 mL 2:1 pentane : chloroform
- 2 x 150 mL 1:1 pentane : chloroform

During each pentane : chloroform wash, the product was agitated and allowed to soak in the wash solution for 5 minutes. The purified product was rinsed through the frit with dichloromethane and dried under reduced pressure. The purity of the gold nanoparticles is confirmed by ^1H NMR spectroscopy in $CDCl_3$.

5.6.4 Synthesis of $Au_{11}(PPh_3)_8Cl_3$

A solution of sodium borohydride (0.3491g, 0.01 mol) in ethanol was added dropwise to a suspension of $Au(PPh_3)Cl$ (4.4464g, 0.013 mol) in ethanol (220 mL) over a 15 minute period. The white suspension immediately started to change to an orange-red solution. The reaction was left to stir for 2 hours, after which period it was poured into hexane (1 L) and allowed to precipitate overnight. The

brown solid was filtered off on a sintered glass funnel and then washed with hexanes (4 × 25 mL), dichloromethane/hexanes (4 ×25 mL) and dichloromethane/hexanes (4 × 25 mL). The remaining solid was dissolved in dichloromethane and filtered through the sintered glass funnel to remove any insoluble by-products. The cluster was recrystallised from a concentrated solution in dicholormethane by vapour diffusion of diethyl ether, resulting in deep red platelets.

5.6.5 Preparation of Au/TiO_2

In a Schlenk tube, Degussa P25-TiO_2 (10 g) was heated at 200 °C (oil bath, magnetic stirrer) under vacuum for 2 hours to remove any moisture absorbed during storage. The titania was cooled under nitrogen to room temperature, and methanol (HPLC grade, 40 mL) was added. The suspension was stirred vigorously under nitrogen for 5 minutes. The gold cluster was dissolved in methanol (40 mL) and rapidly added to the suspension of titania *via* syringe. After 2 hours of stirring, the suspension was left to settle by gravity and the supernatant was syringed off. The precipitate was then washed alternately by methanol and pet ether. Finally, the sample was dried under vacuum.

To calcine these catalysts, the powders were heated to 200 °C (oil bath, magnetic stirrer) under vacuum for 2 hours and then cooled under nitrogen.

5.6.6 Preparation of TiO_2/SiO_2

SiO_2 (5 g) was dispersed in ethanol (50 mL) and added to a dispersion of TiO_2 in ethanol. As previously mentioned there was no drying or cleaning step carried out between synthesis and immobilization on SiO_2. The mixture was stirred for at least 30 minutes and the solvent was then removed under reduced pressure. Once the catalyst was dried, it was calcinated at 200 °C under vacuum for two hours to immobilize TiO_2 on the SiO_2 surface.

5.6.7 Preparation of Au/SiO_2

In a Schlenk tube, SiO_2 (10 g) was heated to 200 $^{\circ}$C under vacuum for 2 hours. The silica was then cooled under nitrogen and then methanol (HPLC grade, 40 mL) was added. The suspension was stirred vigorously under nitrogen for 5 minutes. The gold loading was calculated using the mass of only the gold metal core of the cluster, *e.g.* excluding mass of the ligands. For example, for 1 % loading, 0.110g of Au_{55} or 0.215g of Au_{11} was used. The cluster was dissolved in methanol (40 mL) and rapidly added to the silica suspension. After 2 hours of stirring, the suspension was left to settle by gravity under nitrogen gas and the supernatant was syringed off. The sample was then washed alternately with methanol and hexanes and dried under vacuum. For the Au_{55} clusters, dichloromethane was used as the solvent rather than methanol.

To remove the organic protecting layer on the surface of the clusters, it was necessary to calcine the catalysts. This process involved heating the catalysts at very high temperatures (up to 500 °C), which can result in particle sintering and subsequently decrease the activity of the catalyst. For this study, the powders of catalysts were heated at 200°C under vacuum for 2 hours and then cooled under nitrogen.

5.6.8 Preparation of $Au/TiO_2/SiO_2$

A suspension of Au_{55} was formed in dichloromethane, and this colloidal solution was added to a dispersion of TiO_2 in ethanol. The mixture was allowed to stir for an hour at room temperature accompanied by a colour change from red (unsupported Au55) to purple (Au on TiO_2) indicative of increasing interaction between the Au nanoparticles and the support. After the immobilization of gold nanoparticles was accomplished, the solvent was removed under vacuum, and the material of a catalyst was redispersed in 50 mL ethanol. Immobilization of Au/TiO_2 active ingredient on Silica addition was then performed as detailed in Section 5.1.6.

Chapter 6 – Conclusion and Further Study

6.1 Conclusion

In this study it was found that TiO_2-mediated photocatalytic degradation is an efficient process for dye removal from a wastewater. The results obtained show that photodegradation using titanium dioxide nanoparticles as a photocatalyst is comparatively more efficient than purely chemical catalytic (*e.g.* non-light mediated) degradation, even if the latter was performed at elevated temperature.

The rate of dye degradation is affected considerably by the parameters of the system. In this study it has been shown that pH may affect the degradation rate by changing the ionization properties of both the catalyst surface and the dye. Different dyes, having different chemical structures and thus different pathways of reacting to changes in pH via protonation, deprotonation, or cleavage of chemical bond, will respond differently to changes in pH. In general, at pH $\leq$ 6.8 (the zero charge point for TiO_2), reactions proceeded faster than those at higher pH.

Six dyes from four different classes were used in this study, and all showed different photodegradation behaviour. RB19 (reactive dye) and AR42 (an acid dye) showed relatively similar activity as both are anionic in nature and possess a sulphonic group, which makes them water-soluble. These dyes exhibited a very low propensity to get adsorbed on TiO_2. DY211 (a disperse dye) demonstrated extremely high adsorption on TiO_2, and did not undergo photocatalytic degradation. In addition, MB, BB41, and BY67 (all basic dyes) showed high adsorption and rapid photocatalytic degradation.

Compared with other TiO_2 catalysts, e-TiO_2 showed greater activity than P25-TiO_2 and other custom-made catalysts (c-TiO_2 and p-TiO_2) in all photocatalytic tests. It is hypothesized that this particular photocatalyst displayed such a high activity due to its high surface area.

Immobilisation of gold nanoparticles on the surface of the TiO_2 was proven to enhance the photocatalytic activity of the catalyst in the case of Au_{55}. This finding correlates well with literature reports suggesting that gold nanoparticles can scavenge photoexcited electrons from the conduction band of the TiO_2 support, inhibiting the electron-hole pair recombination and thus facilitating photocatalytic processes by maintaining a high number of longer-living holes. However, this pattern in reactivity is reversed in the case of smaller gold nanoparticles (Au_{11}) as is shown by the higher activity of Au_{55}/TiO_2 as compared to Au_{11}/TiO_2. This is an interesting size-dependant property of such systems which warrants further and detailed study. Recyclability studies on a sample Au_{11}/TiO_2 catalyst demonstrated that these catalysts do not lose activity after being used for photodegradation.

Immobilisation of TiO_2 or Au/TiO_2 on SiO_2 resulted in lower catalyst activity compared to the pure, unsupported-active components in all photocatalytic tests in this study. However, increasing the loading of TiO_2 on SiO_2 was shown to positively affect the activity of the catalyst.

Most photocatalytic degradation reactions displayed first-order character. Confirmation of the first order character is shown by the linear relationship between ln[C] and t of these reactions (Appendix 1).

6.1 Further Study

Due to factors discussed earlier, this study was severely time-limited and lacked the originally planned in-depth analysis of the degradation products of the various dyes studied. Further study on these products should be attempted using total organic carbon analysis (TOC), high-performance liquid chromatography (HPLC), mass spectrometry and other techniques. These will shed light on the degradation pathways of the dyes used, as well as the applicability of these degradation reactions to real-world industrial applications.

The application of photocatalytic reactions to real wastewater processing is another interesting facet to be studied further. The most cost-effective solution (trade-off between efficiency and cost) would be to trial one of the more simple methods e.g. by using e-TiO_2 with H_2O_2.

References

1. Manual Best Management Practices for Pollution Prevention in the Textile Industry. In *EPA/625/R-96/004* September 1996 ed.; U.S. Environmental Protection Agency. 1996.
2. Zollinger, H., *Color Chemistry: Synthesis, Properties and Applications of Organic Dyes and Pigments*. 2nd ed.; VCH: 1991.
3. Catoor, T., European legislation relating to textile dyeing In *Environmental aspects of textile dyeing* Christie, R. M., Ed. Woodhead Publishing Limited: Cambridge, 2007; pp 1-29.
4. Spagni, A.; Grilli, S.; Casu, S.; Mattioli, D., *International Biodetorioration and Biodegradation* **2010,** *64*, 676-681.
5. Koprivanac, N.; Kusic, H., Hazardous Organic Pollutants in Colored Wastewaters. Nova Science Publishers: New York, 2009.
6. Mahmoodi, N. M.; Arami, M., *Journal of Photochemistry and Photobiology B: Biology* **2009,** *94*, 20-24.
7. Akyol, A.; Yatmaz, H. C.; Bayramoglu, M., *Applied Catalysis B-Environmental* **2004,** *54* (1), 19-24.
8. Baldrian, P.; Merhautova, V.; Gabriel, J.; Nerud, F., *Applied Catalysis B: Environmental* **2006,** *66*, 258-264.
9. Somensia, C. A.; L, E.; Simionattoa; L, S.; Bertoli; Jr, A. W.; Radetskib, C. M., *Journal of Hazardous Materials* **2010,** *175*, 235-240.
10. Christie, R. M., *Colour Chemistry*. Royal Society of Chemistry: 2001.
11. Uddin, M. J.; Cesano, F.; Scarano, D.; Bobibo, F.; Agostini, G.; Spoto, G.; Bordiga, S.; Zecchina, A., *Journal of Photochemistry and Photobiology B: Biology* **2008,** *199*, 64-72.
12. Hashimoto, K., *Japanese Journal of Applied Physics* **2005,** *44* (12), 8269-8285.
13. Papic, S.; Koprivanac, N.; Bozic, A. L.; Vujevic, D., *Water Environment Research* **2006,** *78* (6), 572.
14. Sung-Suh, H. M.; Choi, J. R.; Hah, H. J.; Koo, S. M.; Bae, Y. C., *Journal of Photochemistry and Photobiology A: Chemistry* **2004,** *163*, 37-44.
15. Anipsitakis, G. P.; Dionysiou, D. D., *Applied Catalysis B: Environmental* **2004,** *54*, 155-163.
16. Sakthivel, S.; Shankar, M. V.; Palanichamy, M.; Arabindoo, B.; Bahnemann, D. W.; Murugesan, V., *Water Research* **2004,** *38*, 3001-3008.
17. Kumar, P. S. S.; Sivakumar, R.; Anandan, S.; Madhavan, J.; Maruthamuthu, P.; Ashokkumar, M., *Water Research* **2008,** *42*, 4878-4884.
18. Yogi, C.; Kozima, K., *J. Mater Sci.* **2009,** *44*, 821-827.
19. Dozzi, M. V.; Prati, L.; Canton, P.; Selli, E., *Physical Chemistry Chemical Physics* **2009,** *11* (33), 7171-7180.
20. Turner, M.; Golovko, V. B., *Nature* **2008,** *07194*.
21. Koenderink, J., *Color for the Science*. The MIT Press: London, 2010.
22. Broadbent, A. D., Basic Principles of Textile Coloration. Society of Dyers and Colourists: West Yorkshire, England, 2001.
23. Nassau, K., *The Physics and Chemistry of Color*. 2nd ed.; John Wiley & Sons, Inc.: 2001.

24. Shore, J., Classification and general properties of colorants In *Colorants and Auxiliaries Organic Chemistry and Appllication Properties*

2ed.; Shore, J., Ed. Society of Dyers and Colourists: West Yorkshire, UK, 2002; Vol. 1, pp 1-44.

25. Atkins, P.; Paula, J. D., *Atkins' Physical Chemistry*. 9 ed.; Oxford University Press: Oxford, 2010.

26. Renfrew, A. H. M., *Reactive Dyes for Textile Fibres: The Chemistry of activated π-bonds as reactive groups and miscellaneous topics*. Society of Dyers and Colourists: Bradford, 1999.

27. Clayden, J.; Greeves, N.; Warren, S.; Wothers, P., *Organic Chemistry*. Oxford University Press: Oxford, 2001.

28. Beech, W. F., *Fibre-Reactive Dyes*. Logos Press Limited: London, 1970.

29. Hardin, I. R., Chemical treatment of textile dye effluent. In *Environmental aspects of textile dyeing*, Christie, R. M., Ed. Woodhead Publishing Limited: Cambridge, 2007.

30. Konstantinou, I. K.; Albanis, T. A., *Applied Catalysis B: Environmental* **2004,** *49*, 1-14.

31. Pearce, C. I.; Lloyd, J. R.; Guthrie, J. T., *Dyes and Pigments* **2003,** *58*, 179-196.

32. O'Neil, C.; Hawkes, F. R.; Hawkes, D. L.; Lourenco, N. D.; Pinheiro, H. M.; Delee, W., *Journal of Technology and Biotechnology* **1999,** *74*, 1009-1018.

33. Bae, J. S.; Freeman, H. S., *Dyes Pigments* **2007,** *73* (1), 81-85.

34. Verma, Y., *Toxicology and Industrial Health* **2011,** *27* (1), 41-49.

35. Gregory, P., Toxicology of textile dyes. In *Environmental aspects of textile dyeing*, Cristie, R. M., Ed. Woodhead Publishing Limited: Cambridge, 2007.

36. Hunger, K., *Chimia* **1994,** *48*, 520-522.

37. Golka, K.; Kopps, S.; Myslak, Z. W., *Toxicology Letters* **2004,** *151*, 203-210.

38. Moller, P.; Wallin, H., *Mutation Research* **2000,** *462*, 13-30.

39. Sichel, S.; Tello, J.; Cara, M. D.; Fernandez-Ibanez, P., *Catalysis Today* **2007,** *129*, 152-160.

40. Fujishiima, A.; Zhang, X., *C. R. Chimie* **2006,** *9*, 750-760.

41. Fujishima, A.; Zhang, X.; Tryk, D. A., *International Journal of Hydrogen Energy* **2007,** *32*, 2664-2672.

42. Fujishima, A.; Zhang, X.; Tryk, D. A., *Surface Science Reports* **2008,** *63*, 515-582.

43. Diebold, U., *Surface Science Reports* **2003,** *48*, 53-229.

44. Sclafani, A.; Hermann, J. M., *J. Phys. Chem.* **1996,** *100*, 13655-13661.

45. Fusi, M.; Maccallini, E.; Caruso, T.; Casari, C. S.; Bassi, A. L.; Bottani, C. E.; Rudolf, P.; Prince, K. C.; Agustino, R. G., *Surface Science Reports* **2011,** *605*, 333-340.

46. Sapra, S.; Sarma, D. D., Electronic Structure and Spectroscopy of Semiconductor Nanocrystals. In *The Chemistry of Nanomaterials: Synthesis, Properties and Applications*, Rao, C. N. R.; Muller, A.; Cheetham, A. K., Eds. WILEY-VCH: Weinheim, 2004; pp 371-404.

47. Chen, X., *Chin J Catal* **2009,** *30* (8), 839-851.

48. Yan-Fei, H.; Gang, J.; Da-Qiao, M.; Fan-Jie, K., *Acta Physico-Chimica Sinica* **2010,** *26* (6), 1664-1668.

49. Meng-Hsiung, W.; Chuan, C.; Shin-Pon, J., *Chin J Catal* **2009,** *30* (5), 384-390.

50. Barginsky, L., *Physica E.* **2000,** *5*, 142-152.

51. Braginsky, L.; Skhlover, V., *Eur. Phys. J. D.* **1999,** *9*, 627-630.

52. Wu, Y.; Liu, H.; Zhang, J.; Chen, F., *J. Phys. Chem.* **2009,** *113*, 14689-14695.
53. Yang, Y.; Zhong, H.; Tian, C., *Res Chem Intermed* **2011,** *37*, 91-102.
54. Ahmed, S.; Rasul, M. G.; Martens, W. N.; Brown, R.; Hashib, M. A., *Water Air Soil Pollut.* **2011,** *215*, 3-29.
55. Gratzel, M., *Journal of Photochemistry and Photobiology A: Chemistry* **2004,** *164*, 3-14.
56. Campbel, W. M.; Burrell, A. K.; Officer, D. L.; Joley, K. W., *Coordination Chemistry Reviews* **2004,** *248* (1363-1379).
57. Zheng, X.; Zhang, J.; Peng, L.; Yang, X.; Cao, W., *J. Mater Sci.* **2011,** *46*, 5071-5078.
58. Sari, S.; Shishodia, P. K.; Mehra, R. M., *Journal of Renewable and sustainable energy* **2010,** *2*, 043103
59. Burda, C.; Lou, Y.; Chen, X., *Nanoletters* **2003,** *3* (8), 1049-1052.
60. Hermann, J.-M., *Appl. Catal. B: Environ* **2010**.
61. Chen, X.; Mao, S. S., *Chem. Rev.* **2007,** *107*, 2891-2959.
62. akpan, U. G.; Hameed, B. H., *Journal of Hazardous Materials* **2009,** *170*, 520-529.
63. Lachheb, H.; Puzenat, E.; Houas, A.; Ksibi, M.; Elaloui, E.; Guillard, C.; Hermann, J.-H., *Appl. Catal. B: Environ* **2002,** *39*, 75-90.
64. Arbuj, S. S.; Hawaldar, R. R.; Mulik, U. P.; Wani, B. N.; Amalnekar, D. P.; Waghmode, S. B., *Material Science and Engineering B* **2010,** *168*, 90-94.
65. Datye, A. K.; Riegel, G.; Bolton, J. R.; Huang, M.; Prairie, M. R., *Journal of Solid State* **1995,** *115*, 236-239.
66. Ohno, T.; Sakurawa, K.; Tokieda, K.; Matsumura, M., *Journal of Catalysis* **2001,** *203*, 82-86.
67. Hurum, D. C.; Agrios, A. G.; Gray, K. A.; Rajh, T.; Thurnauer, M. C., *J. Phys. Chem.* **2003,** *107*, 4545-4549.
68. Golubko, N. V.; Yanovskaya, M. I.; Romm, I. P.; Ozerin, A. N., *Journal of Sol-Gel Science and Technology* **2001,** *20*, 245-262.
69. Jagadale, T. C.; Takale, S. P.; Sonawane, R. S.; Joshi, H. M.; Patil, S. I.; Kale, B.; Ogale, S. B., *J. Phys. Chem.* **2008,** *112*, 14595-14602.
70. Schwarzenbach, D., *Inorganic Chemistry* **1970,** *9* (11), 2391-2397.
71. Sasirekha, N.; Rajesh, B.; Hen, Y. W., *Thin Solid Films* **2009,** *518*, 43-48.
72. Hutchison, J. E., Tryphenylphosphine-Stabilized Gold Nanoparticles. In *Inorganic Syntheses*, Shapley, J. R., Ed. John Wiley and Son, Inc.: New Jersey, 2004; Vol. 34, pp 228-232.
73. Gao, X.; Wachs, I. E., *Catalysis Today* **1999,** *51*, 233-254.
74. Anderson, C.; Bard, A. J., *J. Phys. Chem.* **1995,** *99*, 9882-9885.
75. Panatoyov, D. A.; Paul, D. K.; Yates, J. T., *J. Phys. Chem.* **2003,** *107*, 10571-10575.
76. Perkampus, H.-H., *UV-Vis Spectroscopy and Its Applications*. Springer: Verlag, 1992.
77. Georgi, A.; Kopinke, F. D., *Appl. Catal. B: Environ* **2005,** *58*, 9-18.
78. Lee, D. K.; Cho, I. C.; Lee, G. S.; Kim, S. C.; Kim, D. S.; Yang, Y. K., *Separation and Purification Technology* **2004,** *34*, 43-50.
79. Santos, V. P., *Journal of Hazardous Materials* **2009,** *162*, 736-742.
80. Lacheb, H.; Puzenat, E.; Houas, A.; Ksibi, M.; Elaloui, E.; C.Guillard; J-M.Hermann, *Appl. Catal. B: Environ* **2002,** *39*, 75-90.

81. Petitjean, M., *Journal of Computational Chemistry* **1994,** *15* (5), 507-523.
82. Miller, C. M.; Valentine, R. L. Catalytic fixed bed reactor systems for the destruction of contaminants in water by hydrogen peroxide. 1998.
83. Han, Y.-F.; Phonthammachai, N.; Ramesh, K.; Zhong, Z.; White, T., *Environ. Sci. Technol.* **2008,** *42*, 908-912.
84. Tanaka, K.; Hisanaga, T.; Harada, K., *J. Photochem. Photobiol. A: Chem* **1989,** *48*, 155-159.
85. Chakrabarti, S.; Dutta, B. K., *J. Hazard. Mater.* **2004,** *B112*, 169-278.
86. Reddy, M. P.; Venugopal, A.; Subrahmanyam, S., *Appl. Catal. B: Environ* **2007,** *69*, 164-170.
87. Kapinus, E. I.; Viktorova, T. I., *Theoretical and Experimental Chemistry* **2010,** *46* (3), 163-167.
88. Liu, W.; Andrew, S. A.; Stefan, M. I.; Bolton, J. R., *Testing Water Res.* **2003,** *37*, 3697-3703.
89. Paulios, I.; Tsachpinis, I., *Journal of Chemical Technology and Biotechnology* **1999,** *74*, 349-357.
90. Gumus, D.; Akbal, F., *Water Air Soil Pollut.* **2011,** *216*, 117-124.
91. Stead, C. V., Chemistry of reactive dyes. In *Colorants and auxiliaries: organic chemistry and application properties*, Shore, J., Ed. Society of Dyers and Colourists: Manchester, 1990; Vol. 1, pp 307-337.
92. Camp, S. R.; Sturrock, P. E., *Wat. Res.* **1990,** *24* (10), 1275-1278.
93. He, Z.; Lin, L.; Song, S.; Xia, M.; Xu, L.; Ying, H.; Chen, J., *Separation and Purification Technology* **2008,** *62*, 376-381.
94. *Textile Dyeing Wastewaters: Characterization and Treatment*; U. S. Environmental Protection Agency: North Carolina, 1978.
95. Correia, V. M.; Stephenson, T.; Judd, S. J., *Environmental Technology* **1994,** *15* (10), 917-929.
96. Neppolian, B.; Choi, H. C.; Sakthivel, S.; Arabindo, B.; Murugesan, V., *Chemosphere* **2002,** *46*, 1173.
97. Shore, J., Dye Structure and Application Properties. In *Colorants and auxiliaries: Organic chemistry and application peoperties*, Shore, J., Ed. Society of Dyers and Colourists: Manchester, 1999; Vol. 1, pp 74-144.
98. Saepurahman; Abdullah, M. A.; Chong, F. K., *Chemical Engineering Journal* **2010,** *158*, 418-425.
99. Liao, D. L.; Liao, B. Q., *Journal of Photochemistry and Photobiology A: Chemistry* **2007,** *187*, 363-369
100. Eiden-Assmann, S.; Widoniak, J.; Maret, G., *Chem. Mater.* **2004,** *16*, 6-11.
101. Primo, A.; Corma, A.; Garcia, H., *Physical Chemistry Chemical Physics* **2011,** *13*, 886-910.

Appendix 1. Relationships of ln[C] *v.s.* t of all reactions in this study

1. Photocatalytic methods

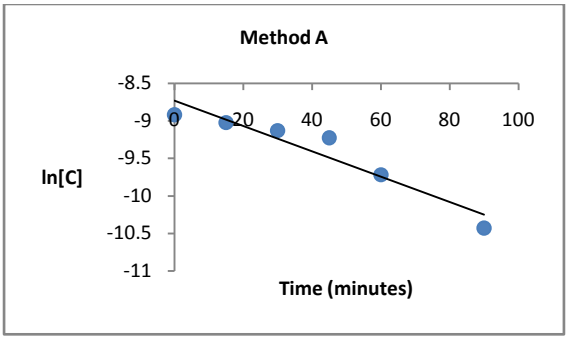

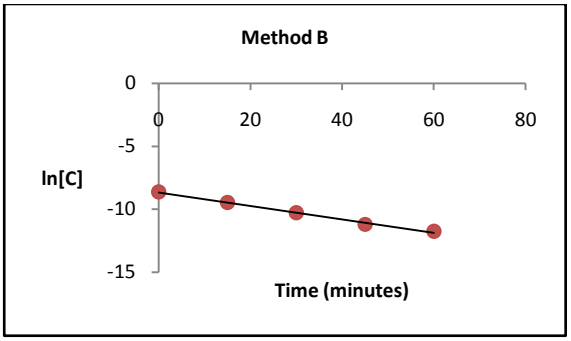

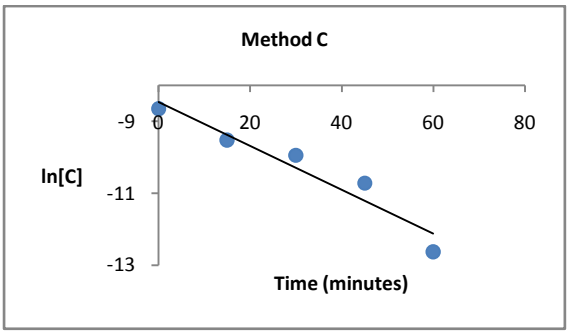

2. Effect of P25-TiO_2 catalyst loadings and concentrations of H_2O_2

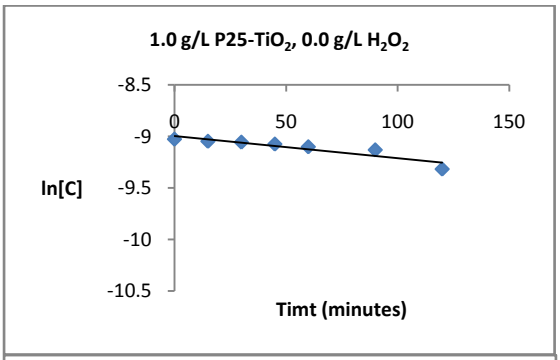

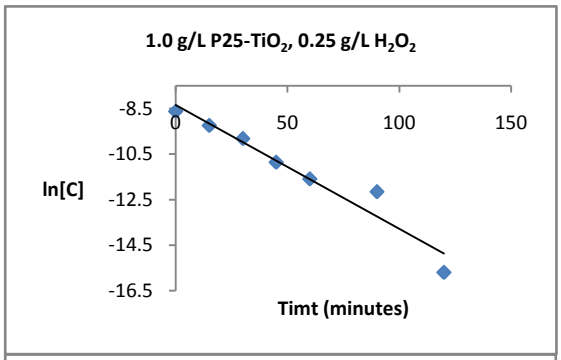

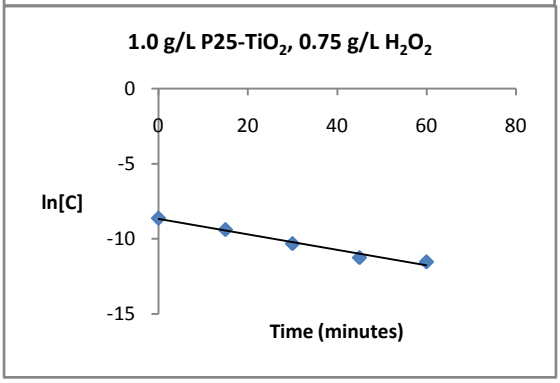

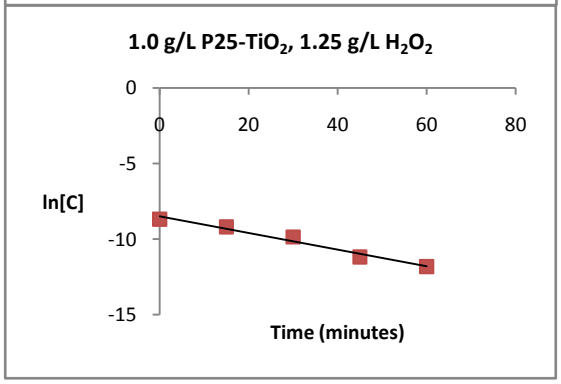

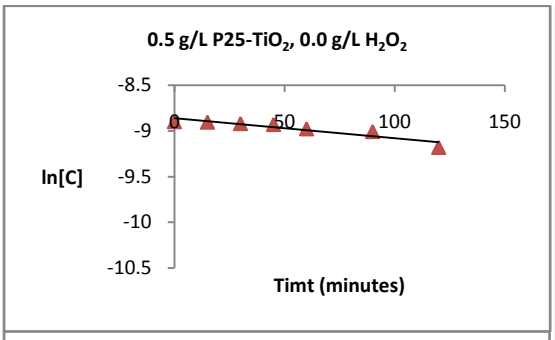
0.5 g/L P25-TiO2, 0.0 g/L H2O2
-8.5
-9
-9.5
-10
-10.5
ln[C]
0
50
100
150
Timt (minutes)

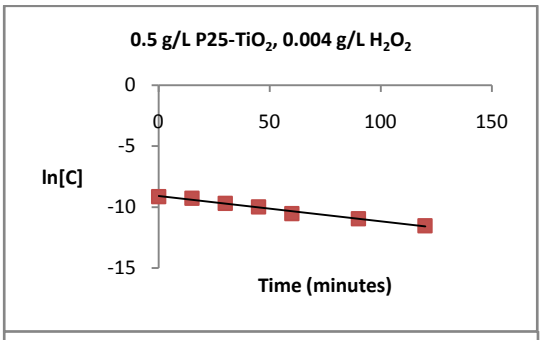
0.5 g/L P25-TiO2, 0.004 g/L H2O2
0
-5
-10
-15
ln[C]
0
50
100
150
Time (minutes)

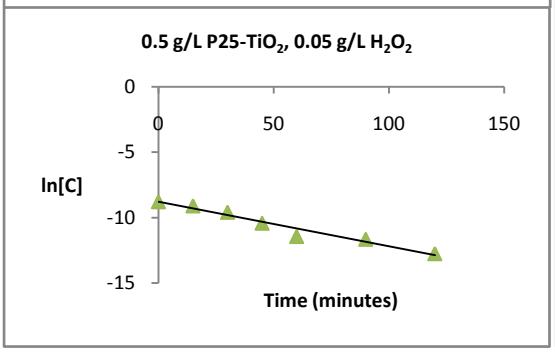
0.5 g/L P25-TiO2, 0.05 g/L H2O2
0
-5
-10
-15
ln[C]
0
50
100
150
Time (minutes)

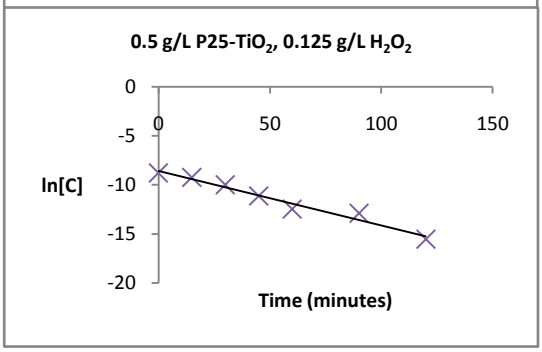
0.5 g/L P25-TiO2, 0.125 g/L H2O2
0
-5
-10
-15
-20
ln[C]
0
50
100
150
Time (minutes)

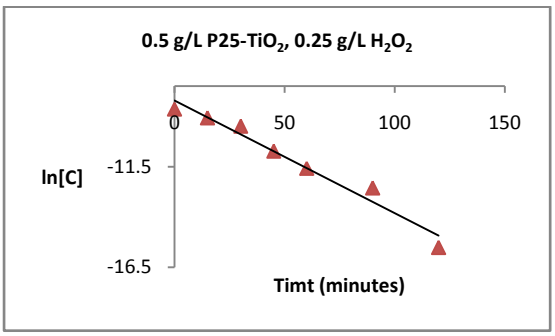
0.5 g/L P25-TiO2, 0.25 g/L H2O2
-11.5
-16.5
ln[C]
0
50
100
150
Timt (minutes)

3. The effect of different pH on photocatalytic degradation of RB19

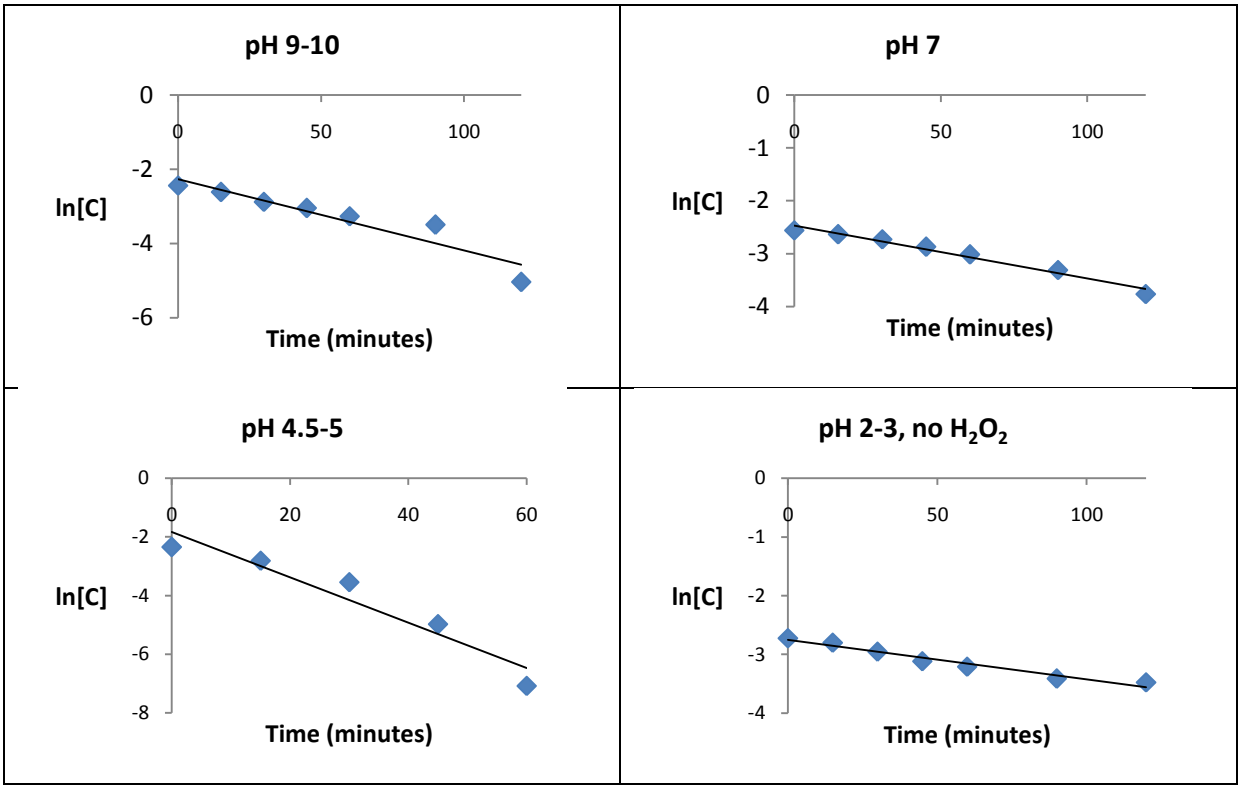

4. The effect of process and natural pH of various dyes

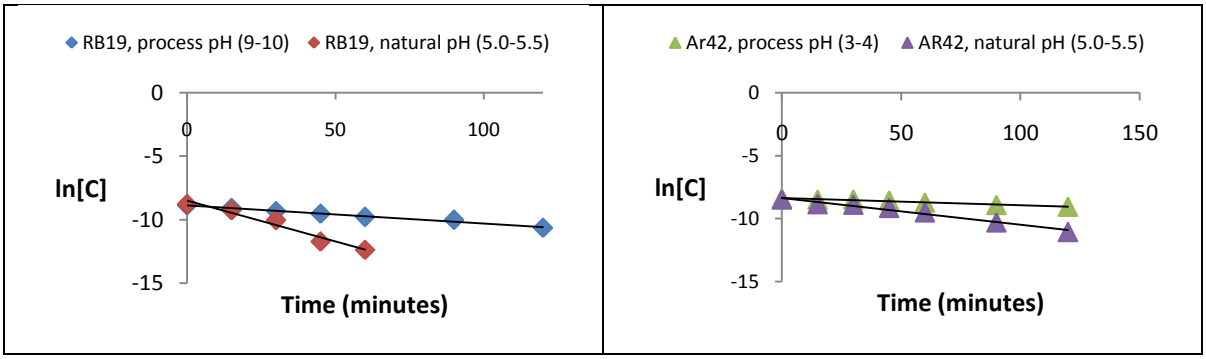

5. Photocatalytic tests of custom-made TiO_2

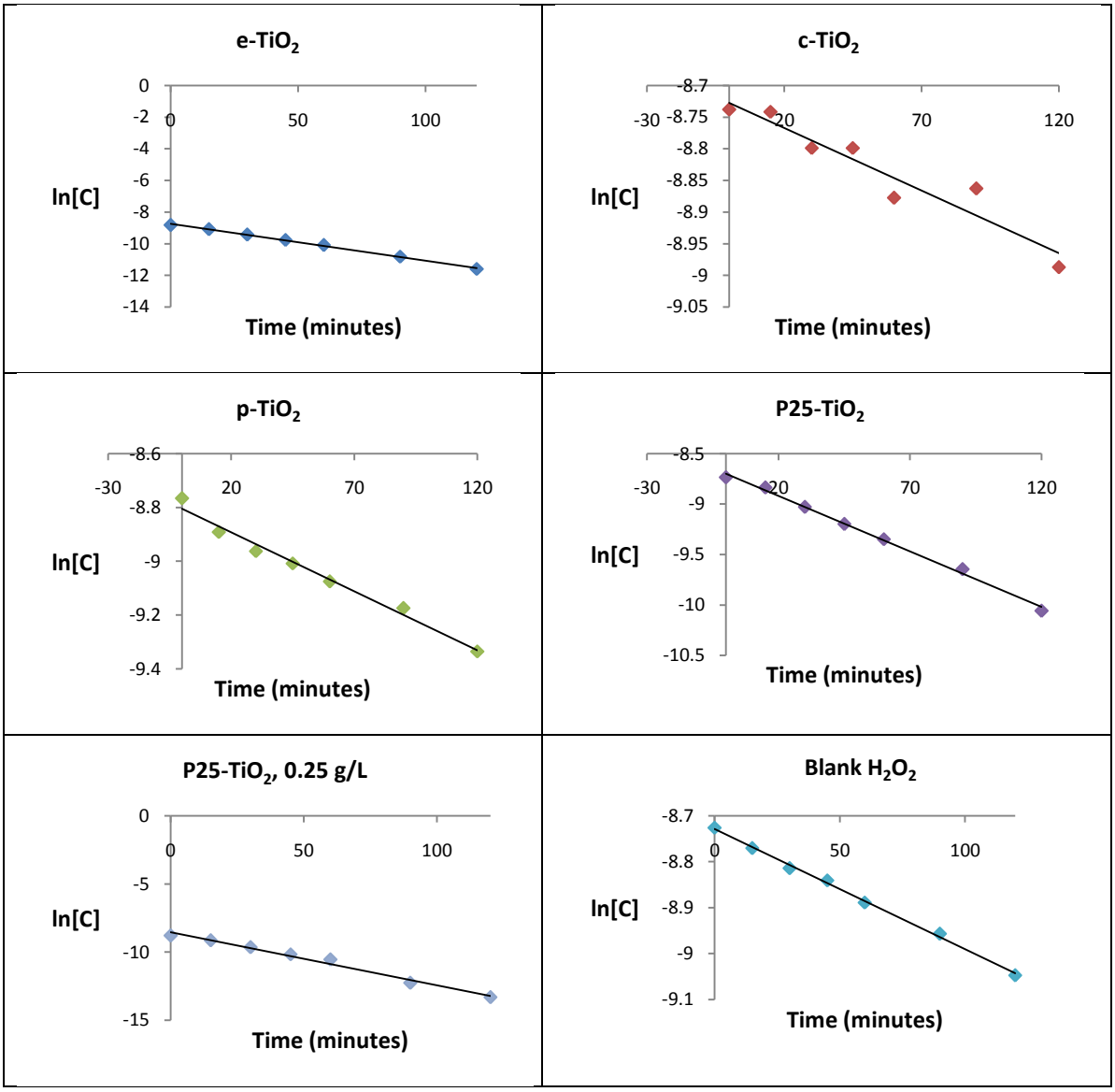

6. Photocatalytic degradation of RB19 using various TiO_2/SiO_2

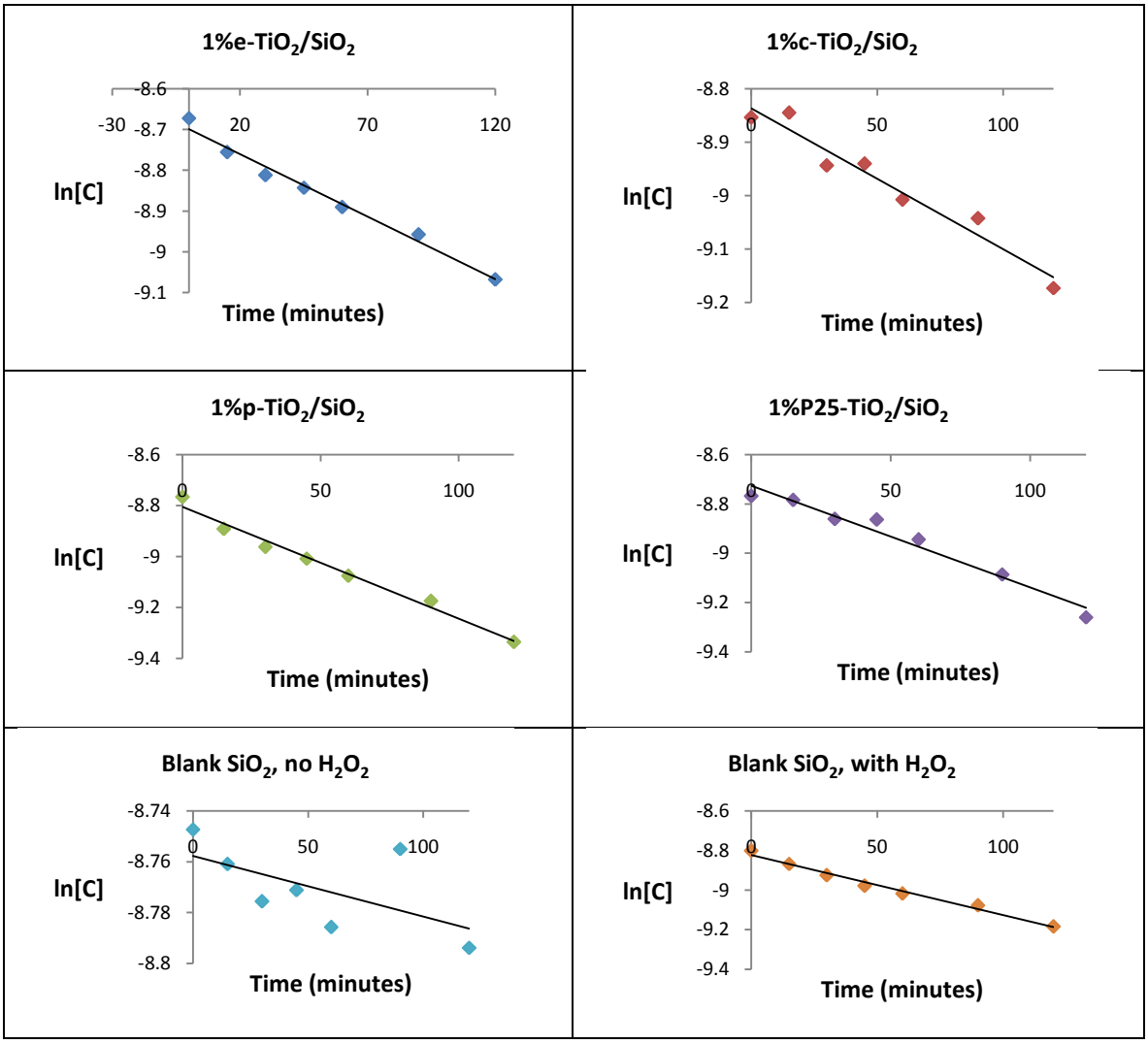

7. Photocatalytic degradation of RB19 using various Au/TiO_2 photocatalysts